

IDENTIFICATION OF DELAMINATION DEFECTS IN CFRP MATERIALS THROUGH  
LAMB WAVE RESPONSES

A Thesis  
Submitted to the Graduate Faculty  
of the  
North Dakota State University  
of Agriculture and Applied Science

By

Taylor John Bruhschwein

In Partial Fulfillment  
for the Degree of  
MASTER OF SCIENCE

Major Department:  
Civil and Environmental Engineering

May 2014

Fargo, North Dakota

North Dakota State University  
Graduate School

---

**Title**

Identification of Delamination Defects in CFRP Materials through  
Lamb Wave Responses

---

**By**

Taylor Bruhschwein

---

The Supervisory Committee certifies that this *disquisition* complies with North  
Dakota State University's regulations and meets the accepted standards for the degree of

**MASTER OF SCIENCE**

SUPERVISORY COMMITTEE:

Mijia Yang

---

Chair

Sivapalan Gajan

---

Frank Yazdani

---

Ghodrat Karami

---

Approved:

05/19/14

---

Date

Dinesh Katti

---

Department Chair

## **ABSTRACT**

Delamination is currently a largely undetectable form of damage in composite laminate materials. This thesis will develop a method to more easily detect delamination damage within composite materials. Using finite element analysis modeling and lab testing, a new method from interpreting the results obtained from existing structural health monitoring techniques is developed.

Lamb waves were introduced and recorded through an actuator and sensors made of piezoelectric material. The data was then analyzed through a novel data reduction method using the Fast Fourier Transform (FFT). Using the data from FFT, the idea of covariance of energy change was developed. By comparing the covariance of energy change in beams with differing delamination size, thickness and depth, correlations were able to be developed. With these correlations, the severity and of damage was able to be detected.

# TABLE OF CONTENTS

ABSTRACT .....	iii
LIST OF TABLES .....	vii
LIST OF FIGURES .....	viii
LIST OF APPENDIX TABLES .....	xii
LIST OF APPENDIX FIGURES.....	xiii
CHAPTER 1. INTRODUCTION .....	1
1.1.    Background.....	1
1.2.    Lamb waves.....	3
1.2.1.  Introduction .....	3
1.2.2.  Theory .....	4
1.2.3.  Previous works .....	7
1.3.    Piezoelectric transducer .....	8
1.3.1.  Introduction .....	8
1.3.2.  Previous works .....	9
1.4.    Summary.....	11
1.4.1.  Literature review summary .....	11
1.4.2.  Research objectives .....	11
CHAPTER 2. MODELING VERIFICATION.....	12
2.1.    Introduction .....	12
2.2.    Modeling of wave propagation in an aluminum beam .....	13
2.2.1.  Wave propagation in an undamaged aluminum beam .....	13

2.2.2.	Wave propagation in a damaged aluminum beam .....	20
2.3.	Summary.....	23
CHAPTER 3. DETECTION OF DELAMINATION IN LAMINATED COMPOSITE BEAMS THROUGH COVARIANCE ENERGY CHANGE OF ULTRASONIC WAVES .....		24
3.1.	Introduction .....	24
3.2.	Data reduction by fast Fourier transform .....	26
3.3.	Parametric study of delamination in composite beams .....	28
3.3.1.	Parameter selection .....	28
3.3.2.	Lamb wave response in undamaged composite beams.....	30
3.3.3.	Lamb wave response in the damaged composite beam.....	33
3.3.4.	Sensor responses of ultrasonic waves in the damaged composite beam.....	33
3.3.5.	Data reduction by FFT .....	36
3.3.6.	Varying delamination thickness.....	45
3.3.7.	Varying delamination location.....	48
3.3.8.	Full section convergence study .....	54
3.3.9.	Multiple delamination detection.....	55
3.4.	Summary.....	56
CHAPTER 4. EXPERIMENTAL DETECTION OF DELAMINATION IN LAMINATED COMPOSITE BEAMS THROUGH COVARIANCE OF ENERGY CHANGE OF ULTRASONIC WAVES .....		57
4.1.	Introduction .....	57
4.2.	Beam manufacturing.....	57
4.2.1.	Creating delamination damage in the beams.....	61
4.3.	Experimental delamination detection in composite beams .....	62

4.3.1. Set up.....	62
4.3.2. Data collection and reduction.....	67
4.4. Results .....	68
4.4.1. Varying delamination size.....	68
4.4.2. Varying delamination depth.....	76
4.4.3. Convergence study of time window.....	77
4.5. Modeling validation.....	79
4.6. Summary.....	81
CHAPTER 5. CONCLUSIONS AND RECOMMENDATIONS .....	82
5.1. Conclusions .....	82
5.2. Recommendations and future work.....	83
REFERENCES .....	84
APPENDIX. COMPOSITE MODELING.....	89
A.1. Loading responses of undamaged composite .....	89
A.2. Loading responses of damaged composite .....	95

## LIST OF TABLES

<u>Table</u>	<u>Page</u>
1. Beam properties .....	25
2. Element size convergence study .....	28
3. Section 1 frequencies and amplitudes.....	40
4. Section 2 frequencies and amplitudes.....	40
5. Covariance of energy change.....	44
6. Damage locations and time of flight.....	49
7. Beam geometry .....	58
8. Beam specifications .....	58
9. Beam properties .....	59

## LIST OF FIGURES

<u>Figure</u>	<u>Page</u>
1. Symmetric and anti-symmetric Lamb waves modes [21].....	5
2. Alumina dispersion curves [22].....	6
3. Dispersion curves for the carbon/epoxy laminate [22].....	7
4. Experimental data confirming “sweet spot” for $A_0$ and $S_0$ wave modes .....	10
5. Diagram from aluminum beam [22] .....	13
6. 5 count, 100 kHz Hanning window wave.....	14
7. Aluminum beam diagram .....	16
8. Sensor 1 (top - Yang, bottom - recreation) .....	17
9. Sensor 2 (top - Yang, bottom - recreation) .....	18
10. Sensor 3 (top - Yang, bottom - recreation) .....	19
11. Damaged aluminum beam .....	20
12. ANSYS model of damaged aluminum beam.....	21
13. Sensor 1 comparison.....	21
14. Sensor 2 comparison.....	22
15. Sensor 3 comparison.....	22
16. Actuator and sensor locations .....	25
17. 100 kHz Hanning window wave.....	26
18. FFT graph of 100 kHz Hanning wave .....	27
19. Element size convergence study .....	29
20. CONTA175 and TARGE169 elements .....	30
21. Undamaged composite beam .....	31



22. Actuator loading nodes .....	32
23. Sensor nodes .....	32
24. Strain-time history of undamaged composite beam.....	33
25. Typical damaged composite beam.....	33
26. Strain-time history of damaged composite beam, 15mm x 0.25mm .....	34
27. Strain-time history of damaged composite beam, 40mm x 0.25mm .....	34
28. Strain-time history of damaged composite beam, 60mm x 0.25mm .....	35
29. Strain-time history of damaged composite beam, 80mm x 0.25mm .....	35
30. Strain-time history comparison.....	36
31. Wave propagation paths.....	37
32. Wave package separation (a) full response (b) Section 1 (c) Section 2.....	38
33. FFT graph of Section 2 of the beam with a 40 mm x 0.25 mm defect .....	39
34. Sum of the square of the difference of the frequencies present .....	41
35. Sum of the square of the difference in present amplitudes present .....	42
36. Covariance of energy change at Section 1 .....	43
37. Covariance of energy change at Section 2 .....	43
38. Covariance of energy change for full section .....	44
39. Comparison of wave responses of different delamination thicknesses .....	46
40. Zoomed in region of wave responses.....	46
41. Covariance of energy change with varying delamination thickness size at section 1 .....	47
42. Covariance of energy change with varying delamination thickness size at section 2 .....	47
43. Covariance of energy change with varying delamination thickness size for full section .....	48

44. Time domain response at section 1 with varying damage locations.....	49
45. Time domain response at section 2 with varying damage locations.....	49
46. Arrival time of peak with varying damage locations.....	50
47. Time domain response at section 1 with varying damage depth .....	51
48. Time domain response at section 2 with varying damage depth .....	51
49. Covariance of energy change at section 1 with varying damage depth .....	52
50. Covariance of energy change at section 2 with varying damage depth .....	52
51. Covariance of energy change for full section with varying damage depth.....	53
52. Covariance of energy change vs distance of damage from center .....	54
53. Convergence study of covariance of energy change of damaged beam based on window size .....	55
54. Wave response comparison for a beam with multiple damages .....	56
55. Tensile test of the composite beam.....	59
56. Tensile test results.....	60
57. Cross section of composite beam.....	60
58. Close up of a damaged (a) and an undamaged (b) beam .....	62
59. Layout of experimental beams.....	62
60. Bonded PZT – top view .....	63
61. Bonded PZT – side view.....	64
62. Agilent 33220A waveform generator .....	64
63. Tektronix TDS 2012B oscilloscope.....	65
64. Wire connection to bonded PZT .....	66
65. Output wave .....	67
66. Time domain comparison of wave responses in beams 4 and 10, sensor 1 .....	67

67. Covariance of energy change at sensor 1, section 1, between 0/90 .....	69
68. Covariance of energy change at sensor 1, section 1, between 90/+45 .....	69
69. Covariance of energy change at sensor 1, section 1, between +45/-45 .....	70
70. Covariance of energy change at sensor 1, comparison .....	70
71. Covariance of energy change at sensor 1, section 2, between 0/90 .....	71
72. Covariance of energy change at sensor 1, section 2, between 90/+45 .....	71
73. Covariance of energy change at sensor 1, section 2, between +45/-45 .....	72
74. Covariance of energy change at sensor 1, section 2, comparison .....	72
75. Covariance of energy change at sensor 1, full section, between 0/90 .....	73
76. Covariance of energy change at sensor 1, full section, between 90/+45 .....	73
77. Covariance of energy change at sensor 1, full section, between +45/-45 .....	74
78. Covariance of energy change at sensor 1, full section, comparison .....	74
79. Covariance of energy change at sensor 2, full section, comparison .....	75
80. Covariance of energy change at sensor 1, full section, comparison .....	76
81. Covariance of energy change at sensor 2, full section, comparison .....	77
82. Convergence of time window size for sensor 1 .....	78
83. Convergence of time window size for sensor 2 .....	78
84. Comparison of model vs experiment wave responses, undamaged beam .....	80
85. Comparison of model vs experiment, damaged beam .....	80

## LIST OF APPENDIX TABLES

<u>Table</u>	<u>Page</u>
A1. Plate properties.....	90
A2. Double cantilever beam properties .....	96
A3. Comparison of results .....	99

## LIST OF APPENDIX FIGURES

<u>Figure</u>	<u>Page</u>
A1. Element type .....	90
A2. Material properties .....	91
A3. Composite layer arrangement .....	92
A4. Composite lay-up .....	92
A5. Composite plate geometry .....	93
A6. Composite plate meshing .....	93
A7. Pressure application .....	94
A8. Double cantilever beam .....	95
A9. Element selection .....	97
A10. Composite properties .....	97
A11. Meshed composite beam .....	98
A12. Solution options .....	99

# CHAPTER 1. INTRODUCTION

## 1.1. Background

Composite materials are becoming more widely used in a variety of structural areas. Whether it is in bridge rehabilitation, aerospace engineering, or other areas, a move toward lighter and stronger materials is being made. Composite laminates are one popular form of these materials and are being used more and more in the aerospace field [1, 2]. While these composite materials have extraordinary benefits with their physical properties, they tend to generate various damages during their usage, including many barely visible damages, due to its composite components and layered structure [3, 4]. One of these most critical damage modes in these composites is delamination [5, 6]. Since failure of structures in the aerospace field can be extremely costly and possibly causes great danger to thousands of travelers, there comes an urgent demand for accurate methods of delamination detection.

Delamination is a result of the method in which the laminates are produced, namely a layer by layer process [6]. Delamination may occur between any two neighboring layers of the laminate, making detection from purely exterior visual inspection all but impossible. This is referred to as barely visible damages, BVD [1]. Once delamination has occurred, the physical strength properties of the composite material may be greatly reduced or even completely compromised [6]. While there have been numerous studies to locate damage in both metallic and composite materials, there is still difficulty with accurately detecting delamination damage due to its special planar shape.

In addition to real-time detection of the damage, the weight of the monitoring system is also of great importance. Since the light weight of the material is one of the desirable qualities, it

is important the sensors being used will not affect the overall weight significantly. From previous studies, it has been shown that piezoelectric sensors (PZTs) are an appropriate choice for health monitoring while not being over cumbersome [7, 11-15].

Piezoelectric sensors are able to be applied directly to the laminates, while not hindering the overall performance of the composite. By using the PZT as a series of actuators and sensors, it is possible to detect damage location as well as severity throughout the composite materials. The actuators are used to create waves which are then altered by changing conditions, such as boundaries or damage. Using the feedback from the sensors, one is able to effectively evaluate the damage. In this thesis, PZTs will be used to generate and receive Lamb waves. Lamb waves have long been used in the SHM field and are discussed in Section 1.2.1.

While there are currently methods for structural health monitoring available for composite laminates, there is room for improvement of the methods. As mentioned before, delamination remains an area in which current SHM systems struggle. Another current problem is the data reduction methods. Data reduction based on time of flights has been proven to be limited in determining multiple damages and damage severity [22].

This thesis paper will be divided into 5 chapters. Chapter 1 will provide an introduction and literature review of techniques to be used in the research, including Lamb wave generation and PZT sensors and actuators. Chapter 2 will explore using commercial software ANSYS to perform wave propagation and composite material modeling. The modeling parameters used in the research will include wave modes, frequency, and different lay-up configuration of composites. Validation of the modeling techniques will be provided through comparison with previous experimental and numerical works. The modeling process will then be expanded to new areas including multiple delamination/damage detection and new data reduction methods

will be invented to correlate damages with signal processing indexes, which will comprise Chapter 3. Chapter 4 includes the experimental validation of the suggested data reduction method obtained in Chapter 3. Finally, Chapter 5 provides a summary of the thesis, including conclusions and recommendations for further study.

## **1.2. Lamb waves**

### **1.2.1. Introduction**

Lamb waves have long been used as a method for damage detection. Lamb waves provide a non-destructive method for detecting both damage location and severity. As far back as 1961, Worlton already used Lamb waves in Structural Health Monitoring [10]. In 1967, Viktorov provided the theoretical foundation for Lamb wave propagation through elastic media and damage detection applications [8]. Since location is a key component to useful SHM systems, the wave velocity must be known for the media being monitored. Coppens and Wilson analyzed the governing equations of Lamb waves during their research in the 1970s [9]. From these governing equations, propagation of the Lamb waves can be described through dispersion curves which will be discussed later in this chapter. Since their introduction to SHM, there have been numerous studies on the usage of Lamb waves, some of which are summarized in Section 1.2.3.

It has been shown that Lamb waves are able to span large distances quickly and respond to interference in the propagation path, such as a boundary or damage [16, 17, 19]. In addition, it was shown that Lamb waves are able to monitor the entire thickness of material they are propagating through [19, 20]. This is especially relevant since the major damage type to be



investigated in this thesis is delamination. Since delamination may occur at any depth, it is important to inspect the entire laminates.

Structural health monitoring, including the Lamb wave method, can be broken down into levels of detection based on their level of demands. In order of increasing difficulty the following pieces of information may be obtained: 1) indication whether or not damage has occurred, 2) location of the damage, 3) severity of the damage, and 4) prediction of structural safety [18]. For this thesis, the focus will be limited to detecting damage location and severity. In addition, the ability to detect several instances of damage within one material, namely several areas of delamination in a composite laminate, will be explored.

### 1.2.2. Theory

Lamb waves were discovered in 1917 by Horace Lamb. Lamb waves are able to exist in thin plates with parallel free boundaries, which will be the medium used for this thesis. Lamb waves are made up longitudinal and shear components, characteristics of which depend on the geometry of the structure, excitation method, and angle of introduction [21]. There are two distinct modes of Lamb waves: anti-symmetric and symmetric. The formulation of each of these modes can be represented as [21]:

$$\frac{\tan(qh)}{\tan(ph)} = -\frac{(k^2 - q^2)^2}{4k^2qp} \quad \text{for anti-symmetric modes,} \quad (1)$$

$$\frac{\tan(qh)}{\tan(ph)} = -\frac{4k^2qp}{(k^2 - q^2)^2} \quad \text{for symmetric modes,} \quad (2)$$

$$p^2 = \frac{\omega^2}{c_L^2} - k^2, \quad q^2 = \frac{\omega^2}{c_T^2} - k^2, \quad k = \frac{\omega}{c_P} \quad (3)$$

Where  $h$ ,  $k$ ,  $c_L$ ,  $c_T$ ,  $\omega$  represent plate thickness, wavenumber, velocities of longitudinal and transverse modes, and wave circular frequency, respectively.

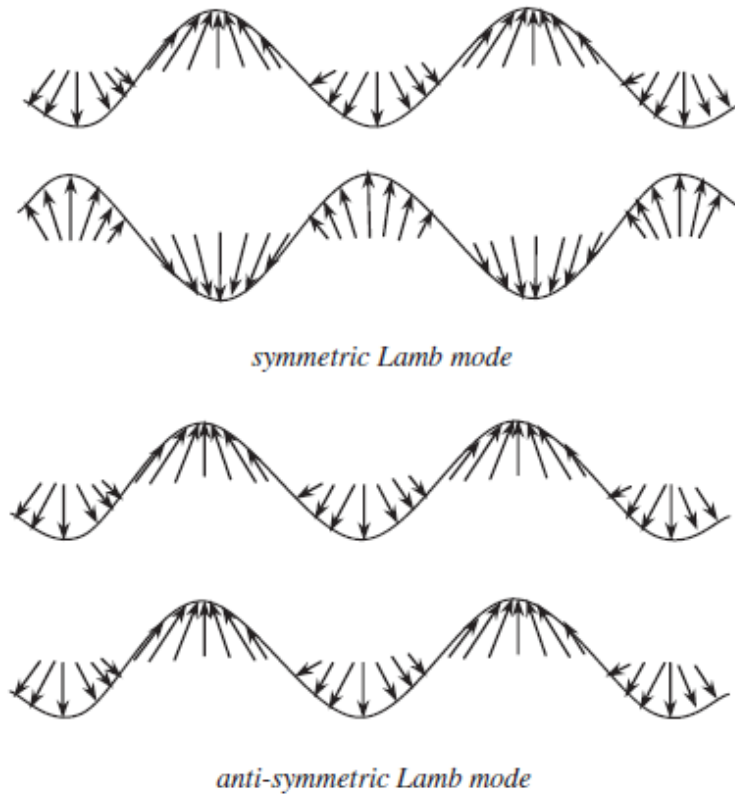


*Figure 1. Symmetric and anti-symmetric Lamb waves modes [21]*

These equations show that the velocity of the waves is correlated to the frequency. A wave exhibiting this behavior is said to be dispersive. Exactly how the velocity of the wave propagation is related to frequency is vital to using Lamb waves as a detection method effectively. With a known velocity, one is able to determine locations of interference, in our case delamination, with relative ease. Therefore the dispersion curves of Lamb modes are an integral part of the process. This paper will first look into thin aluminum beams as a starting point for damage detection. In their research paper (Yang and Qiao, 2005), Yang plotted the dispersion curves for Lamb waves in alumina [22].

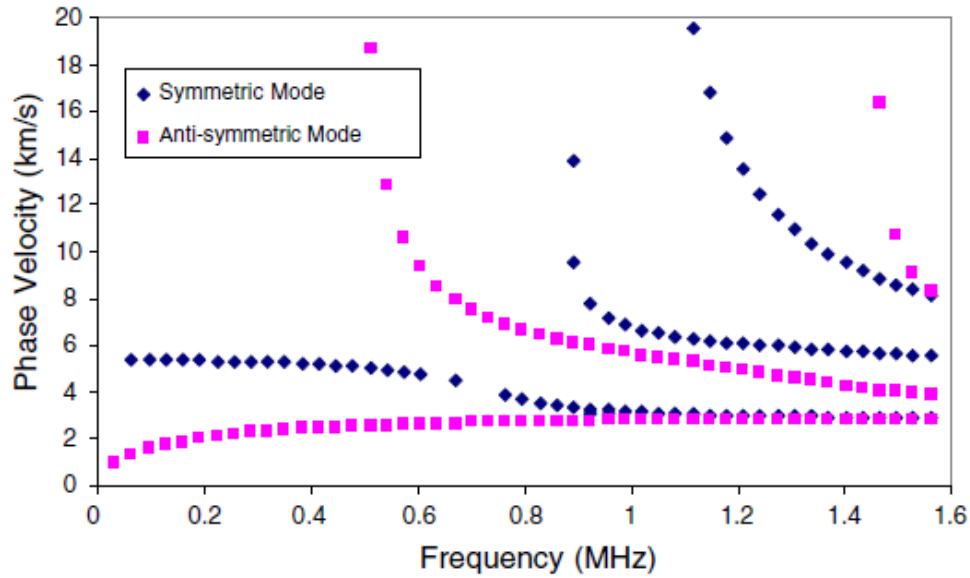


Figure 2. Alumina dispersion curves [22]

From the curves, it can be seen that for frequencies less than roughly 0.5 MHz, only two wave modes exist. These are called the fundamental symmetric ( $S_0$ ) and anti-symmetric ( $A_0$ ) waves. Since there are only two wave modes existing at these frequencies, this thesis will use the frequency range between 10 to 100 kHz, and it will be easier to distinguish which wave is producing the feedback. It can be seen the symmetric wave travels much more quickly than the anti-symmetric wave. Due to this, a higher frequency should be used when dealing with the symmetric wave propagation so as not to have damage passed over by too long of a wavelength.

Similarly, dispersion curves can be developed for anisotropic materials such as composite laminates. Many papers have these propagation characteristics of composite laminates, including dispersion curves [22-31]. The equations of motion become more complex as layers are incorporated and are discussed in Yang's 2005 paper [22]. From these equations of motion, the respective dispersion curves are developed.

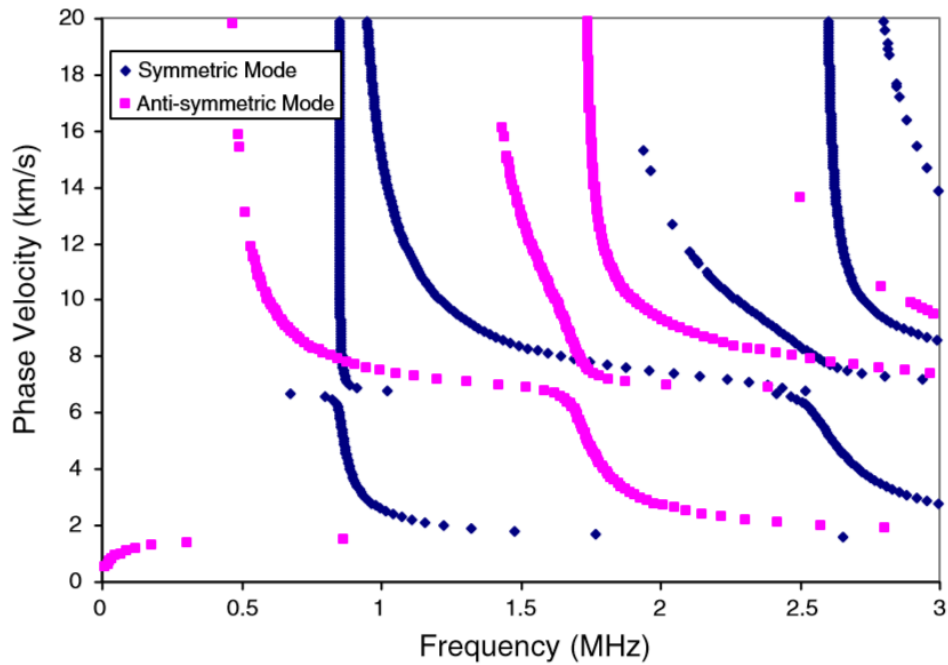


Figure 3. Dispersion curves for the carbon/epoxy laminate [22]

### 1.2.3. Previous works

There have been numerous studies on the use of Lamb waves as a damage detection method both in metals and composite materials. One study similar to this research was done at the Naval Academy by Palmos in 2009 [32]. This thesis discussed the use of Lamb waves to detect crack formations and generated Lamb waves through the use of PZT wafers. It was found that Lamb waves were a viable method of detection for this type of damage. The modeling was done with ANSYS software, which will also be used in this thesis.

Another study explored the response of Lamb waves in aluminum plates [33]. ABAQUS was used as the finite element analysis software for the modeling. Further modeling techniques were explored by the Air Force Research Laboratory in 2006 [34]. There the use of forces and moments as a means to model Lamb waves was validated. While studies such as the

aforementioned give validity to the Lamb wave method of damage detection, there has still been difficulty using this method to detect certain types of delamination in composite laminates [32]. The difficulty comes when the layers between which delamination occurs do not lose contact, but rather they simply no longer transfer loads effectively. Due to the conversion of wave modes from the delamination, it has been difficult to interpret data recorded by sensors [35]. Through different data reduction methods, such as FFT or wavelet analysis, this thesis will attempt to bring clarity to such results.

### **1.3. Piezoelectric transducer**

#### 1.3.1. Introduction

In order to monitor the structural health of materials still in use, the detection method must be non-destructive. Non-destructive evaluation (NDE) is common among SHM systems. There are two types of NDE currently in use, active and passive. While passive evaluation simply collects data from the structure, active evaluation interacts with the material to determine structural health [36].

One popular form of active NDE is using piezoelectric transducers (PZTs). PZTs operate on the piezoelectric principle and can transform electric energy into elastic energy and vice versa [36]. This allows one to send ultrasonic waves through a given material while controlling the amplitude of the wave through voltage. Other methods of active NDE have been used, but the majority of studies have shown PZTs to be the most effective in both generating and receiving Lamb waves.

### 1.3.2. Previous works

For nearly 20 years, research using PZTs as part of a SHM system to introduce and sense Lamb waves has been done. Beginning in 1995 with Chang's research [38], piezoelectric wafer active sensors (PWAS) have been explored as a NDE sensor or actuator. A more comprehensive review of the use of PWAS can be found in Giurgiutiu's 2008 book [37]. PWAS are a fitting choice as they weigh less than 0.1g and are smaller than 0.5mm thick for composite laminates [36].

There were numerous studies of nondestructive material evaluation techniques using finite element analysis, which can be found in Marckerle's review [39]. A breakthrough, as it relates to the current research, came with Moulin's work that showed that PZTs may be embedded in a composite plate to generate Lamb waves [40]. While we will be using bonded PZTs rather than embedded ones, this research first showed the ability of PZTs to noninvasively be part of the composite structure.

More specific research involving sensor placement and signal processing has also been conducted. Valdez and Soulis have published several papers on this topic [41-43]. Included in this work, PZTs were compared with another method, polyvinylidenedifluoride (PVDF). They chose PZTs since they required a much lower voltage to generate the waves needed. At the time of their research they noted that PZTs were not conformable to the material surface, but that issue has since been resolved.

The ability to isolate desired Lamb wave modes is another important consideration when choosing the wave generation method. By using PZT bonded to both sides of the composite, Su et al. [21] were able to verify that symmetric and anti-symmetric waves could be produced using actuation in phase and out of phase, respectively. Further, it was shown that frequency can be

controlled such that the symmetric wave dominates the anti-symmetric wave, or vice versa (Figure 4) [36].

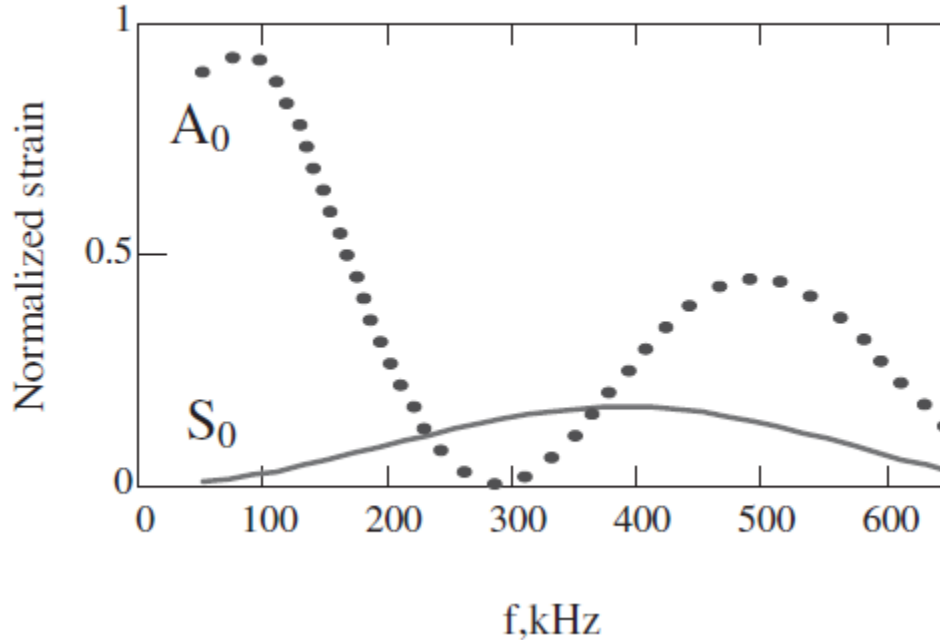


Figure 4. Experimental data confirming “sweet spot” for  $A_0$  and  $S_0$  wave modes

This isolation of wave mode is particularly important as it relates to this research, as the effectiveness of damage detection varies with wave mode and damage type. For example, it has been shown that the  $A_0$  mode is better suited for the detection of delamination [36].

In summary, using active piezoelectric transducers will be the most effective means of producing and receiving Lamb waves for this project. They are both cheap and noninvasive when compared to other actuators/sensors. As remarked in the conclusions by Su et al. [21]

“Active piezoelectric actuator/sensors are capable of generating and capturing Lamb waves most cost effectively for damage identification purposes, compared with other techniques. Large-scale integrated or embedded sensor networks can be customized using a certain number of distributed PZT elements. However, PZT-generated Lamb waves unavoidably create

difficulty in signal interpretation. Sophisticated signal processing with interpretation software is an integrated part of the approach.”

As mentioned earlier, one focus of this research paper is to simplify the interpretation of results from PZTs. This will address the concern shown in the conclusion from [21].

## **1.4. Summary**

### 1.4.1. Literature review summary

From the literature review, it was clearly seen that using Lamb waves is an acceptable and effective method to monitor structural materials. The method of introducing waves by PZT is preferable due to their small size and ease of bonding to the surface of such material. Current techniques have had trouble finding and classifying delamination damage with such methods.

### 1.4.2. Research objectives

The objective of this thesis is to develop a new data reduction method to locate and determine severity of delamination damage within composite materials. By developing such a method, the first step toward developing an index for damage severity in composites will be made.



## CHAPTER 2. MODELING VERIFICATION

### 2.1. Introduction

In order to validate modeling techniques adopted in this thesis, it is necessary to show all modeling are conducted accurately. By recreating the results of previous research, it will be proven that the modeling conducted is valid. For completeness, one example will be included for each type of modeling that will be seen in this thesis.

Included in this chapter will be results from two previous modeling examples alongside a reproduction of the respective results. The software to be used in this research will be the commercial software ANSYS. ANSYS is a finite element modeling software capable of producing all the necessary parts for the current research. Previous works involving Lamb wave propagation as a means of structural health monitoring have been completed using both ANSYS and the similar ABAQUS software. At least one example from each model will be recreated using ANSYS.

The examples to be recreated will include undamaged and damaged aluminum beams as well as a layered composite laminate. The aluminum beam examples will provide the basis for Lamb wave propagation and damage detection. The composite examples will exhibit the ability to create a layered composite material as well as the ability to effectively represent a delamination. Due to limitation of space, the composite laminate example will be included as an appendix. Once it is proven that all these aspects can be accurately modeled, one can be assured the rest of the modeling in the research has a sound basis.

## 2.2. Modeling of wave propagation in an aluminum beam

### 2.2.1. Wave propagation in an undamaged aluminum beam

The objective of this first model is to show that the methods to be used for modeling Lamb wave generation and reception are accurate. The undamaged aluminum beam example to be recreated comes from the 2005 paper by Yang [22]. The beam to be studied has the dimensions: 914mm x 14mm x 1.6mm. The properties of the aluminum used were:  $E = 7.0 \text{ GPa}$ ,  $\nu = 0.35$ ,  $\rho = 2,700 \text{ kg/m}^3$ . In the paper, one actuator and three sensors were used in monitoring the beam. Free-free boundary conditions were used.

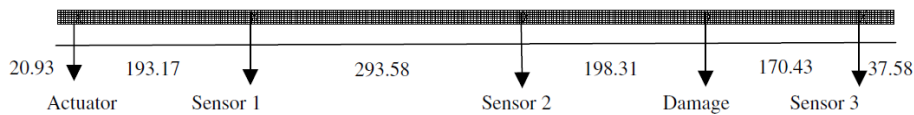


*Figure 5. Diagram from aluminum beam [22]*

Excluding the damage, since a healthy aluminum beam is being used, this model was recreated using the ANSYS software.

In Yang's simulation, the model was subjected to a 5 count, 100 kHz Hanning window axial wave (Figure 6) generated from the actuator at the left-hand side of the beam. The strain at each sensor was then recorded and plotted against time. The time period of the loading was  $5 \times 10^{-5} \text{ s}$ , with a time step of  $10^{-7} \text{ s}$ . The total length of the simulation was given as 0.001 seconds.

Reasoning for the determination of time step can be found in [21] and as a general guideline:

$\Delta t \leq \Delta x / v$  where,  $\Delta t$  = time step,  $\Delta x$  = element size,  $v$  = wave velocity. Given these parameters, the simulation was recreated using the ANSYS software.

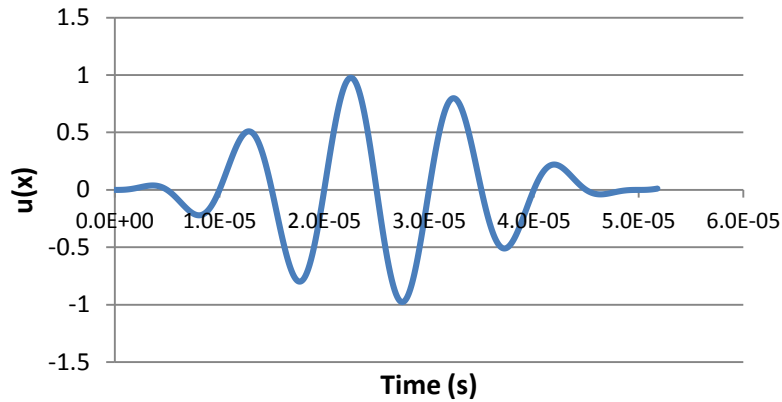


*Figure 6. 5 count, 100 kHz Hanning window wave*

**i) *Creating the Material***

With the given material properties, the aluminum material was defined.

**ii) *Element Type***

The element type was chosen as SOLID 182, 4-node. Six degrees of freedom were defined for each node: UX, UY, UZ, ROTX, ROTY, ROTZ.

**iii) *Creating Geometry***

The geometry of the beam was created using a 2-D shape that was later given a thickness.

**iv) *Creating a Section***

The section was defined as a beam section with thickness 1.6 mm.

**v) *Meshing***

When determining element size, the guideline given in Han's thesis [33] of  $\Delta x \leq \lambda/10$  is adopted. The wavelength was determined using a wave velocity of 5000 m/s, approximated

from the dispersion curve shown in Figure 2. The average element edge length was taken to be 5 mm, the magnitude of wavelength/10.

**vi) Boundary Conditions**

Boundary conditions were given as free-free. To isolate the deflections of interest the beam was constrained of twisting about the x and y axes.

**vii) Loading**

The loading is applied as the 100 kHz Hanning window shown in Figure 6. The load will be applied as a force, rather than a displacement in order not to constrain the model after applying the pulse. First, the function must be defined within ANSYS. This is captured as a multiple regime function defined as:

$$f(t) = \begin{cases} A * \left(1 - \frac{\cos(2\pi ft)}{5}\right) * \sin(2\pi ft), & 0 \leq t < 0.00005 \\ 0 & , \quad 0.00005 \leq t \end{cases} \quad (4)$$

Where  $A$  = Amplitude (N),  $f$  = Frequency (Hz),  $t$  = time(s), and  $f(t)$  = loading force history.

For this case frequency is 100 kHz and amplitude was taken as 1 kN. The amplitude is arbitrary and will only affect the magnitude of deflection, while propagation speed and wave response frequency remain unchanged.

The load is then applied to nodes which correspond to the front and back of the actuator as a positive and negative load, respectively. This will effectively simulate the expansion and contraction of the PZTs used in experimental practice.

### viii) *Defining Analysis Type*

The simulation requires a transient analysis type. The total analysis period is set to 0.001 seconds to be consistent with the literature model. Using the equation mentioned earlier, the time step is calculated from,

$$\Delta t \leq \Delta x / v \quad (5)$$

$$\Delta t = 1.25 \times 10^{-6} \text{s}$$

Where,  $\Delta t$  = time-step,  $\Delta x$  = element size,  $v$  = wave velocity. The model is now ready for analysis.

### ix) *Results*

From ANSYS, the displacement of each node is able to be observed over the analysis period. Nodes along the center of the beam at locations that represent the near and far edges of each sensor are observed. For example:

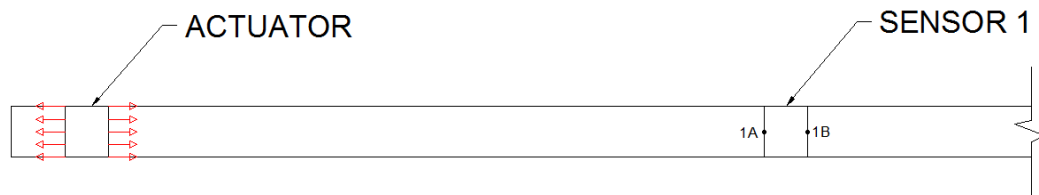


*Figure 7. Aluminum beam diagram*

Change in deflection can then be determined. In this case,  $\Delta U = U(1A) - U(1B)$ , where 1A and 1B are the middle points of the sensor boundary line. This will mimic the strain data collected by the PZT during the experiment.

Comparison with Yang's paper shows the modeling was indeed effective at reproducing the results. It can be noted there is a difference in amplitude of  $\Delta U$ , however this may be

attributed to differences in wave amplitude. Another cause of this may be the difference in sensor width used, as none was specified in the paper.

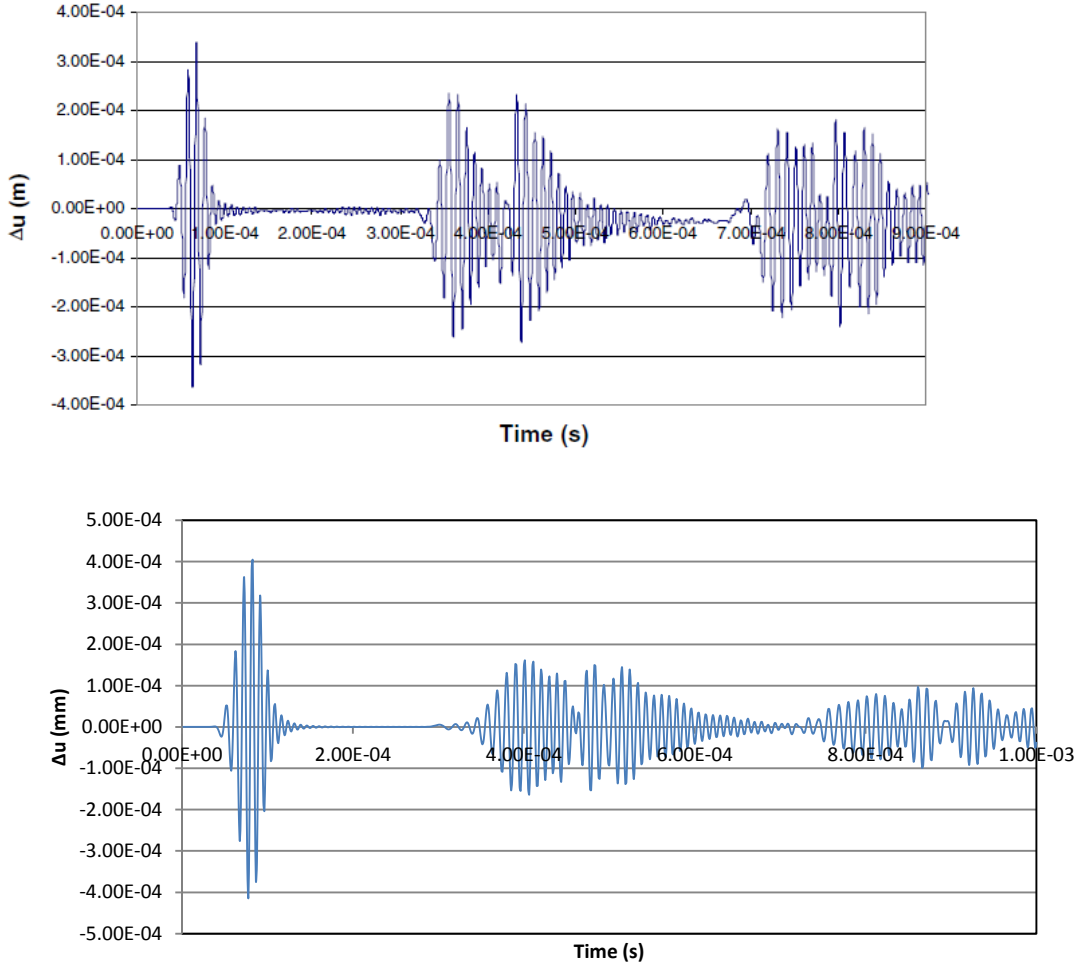


Figure 8. Sensor 1 (top - Yang, bottom - recreation)

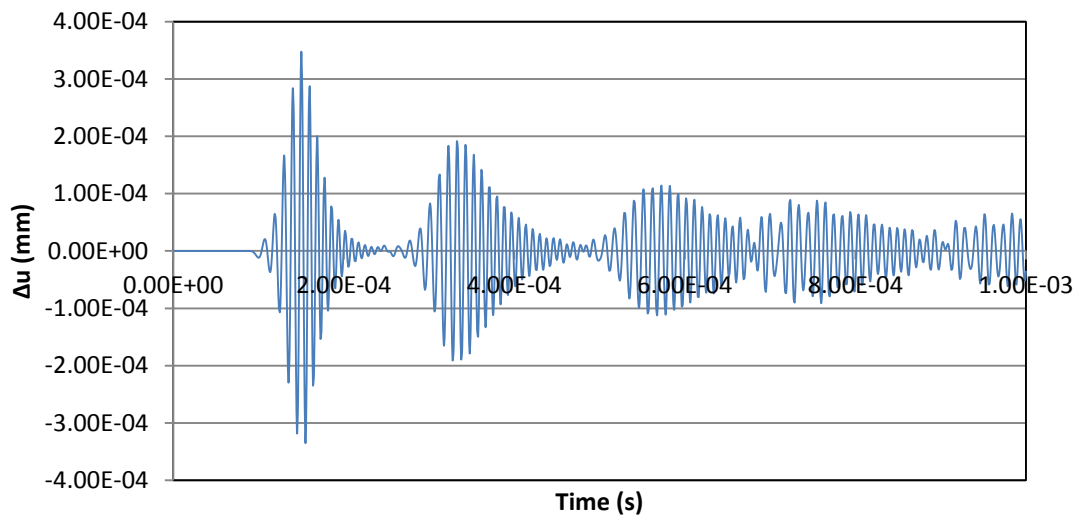
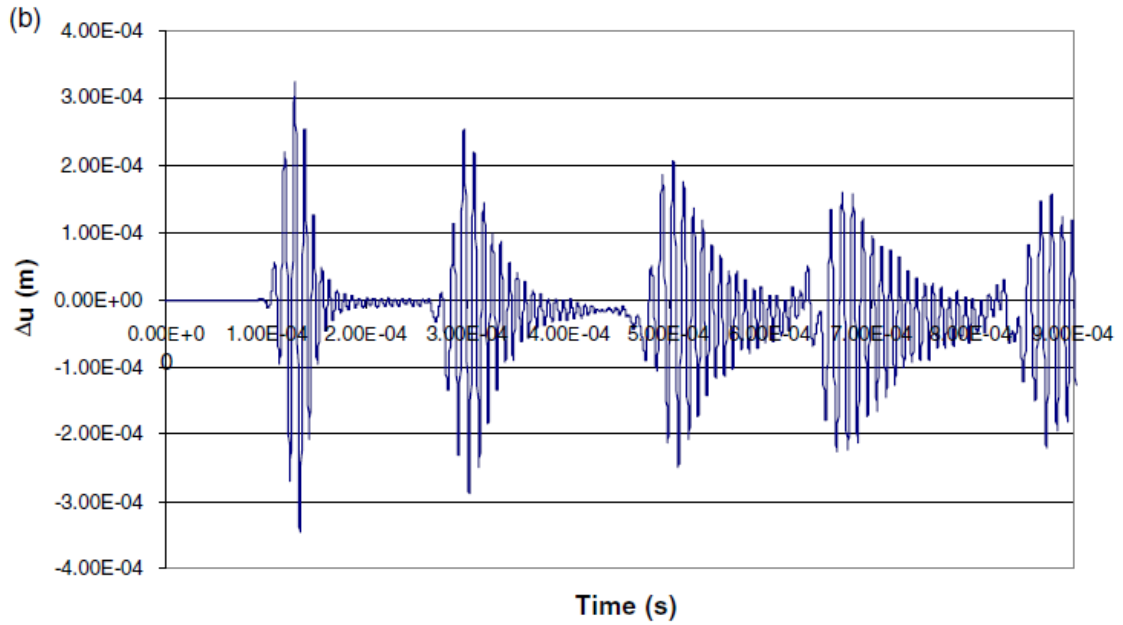


Figure 9. Sensor 2 (top - Yang, bottom - recreation)

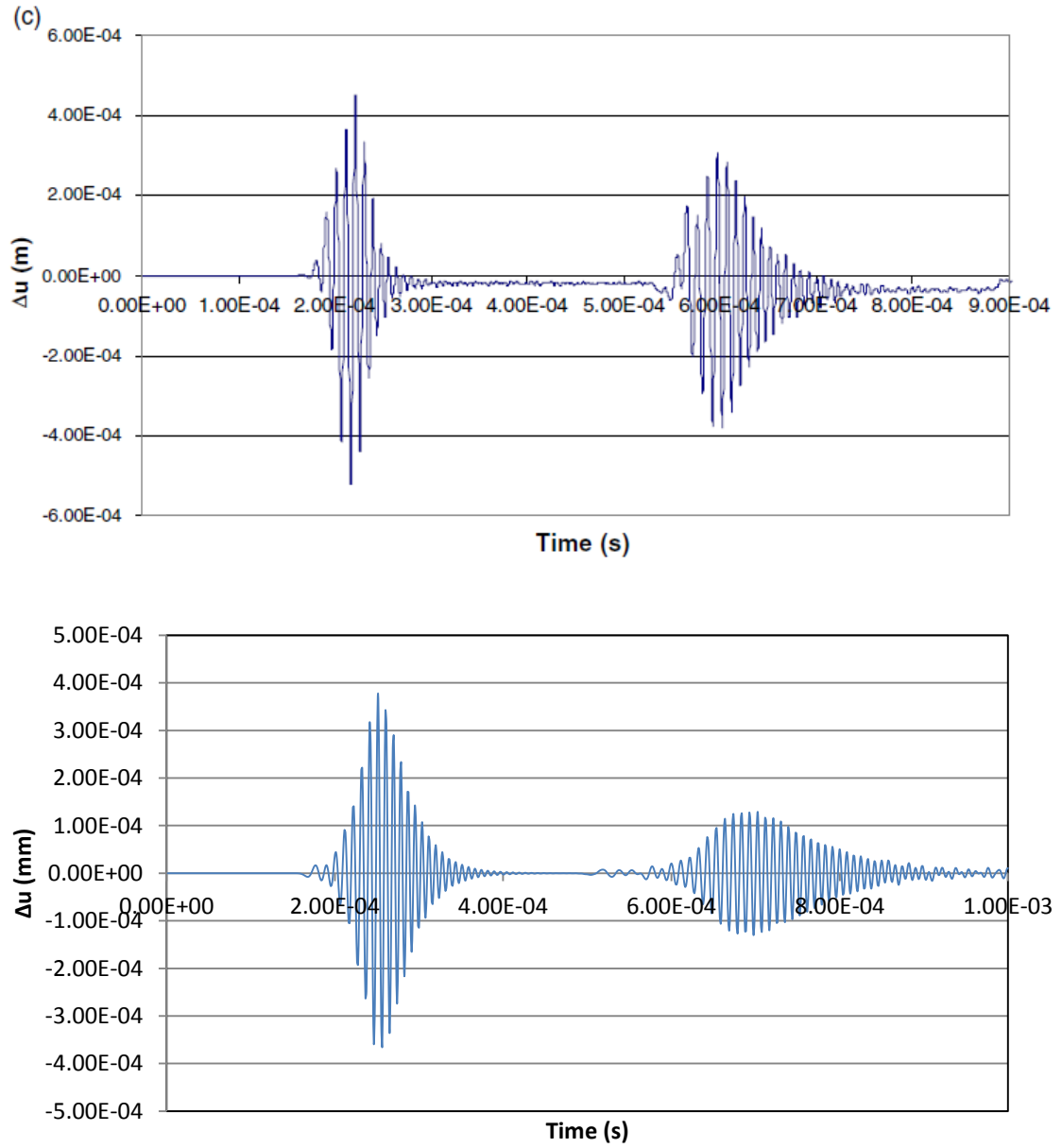


Figure 10. Sensor 3 (top - Yang, bottom - recreation)

The results show the ability to effectively model Lamb wave propagation using the ANSYS software.



### 2.2.2. Wave propagation in a damaged aluminum beam

The objective of this section is to confirm that damage can be correctly modeled using ANSYS software and that reflections due to damage will indeed be shown in the Lamb wave response. Again the example to be used comes from Yang's 2005 paper [21]. The aluminum beam is identical to the beam recreated in Section 2.2.1, except for a missing square section which will represent the damage.

#### ***i) Modeling***

The procedure of the modeling process is similar to Section 2.2.1, steps *i-vii*.

#### ***ii) Simulating Damage***

The damage to the aluminum beam is simulated by removing a section of the beam. Simulations were done with a 7mm x 7mm section removed in the reference. To remove this portion of the beam, one must simply create an area at the desired spot, and use Boolean operators to remove the section.

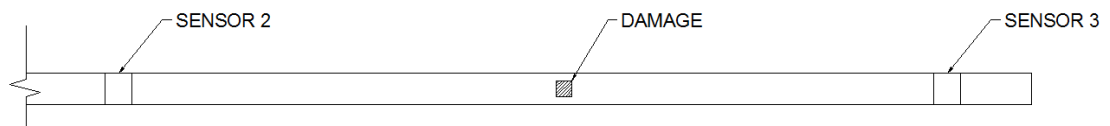


*Figure 11. Damaged aluminum beam*

Due to the damage, meshing may need to be refined in the area near damage. When using SOLID 182 elements, all elements must maintain a quadrilateral shape.

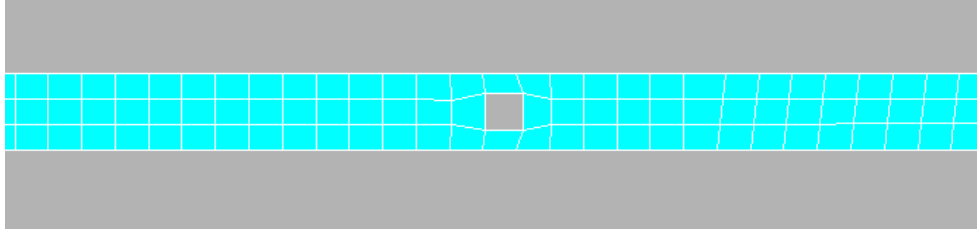


Figure 12. ANSYS model of damaged aluminum beam

### iii) Analysis/Results

The same analysis method was used as described in Section 2.2.1, step *viii*. Results are compared with their undamaged counterparts from Section 2.2.1.

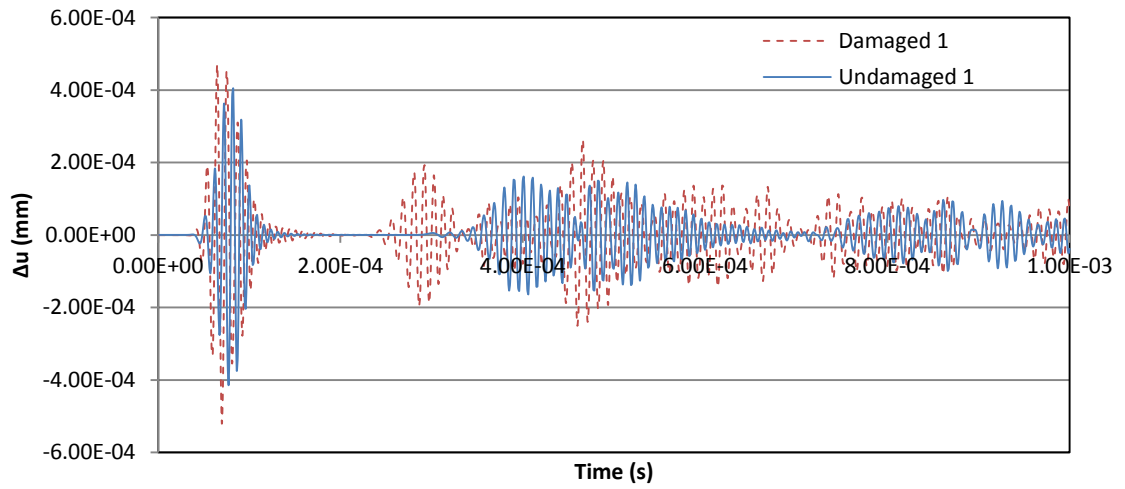
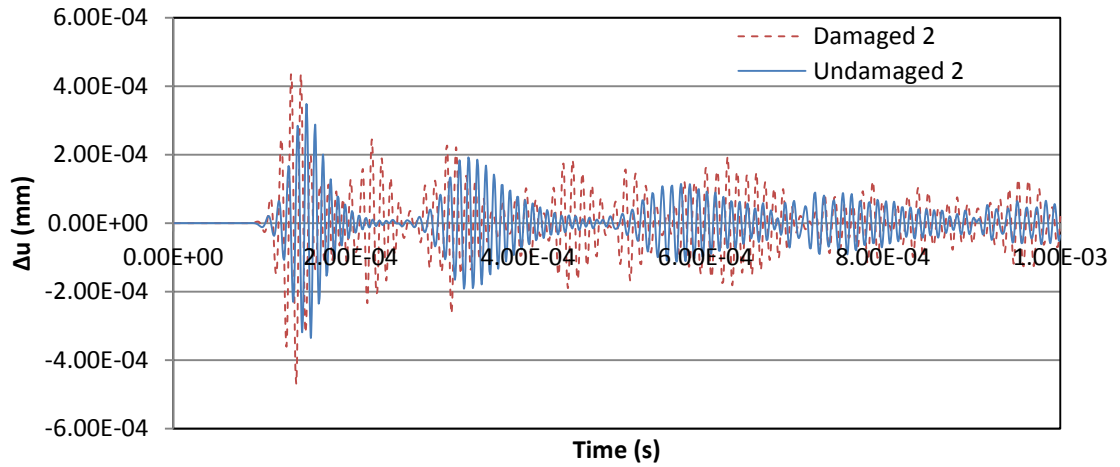
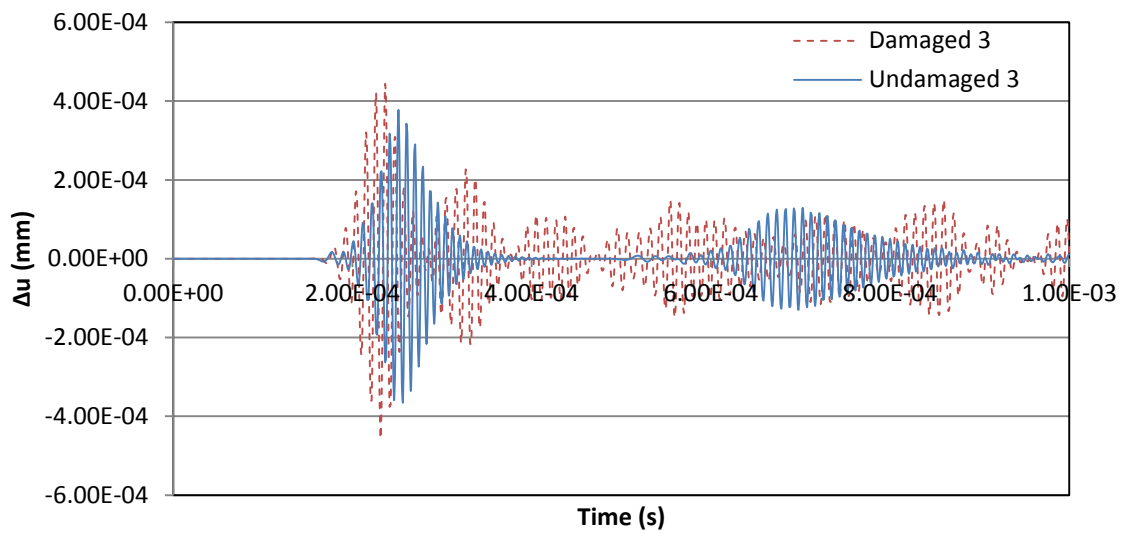


Figure 13. Sensor 1 comparison



*Figure 14. Sensor 2 comparison*



*Figure 15. Sensor 3 comparison*

**iv) Comments**

From the comparisons, it can be seen that the damage did in fact alter the Lamb wave propagation. The results reflect the same behavior exhibited by the experimental data of

damaged aluminum beams in the reference [21]. This confirms that ANSYS is a viable method to model and detect damages using Lamb waves.

The changes may be due to wave reflection from the boundary and the damage. Sometimes, it may be due to wave mode transformation through the damage, or another source. These possibilities will be further discussed and investigated in Chapters 3 and 4.

### **2.3. Summary**

Multiple validations have been conducted in ANSYS software to validate the modeling techniques in wave propagation, wave scattering, composite, and composite delamination modeling. The accuracy of these results confirms the ability to effectively model delamination damage with ANSYS. The principles from this section will be used in Chapter 3 to simulate delamination in more complex composites.

# **CHAPTER 3. DETECTION OF DELAMINATION IN LAMINATED COMPOSITE BEAMS THROUGH COVARIANCE ENERGY CHANGE OF ULTRASONIC WAVES**

## **3.1. Introduction**

Delamination in composite materials is pervasive and difficult to detect as discussed in Ye's paper. In this chapter, composite beams similar to those used in experiments in Chapter 4 will be adopted. The same Lamb wave detection method shown in Chapter 2 is used. As mentioned earlier, detecting delamination damage only through time of flights has proven to be difficult in previous studies. In this chapter a new delamination detection methodology through the covariance energy change of ultrasonic waves will be sought. By using the innovative data reduction method, it was proven that a strong correlation between delamination size and wave response is seen, which can be used to detect delamination locations and delamination sizes.

All beams were modeled with free-free boundary conditions and were modeled with the following properties.

Table 1. Beam properties

$L$	1200 mm	$G_{xy}$	5.2 GPa
$t$	12 mm	$G_{xz}$	5.2 GPa
$w$	Unit width	$G_{yz}$	3.08 GPa
$E_x$	135.3 GPa	$\nu_{xy}$	0.24
$E_y$	135.3 GPa	$\nu_{xz}$	0.24
$E_z$	9.0 GPa	$\nu_{yz}$	0.46
$\rho$	1.600 g/cm <sup>3</sup>		

Where  $L$  = beam length,  $t$  = beam thickness  $w$  = beam width,  $E$  = modulus of elasticity,  $\rho$  = material density,  $G$  = shear modulus, and  $\nu$  = Poisson's ratio.

At the time of modeling, the beams used in experiments were not yet manufactured. The material constants were taken as values for an arbitrary composite with similar composition of that to be used in the lab.

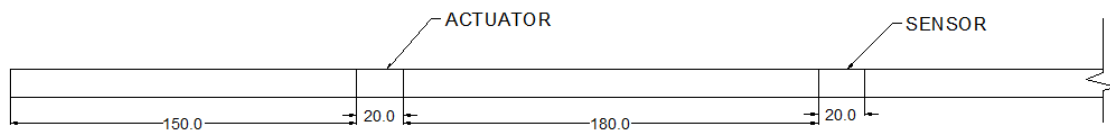


Figure 16. Actuator and sensor locations

Lamb waves were produced and recorded using an actuator and a singular sensor. First, an undamaged beam was analyzed for a benchmark. Next, beams of varying delamination sizes were analyzed and compared with the healthy beam results in order to develop a correlation. This chapter will discuss the data reduction methods used, a parametric study incorporating these methods, and finally the results and conclusions obtained from the study.

### 3.2. Data reduction by fast Fourier transform

Due to issues detecting small changes in a wave response from deflection or strain curves, it is helpful to use a different data reduction method to summarize the results in a better way. The data reduction method used in this thesis is to calculate the frequency bandwidth, the frequency amplitudes, and the covariance energy change through the fast Fourier transform or FFT.

FFT is a variation of the discrete Fourier transform. It is a well-established analysis tool used since the 1965 paper by Tukey and Cooley [24]. For the purposes of this thesis, FFT will be used to transform data of strain over time to frequency domain. This is helpful for this study, as the different wave types can be more easily separated and compared when looking at FFT graph instead of the time-strain graph. To exhibit the behavior of FFT, an example is performed on the input signal used for the modeling.

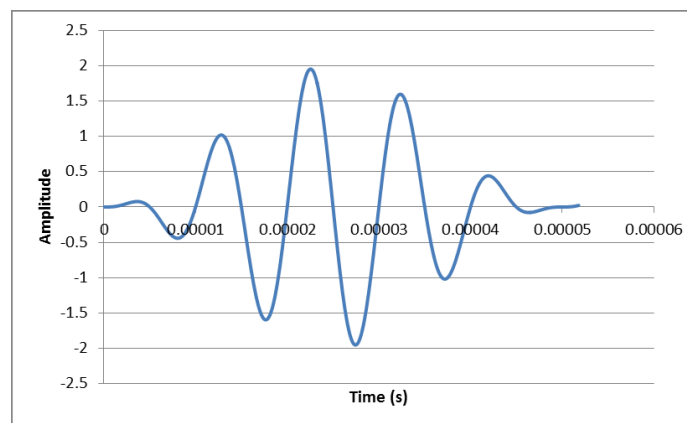


*Figure 17. 100 kHz Hanning window wave*

A five-count Hanning wave is shown graphically over time in Figure 17. Using FFT function from MATLAB the frequencies present in this wave can be extracted. MATLAB is

commercial mathematical software, which will be used in all FFT conversions in this thesis.

Figure 18 shows FFT conversion of the input signal used in modeling.

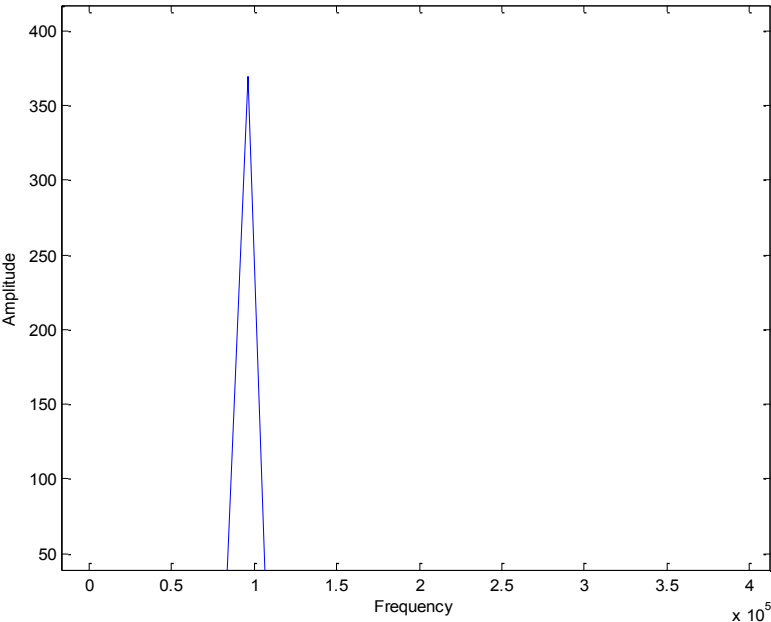


*Figure 18. FFT graph of 100 kHz Hanning wave*

It is seen that after the transform is applied to the wave, a singular peak at 100 kHz shows up. While changes in time domain are easy to detect if and only if one wave is present and the changes are drastic, it becomes much more difficult when dealing with multiple waves and very small changes. This is where FFT becomes a very useful tool. Since delamination damage is very thin, Lamb waves are not reflected as clearly as seen in other damage types, such as the aluminum beam damage seen in Chapter 3. By using FFT, even very small changes to the waves can be extracted and analyzed more easily.



### 3.3. Parametric study of delamination in composite beams

#### 3.3.1. Parameter selection

##### 3.3.1.1. Dimensions

The dimensions of the beam were chosen to closely resemble the beams to be tested in laboratory. The beam length of 1200 mm is the same as the experimental beams, and the thickness of 12 mm was chosen from the example composite given in Chapter 2.

##### 3.3.1.2. Element size

The size of the elements was selected by means of a convergence study. Based on the maximum amplitude in the sensor readings from the undamaged beam, a convergence study was performed to determine a suitable element size.

*Table 2. Element size convergence study*

<b>Element Size (mm)</b>	<b>Max Amplitude</b>
0.75	2.433E-02
1.5	2.433E-02
3	2.439E-02
6	2.476E-02

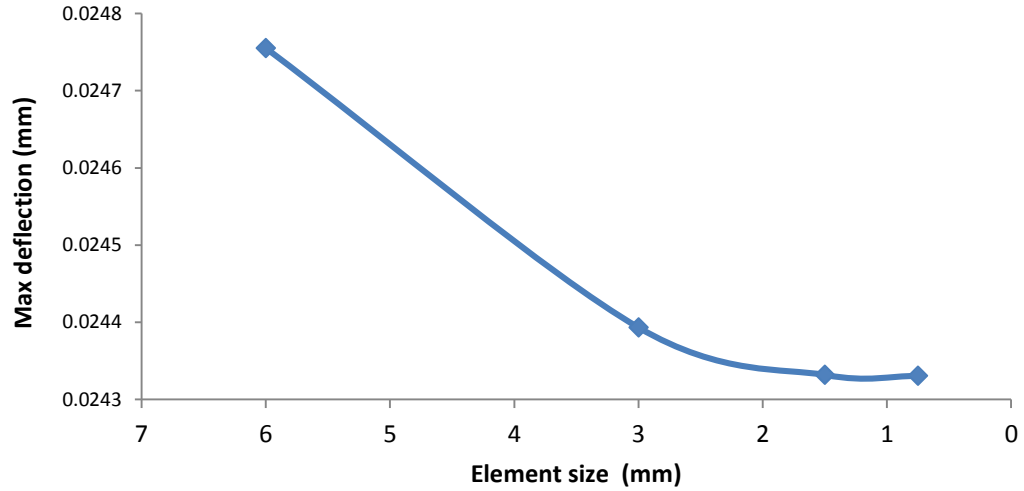


*Figure 19. Element size convergence study*

It was proven that 1.5 mm elements will provide accurate results for the modeling. This was taken as the maximum side length for elements to be used. In the case of damaged models, mesh refinement near the damaged area created smaller element sizes. By using only 1.5 mm elements and smaller it is assured results are sound. However, decreasing element size increases the time of computer simulation. In order to minimize simulation time, elements will be sized as close to 1.5 mm as possible.

### **3.3.1.3. Damage size**

The thickness of the damage was taken from typical resin layer thickness. As expected, resin layer thickness depends on the manufacturer and material type. A range of 0.10-0.50 mm can be considered typical [26]. It was chosen to use 0.25 mm thickness for most models in the parametric study. Further discussion on this selection can be found later in the chapter.

### 3.3.2. Lamb wave response in undamaged composite beams

The modeling process very closely follows the same steps discussed in Section 2.2. Material properties and element types have been modified but the overall process follows the same steps. The element types used in the composite modeling are PLANE182, CONTA175 and TARGE169. The PLANE182 element is used for the orthotropic material. The CONTA175 and TARGE169 elements are used to define the delamination surfaces.

The contact elements prevent overlap of material during vibration. Instead of overlapping, if the surfaces come in contact they are subjected to normal and tangential loads similar to those that would be observed in real applications. The CONTA175 element is applied to a point, in this case to all the points along one side of the delamination. The TARGE169 element is used to create a 2-D surface on the other side of the delamination.

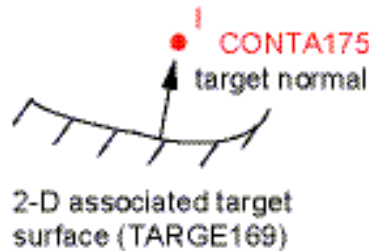


*Figure 20. CONTA175 and TARGE169 elements*

When the CONTA175 element comes in contact with the target surface, forces are generated to simulate contact. To prevent penetration, FTOLN, is set to zero in ANSYS and the default stiffness values are used. The default values are dependent on material properties, element size and degrees of freedom in the model. Stiffness values are updated automatically throughout the simulation using KEYOPT(10) = 2. The stiffness changes are based on the mean

stress of the underlying elements and the previously defined allowable penetration. With these properties, the model will more accurately simulate real applications. First an undamaged beam was modeled for benchmark values. The properties of the beam can be found in section 3.1. The beam was modeled using a 2D side view prospective, with length in the X-axis and thickness in the Y-axis. This orientation was used to ensure a “through the thickness” analysis. By orienting the thickness in the Y-axis, damage was able to be placed inside the beam, simulating non-visible delamination damage.

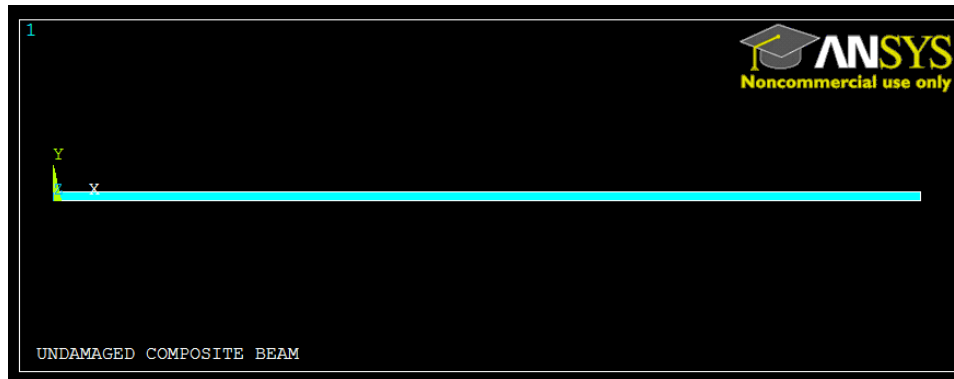


Figure 21. Undamaged composite beam

Loading was applied to the beam at the actuator location in the form of a 100 kHz Hanning window flexural wave. The load was applied via four nodes, two at the top and two at the bottom of the beam. The five count Hanning wave was applied using the function

$$F(t) = \begin{cases} A * \left(1 - \frac{\cos(2\pi ft)}{5}\right) * \sin(2\pi ft), & 0 \leq t < 0.00005 \\ 0, & 0.00005 \leq t \end{cases} \quad (6)$$

Where  $A = 1000 \text{ N}$ ,  $f = 100 \text{ kHz}$ ,  $t = \text{time}$  and  $F(t) = \text{loading force history}$ .

The loads on the top two nodes were applied as compression while the bottom two nodes were loaded in tension initially, and alternate direction after each cycle. This accurately simulates actuators applied to the top and bottom of the beam.

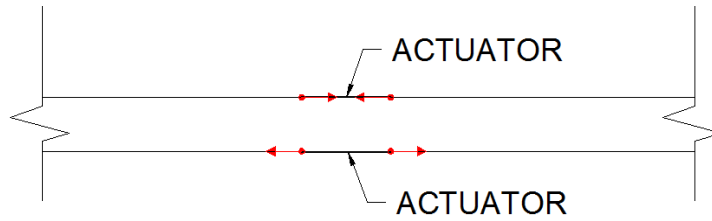


*Figure 22. Actuator loading nodes*

After the load is applied, results were obtained at the sensor. The data collected was the difference of displacement in the x direction between two nodes. The nodes used are at the top of the beam to simulate the surface the sensor will be applied to in experiments.

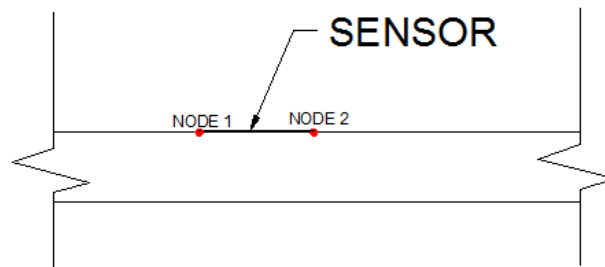


*Figure 23. Sensor nodes*

The results from the undamaged beam will provide the benchmark against which damaged results can be compared.

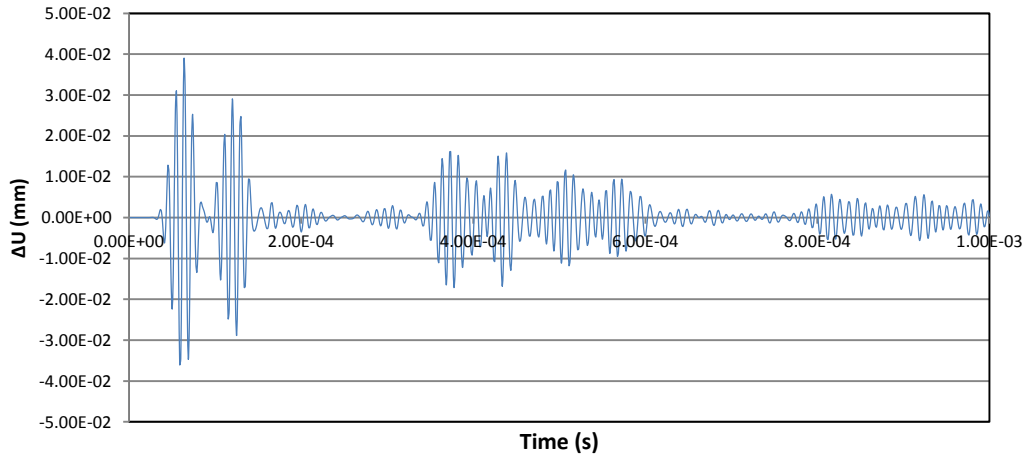


*Figure 24. Strain-time history of undamaged composite beam*

### 3.3.3. Lamb wave response in the damaged composite beam

To simulate delamination damage in the composite beams, small sections of the beam were removed. The section removed represents the damaged interface bond in the composite material. The thickness of the section removed was based upon the typical thickness of the resin layer of composite laminates.

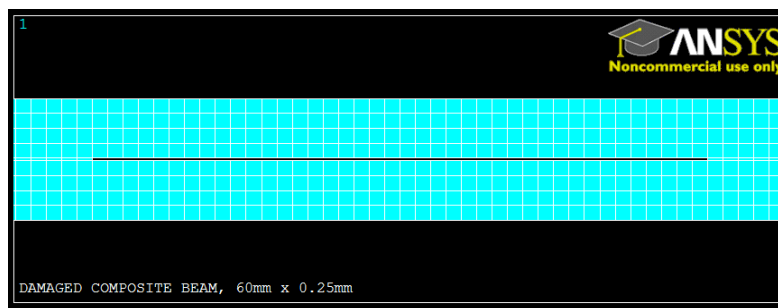


*Figure 25. Typical damaged composite beam*

### 3.3.4. Sensor responses of ultrasonic waves in the damaged composite beam

Results from the damaged beam simulated are summarized and shown in Figures 26-29.

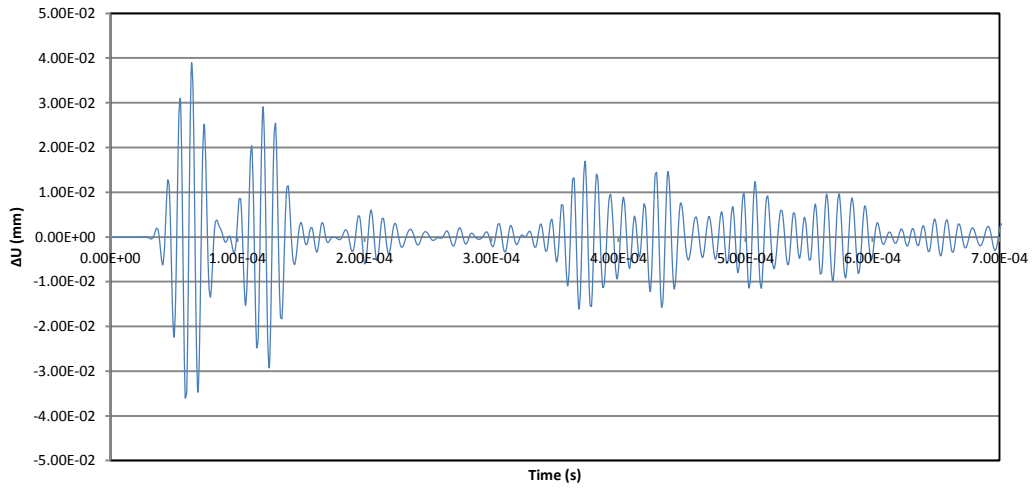


Figure 26. Strain-time history of damaged composite beam, 15mm x 0.25mm

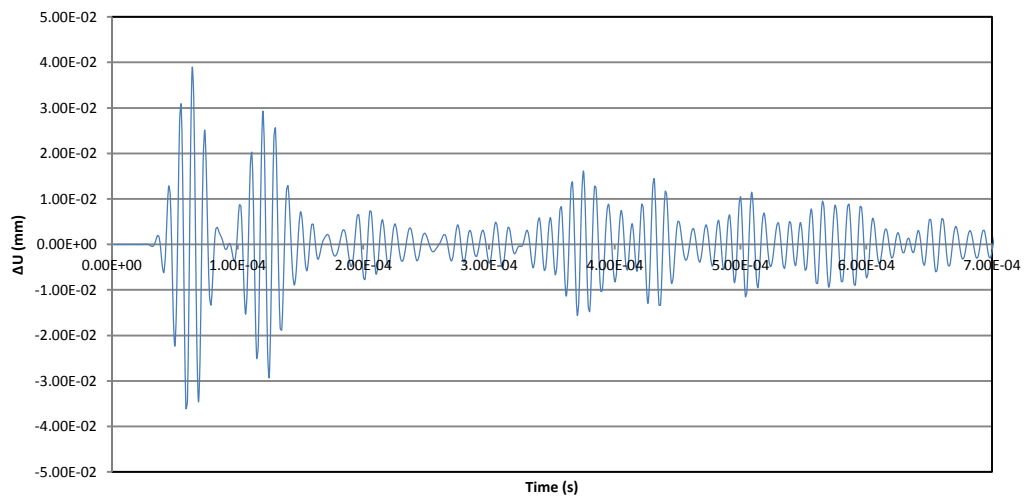
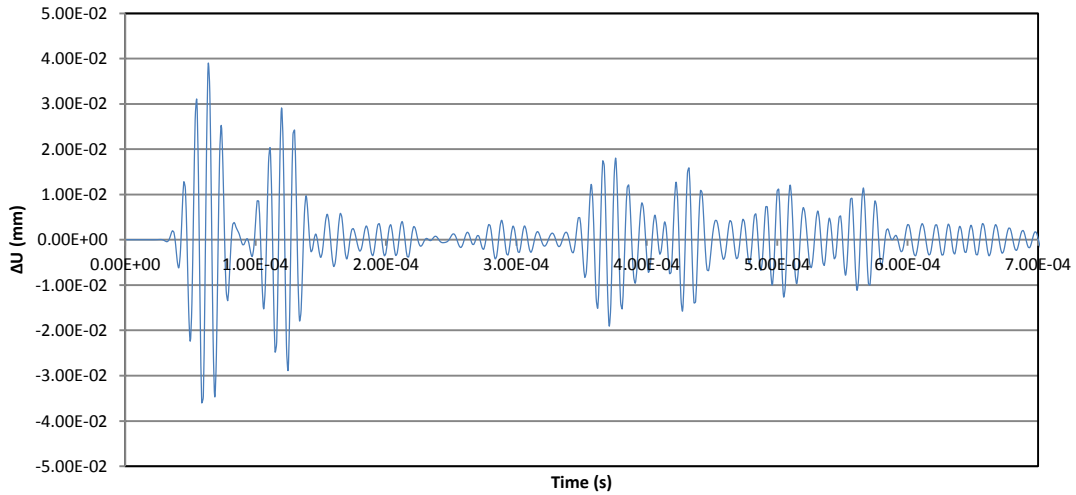
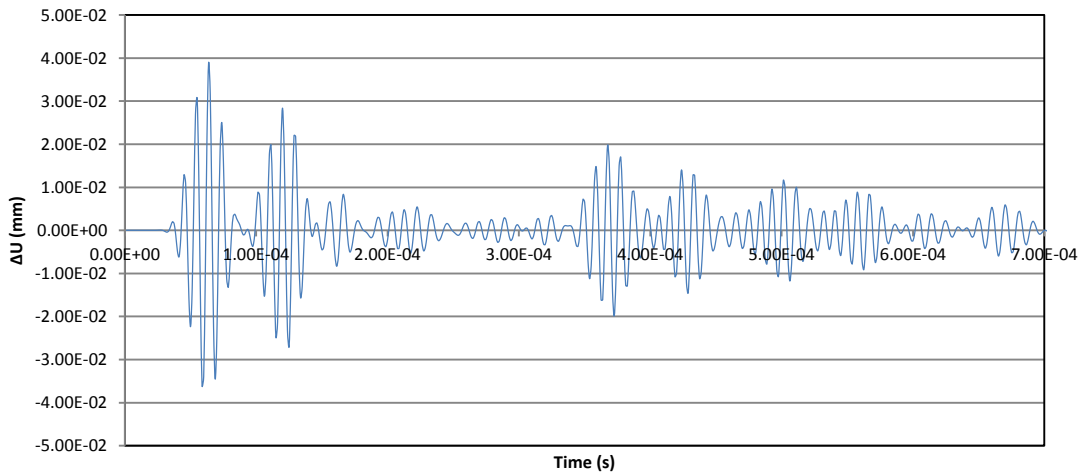


Figure 27. Strain-time history of damaged composite beam, 40mm x 0.25mm



*Figure 28. Strain-time history of damaged composite beam, 60mm x 0.25mm*



*Figure 29. Strain-time history of damaged composite beam, 80mm x 0.25mm*

It is difficult to see the difference in the responses at varying levels of damage from these graphs alone. Even when the graphs are superimposed it is very difficult to determine the change between them.



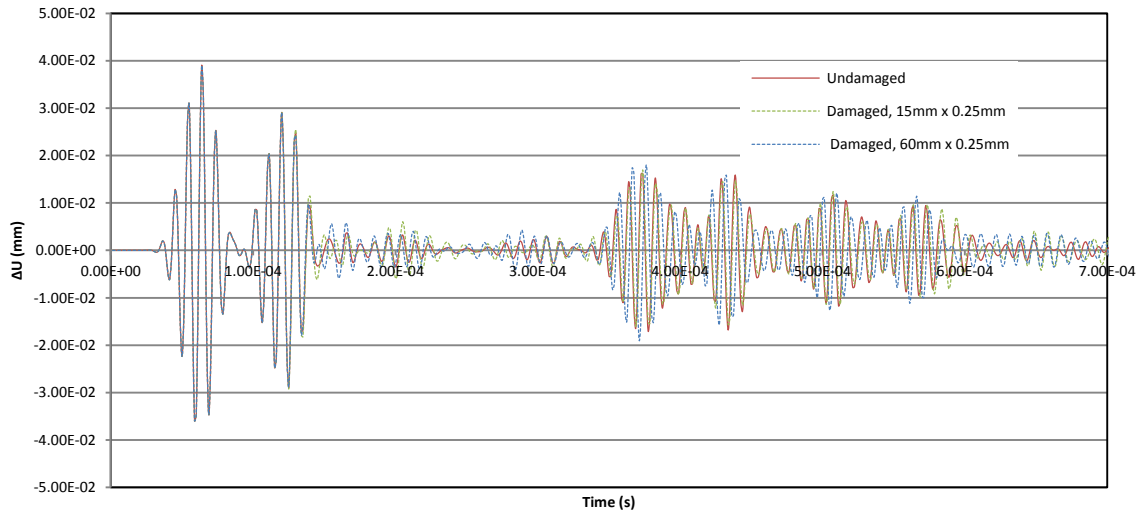


*Figure 30. Strain-time history comparison*

It is apparent that further data reduction methods are needed. While some changes in the time domain responses can be seen, determining the level of damage from these graphs alone is near impossible. This is where FFT will help clarify the results.

### 3.3.5. Data reduction by FFT

In order to make the results from the previous section easier to analyze, FFT is applied. The goal of the data reduction is to develop a method for relating damage to parameters obtained from FFT.

#### i) Wave Package Selection

A question that arises is which portion of the response should be used to calculate the potential index and relate them to damage. To answer this question, several packages were analyzed. First, two sections showing distinct differences in the time domain graphs were analyzed. In some cases, such differences may not be as apparent and another method must be

used. To account for this, a relationship between time of flight and the wave section was developed. The propagation of the incident wave will follow several paths to reach the sensors. The diagram below show the fastest possible wave paths to the sensor.

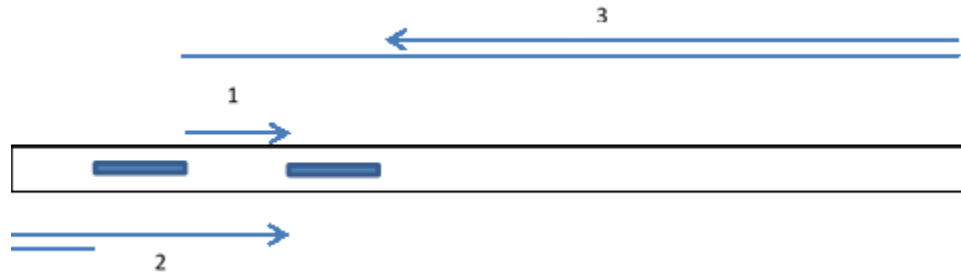
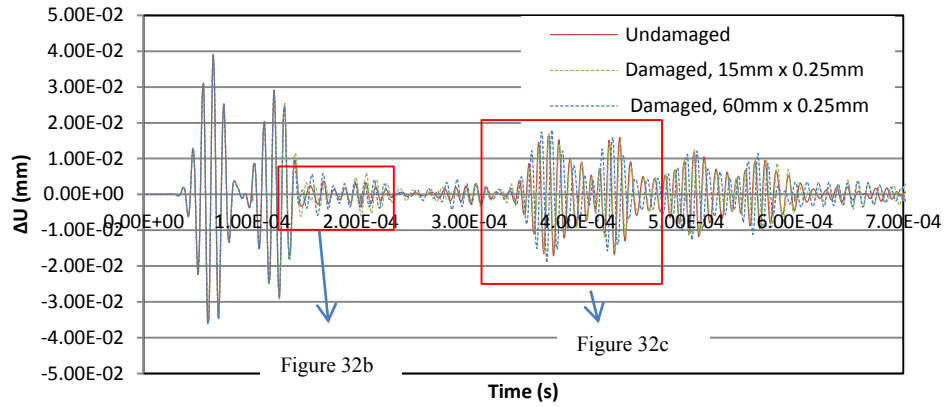


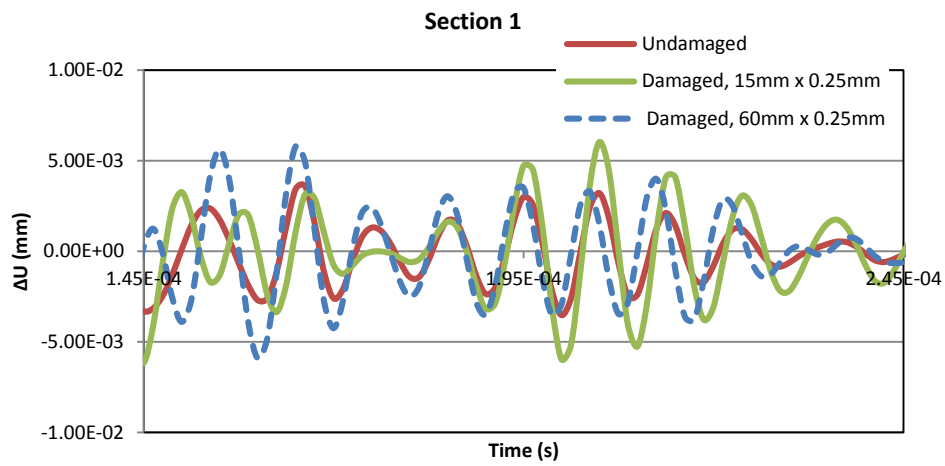
*Figure 31. Wave propagation paths*

We are most interested in these three paths, as any further interaction with the boundary will further dissipate the waves. Using the distance of the wave paths and approximate speed based on the time between responses 1 and 2, an approximate window was developed to capture all wave paths shown in Figure 31. A convergence study on this window was performed and is included later in the chapter.

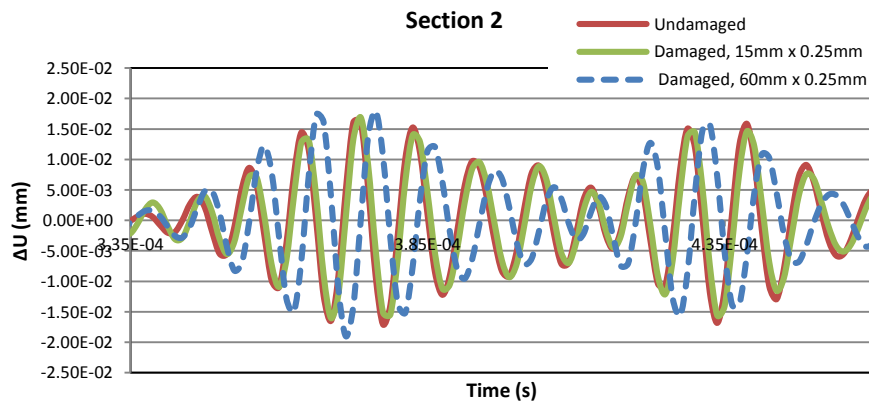
By using both methods of window selection for data reduction, a better understanding of the data reduction will be developed. This section will incorporate results and discussion on all three sections chosen. For clarity, the sections picked based on time domain differences are labeled Section 1 and 2, while the section based on time of flight is labeled Full Section. Discussion on the methods used and results for Sections 1 and 2 will first be given, followed by the results of the full section.



(a)



(b)



(c)

Figure 32. Wave package separation (a) full response (b) Section 1 (c) Section 2

These sections were selected because of the apparent differences in response based on damage size. The wave types in these sections may not be able to be identified individually, but by keeping the analysis region the same throughout, changes to the total wave package can be recorded. FFT data for each delamination size was obtained through MATLAB. One such FFT plot is shown below.

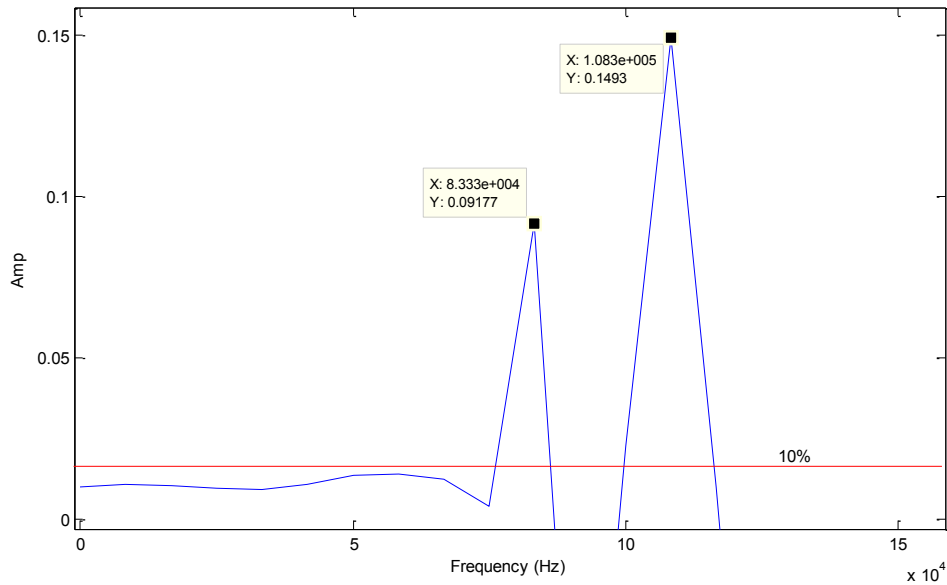


*Figure 33. FFT graph of Section 2 of the beam with a 40 mm x 0.25 mm defect*

The major wave frequencies were defined as peaks above 10% of the maximum amplitude, shown by the red line in Figure 33. This cutoff mark ensured separation of the noise from the key frequencies. In addition, the energy of a wave is related to the amplitude squared. At 10% amplitude, the energy level would only be 1% of the largest peak, making it insignificant. For all sections, the frequencies and corresponding amplitudes were recorded. In the sections where frequencies present in the undamaged beam were not found, a “0” was used as a placeholder.

Table 3. Section 1 frequencies and amplitudes

Frequency (kHz)					
Beam	F1	F2	F3	F4	F5
Undamaged	74	84	94	126	158
15mm	75	0	96	128	160
40mm	75	0	107	128	0
60mm	0	85	0	128	160
80mm	75	0	0	128	0
Amplitude					
Beam	A1	A2	A3	A4	A5
Undamaged	0.025	0.029	0.042	0.025	0.01
15mm	0.027	0	0.056	0.028	0.013
40mm	0.01436	0	0.1115	0.0276	0
60mm	0	0.041	0	0.026	0.009
80mm	0.069	0	0	0.007	0

Table 4. Section 2 frequencies and amplitudes

Beam	Frequency (kHz)			Amplitude		
	F1	F2	F3	A1	A2	A3
Undamaged	85	111	125	0.13	0.236	0.16
15mm	83	108	0	0.0609	0.38	0
40mm	83	108	0	0.092	0.149	0
60mm	0	100	0	0	0.142	0
80mm	0	92	0	0	0.269	0

This data allows for some understanding of wave behavior with increasing damage. For example, it is easy to see that in section 2 as damage increases, frequencies are either completely removed from the wave or lessened. The loss of a wave frequency may be due to wave transformation due to damage or dissipation to the point of insignificance.

Using this data, information about the energy of the wave can be obtained. The general equation for power transmitted by a wave is given as

$$E = \frac{1}{2} \mu \omega^2 A^2 v. \quad (7)$$

Where,  $\mu$  = material density,  $\omega$  = angular frequency,  $A$  = Amplitude,  $v$  = wave speed.

Density remains constant for all beams. Since the calculation time period is held constant for all tests, the wave velocity can also be assumed constant for all cases. This leaves energy as a function dependent on the squares of frequency and amplitude.

From here, the data obtained from FFT graphs can be used to compare the squares of the differences in both frequency and amplitude. Using the equations  $\sum_i^n (F_i - F_{oi})^2$  and  $\sum_i^n (A_i - A_{oi})^2$ , where  $A_o$  and  $F_o$  represent the undamaged amplitude and frequency, and  $A_i$  and  $F_i$  represent the damaged amplitude and frequency, the relationships with the damage characteristics can be studied.

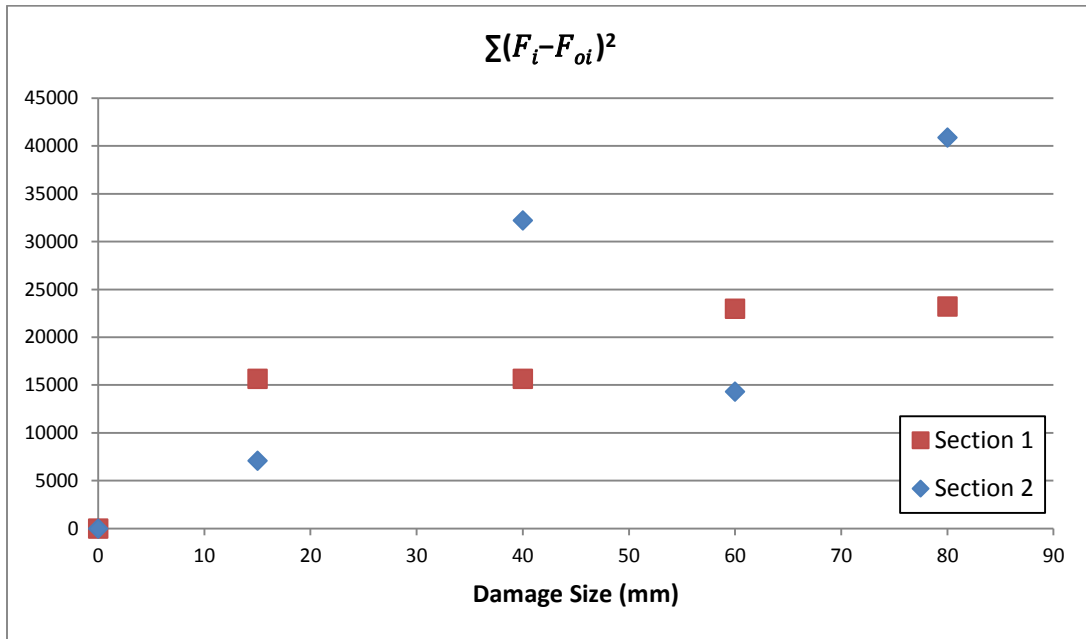


Figure 34. Sum of the square of the difference of the frequencies present

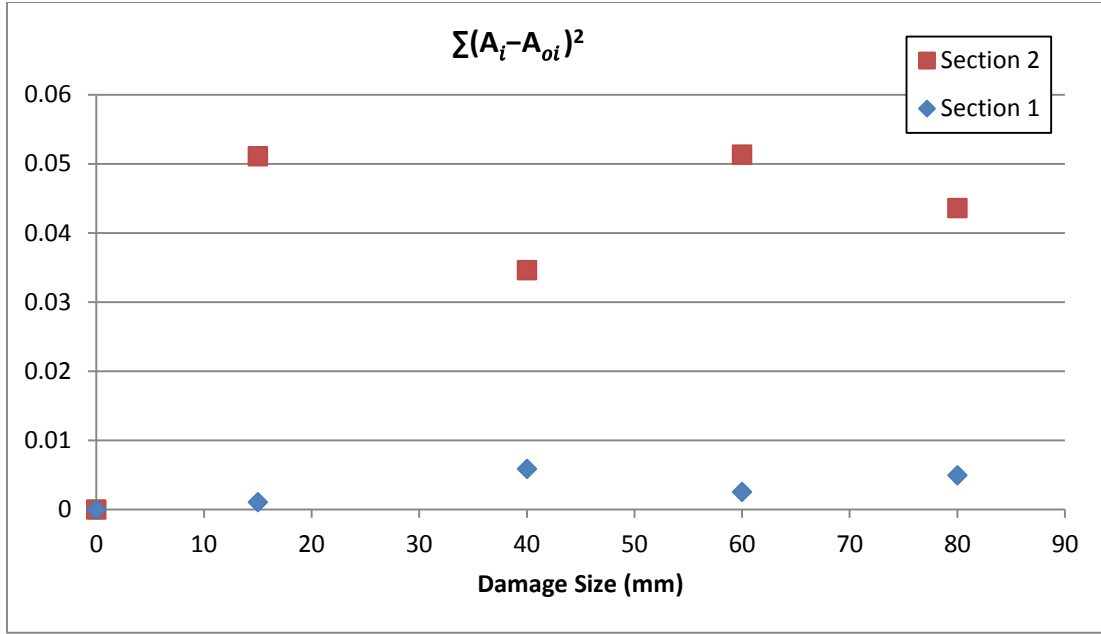


Figure 35. Sum of the square of the difference in present amplitudes present

Some small relations may be able to be formed from these graphs; however they are still not conclusive in showing a definite trend. The changes to one variable alone cannot be used to indicate damage. Instead, how both variables change simultaneously may be more indicative. Using the data, a covariance study of the energy can be calculated. Covariance is a measure of how two variables change together, in our case frequency and amplitude. When both amplitude and frequency of a wave is changed there is large indication of damage. By finding the covariance, an index relating the damage to the covariance of energy change can be formed. The following equation was used to find the covariance of energy change.

$$\Sigma[(F_i - F_{oi})^2 * (A_i - A_{oi})^2] \quad (8)$$

Using this equation, the following results were obtained.

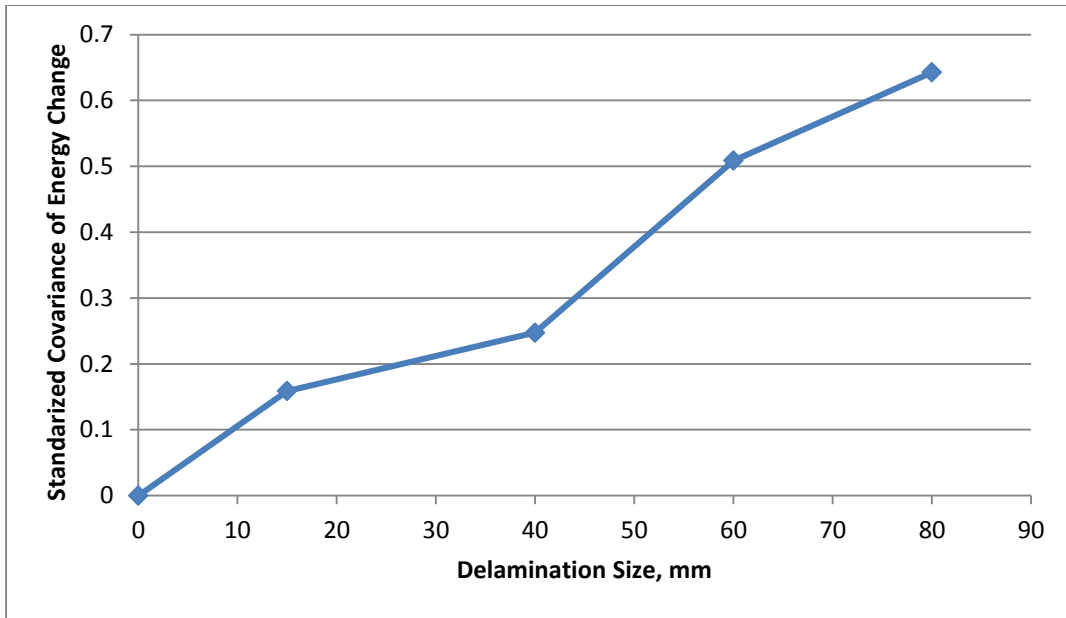


Figure 36. Covariance of energy change at Section 1

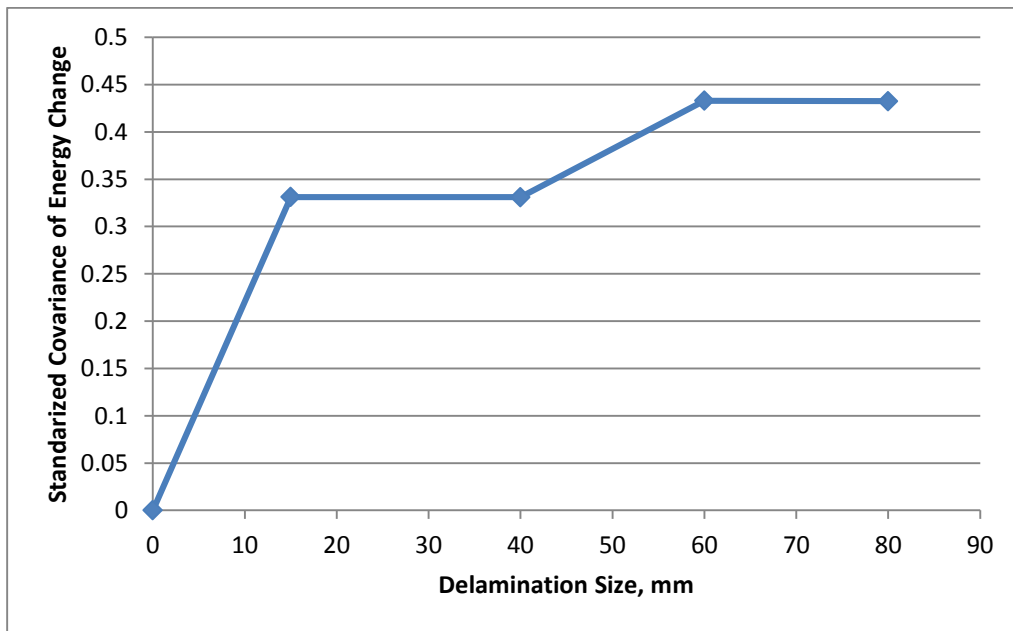
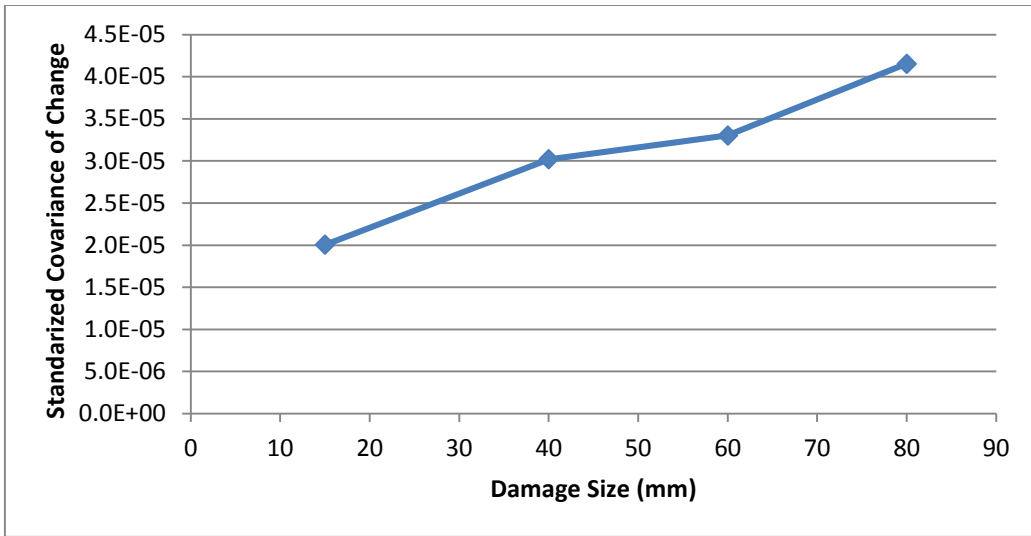


Figure 37. Covariance of energy change at Section 2





*Figure 38. Covariance of energy change for full section*

The graphs show a trend of increasing change of energy with increasing delamination size. It is important to note here that the values are not exactly the change in energy but rather a proportional value that indicates change of energy.

From here, an index was created relating covariance of energy change to damage size. As a baseline, the energy present in the undamaged beam was calculated from the equation  $\sum_i^n (F_{oi}^2 * A_{oi}^2)$ . Using this value the ratio of total energy change to that of the undamaged beam can be calculated.

*Table 5. Covariance of energy change*

Section 1	
Damage size (mm)	Covariance of energy change
15	0.1588
40	0.2475
60	0.5088
80	0.6429
Section 2	
Damage size (mm)	Covariance of energy change
15	0.3312
40	0.3311
60	0.4330
80	0.4324
Full Section	
Damage size (mm)	Covariance of energy change
15	2.005E-05
40	3.020E-05
60	3.302E-05
80	4.154E-05

From Table 8 the damage sizes can be divided into two groups for Sections 1 and 2; small damage, roughly 1-3% total length and large damage, 5-7% total length. The corresponding ranges of covariance of energy changes are 15-35% and 40-65%.

By using the full section, it is seen that the total energy change is also increasing with damage size, but at a much smaller scale than in either of the individual wave packages.

### 3.3.6. Varying delamination thickness

As mentioned earlier, literature suggested 0.1-0.5 mm thickness is a typical range of resin layer [26]. Simulations at 0.1, 0.25 and 0.5 mm were performed, with a delamination length of 60 mm.

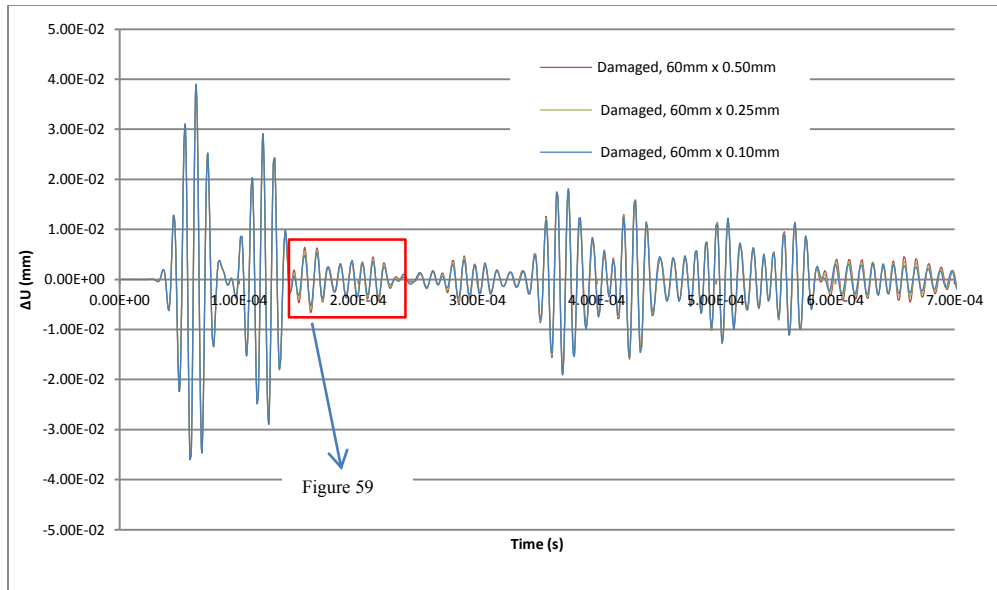


Figure 39. Comparison of wave responses of different delamination thicknesses

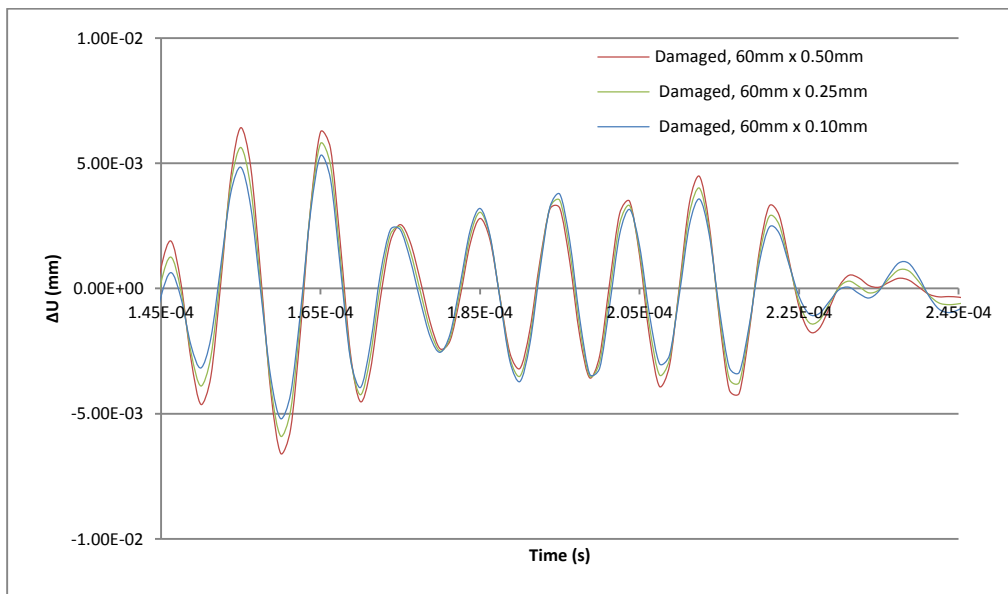


Figure 40. Zoomed in region of wave responses

It is seen that the thickness of delamination at these sizes does not greatly influence the responses in the time domain. Data reduction by means of FFT helps clarify the results. Using the same method shown in section 3.2.5, the effect of delamination thickness can be further

examined. The same two wave packages were analyzed and the change of covariance of the energy was found for each model.

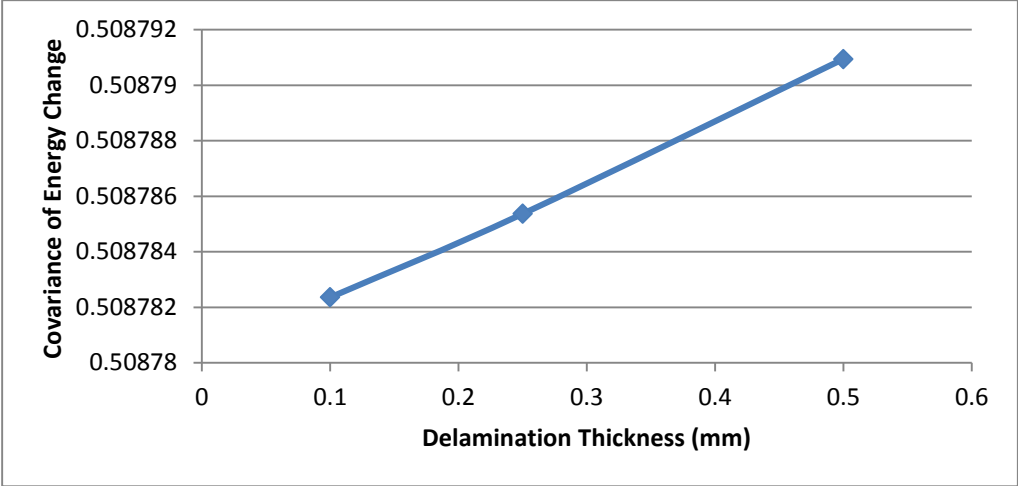


Figure 41. Covariance of energy change with varying delamination thickness size at section 1

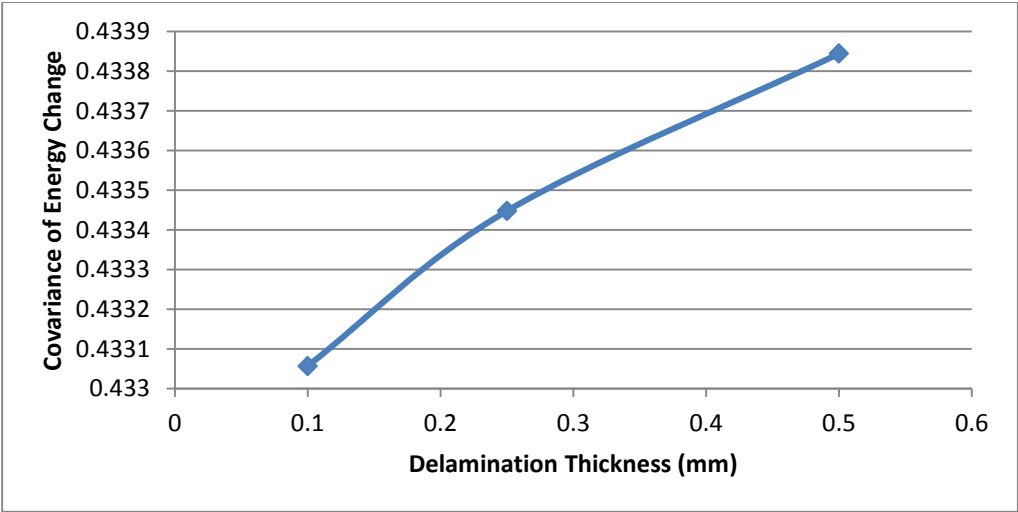


Figure 42. Covariance of energy change with varying delamination thickness size at section 2

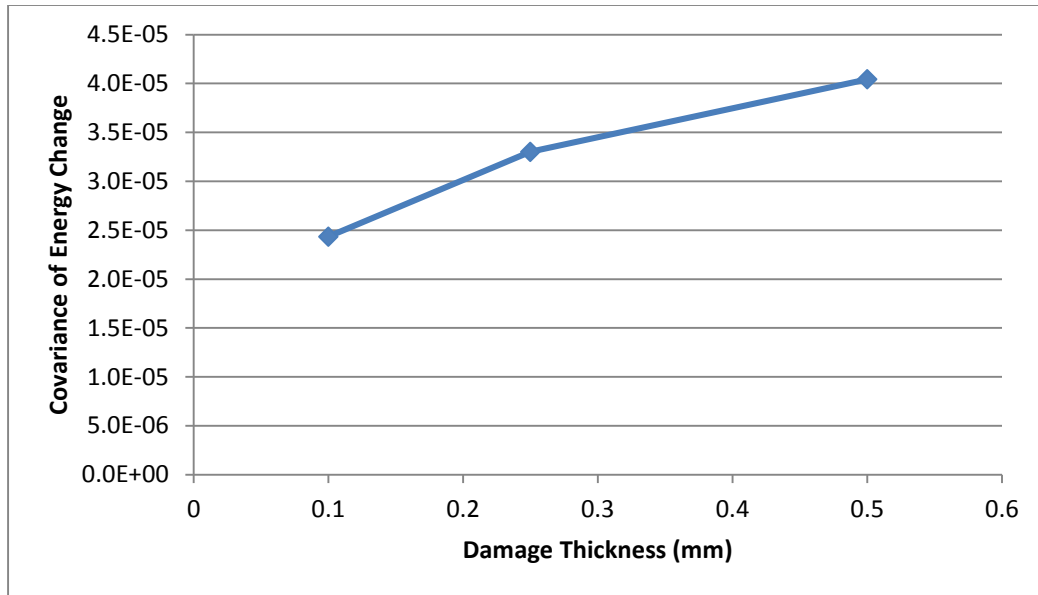


Figure 43. Covariance of energy change with varying delamination thickness size for full section

The effect of varying delamination thickness is now much more apparent. The graphs show what is to be expected, no matter if the wave package is reflected by the damaged or transformed. A larger damage would reflect more of the incident wave and reduce the energy of waves traveling through it. While the changes at this scale are quite small, the trend is apparent and gives validity to the data reduction method.

### 3.3.7. Varying delamination location

Detecting the location of the damage is also an important aspect of structural health monitoring of composites. Models with delamination damage at varying locations and depths of the beams were tested. First let us look at varying  $x$ -coordinates of the delamination with the depth held constant. Beams with damage centered at  $x = 500$  mm,  $600$  mm,  $700$  mm were modeled. Since horizontal location is based on time of flight, only the time domain was used. For consistency, the same two wave packages used throughout this chapter were observed.

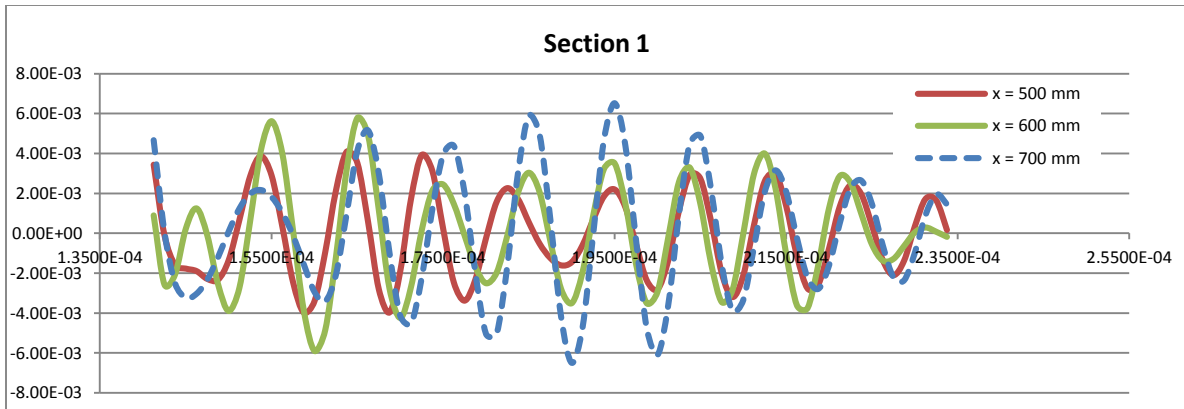


Figure 44. Time domain response at section 1 with varying damage locations

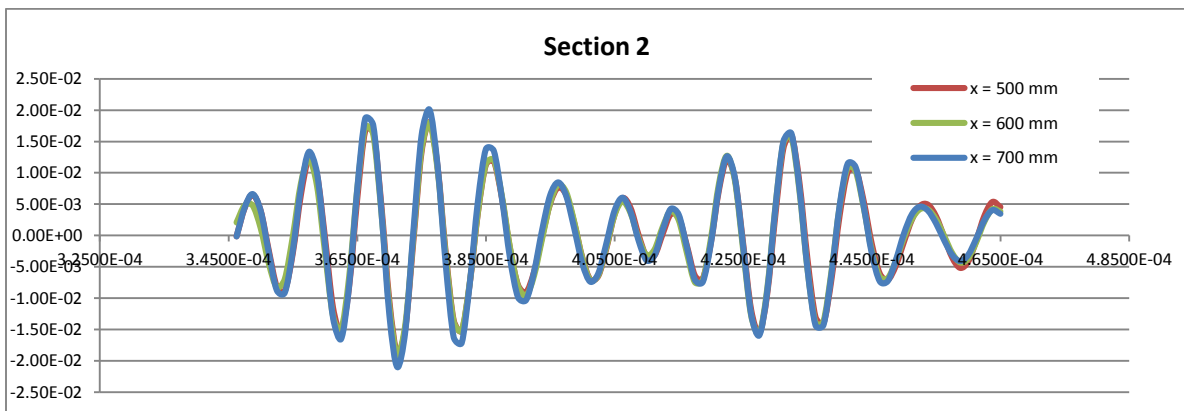
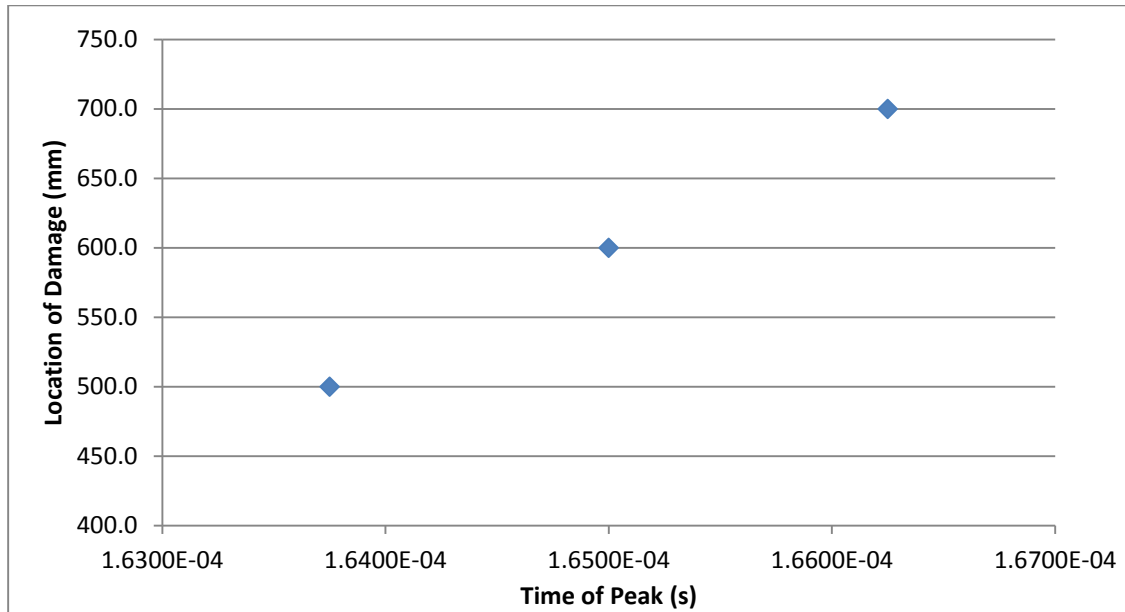


Figure 45. Time domain response at section 2 with varying damage locations

From the time of flight of arrival of package one, it can be assumed this wave is reflected from the damage. The wave occurs after the incident wave and the wave from the left boundary, but too soon to be a reflection from the right boundary. It is not possible to distinguish wave types within the package 2, so exact location cannot be found. It is possible to compare the time of flight within section 1 to gather evidence to support the assumption this wave package is reflected. By simply comparing the time of arrival of the peak in the first wave this can be tested.

Table 6. Damage locations and time of flight

Location of Damage (mm)	Time of Peak (s)
500.0	1.6375E-04
600.0	1.6500E-04
700.0	1.6625E-04



*Figure 46. Arrival time of peak with varying damage locations*

The results are consistent with that of a wave being reflected by the damage. With the time of flight of peak arrival, the wave speed can be calculated.

Next the depth of the delamination damage was examined. The variation of depth will simulate delamination between different layers of the composite laminates. Beams with damage at depths  $y = 3$  mm, 4.5 mm, 6 mm, 7.5 mm, 9 mm. For this section the horizontal damage location and delamination thickness were held constant, at 600 mm and 0.25 mm respectively. The depths correspond to the interfaces of 1.5 mm thick layers within the composite. Looking at the time domain responses at the two previously used sections, some variation is seen.

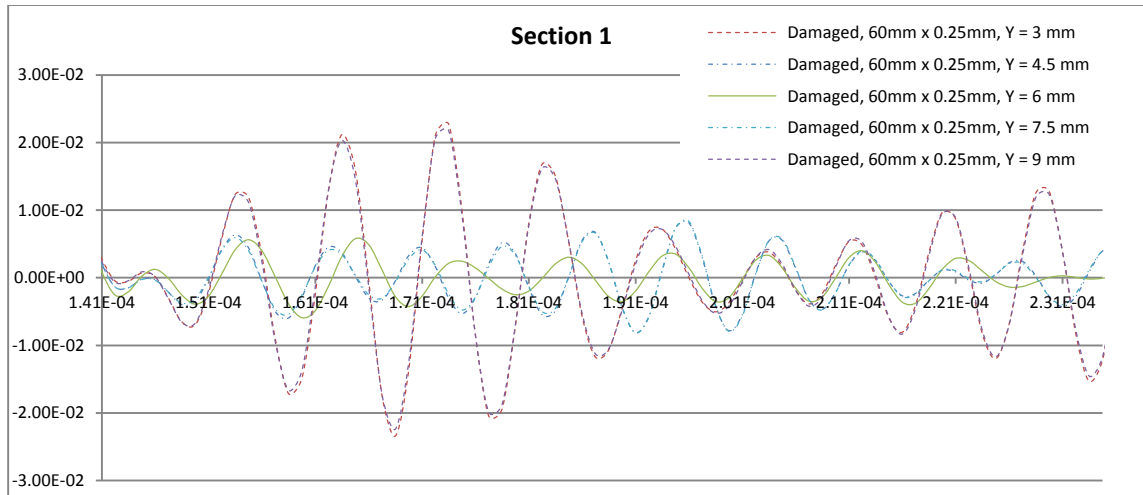


Figure 47. Time domain response at section 1 with varying damage depth

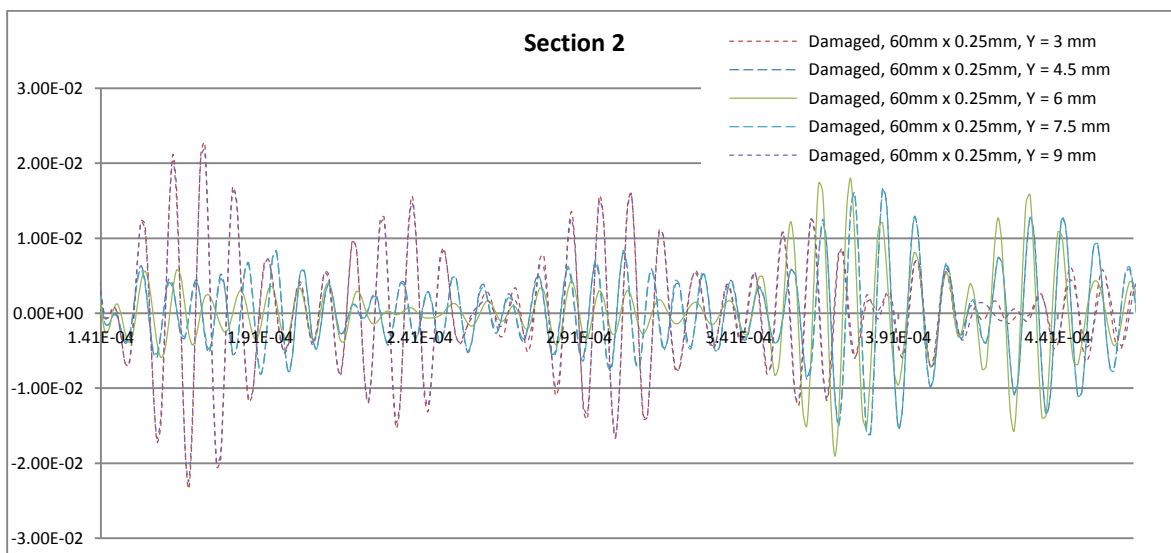


Figure 48. Time domain response at section 2 with varying damage depth

The variation in response shows more movement in damage closer to the edge of the beam. This makes sense since the closer to the center of the beam the damage is, the more it is constrained by the material surrounding it. In addition, the moment of inertia is more affected by removing a section away from the centroid. This reduction of  $I$  reduces the stiffness of the material, further explaining the larger displacements from such damage. Also the response looks



to be near symmetrical about the center of the beam. To further understand the behavior, FFT data reduction method is again used. The change of covariance of energy shows the relationships more clearly.

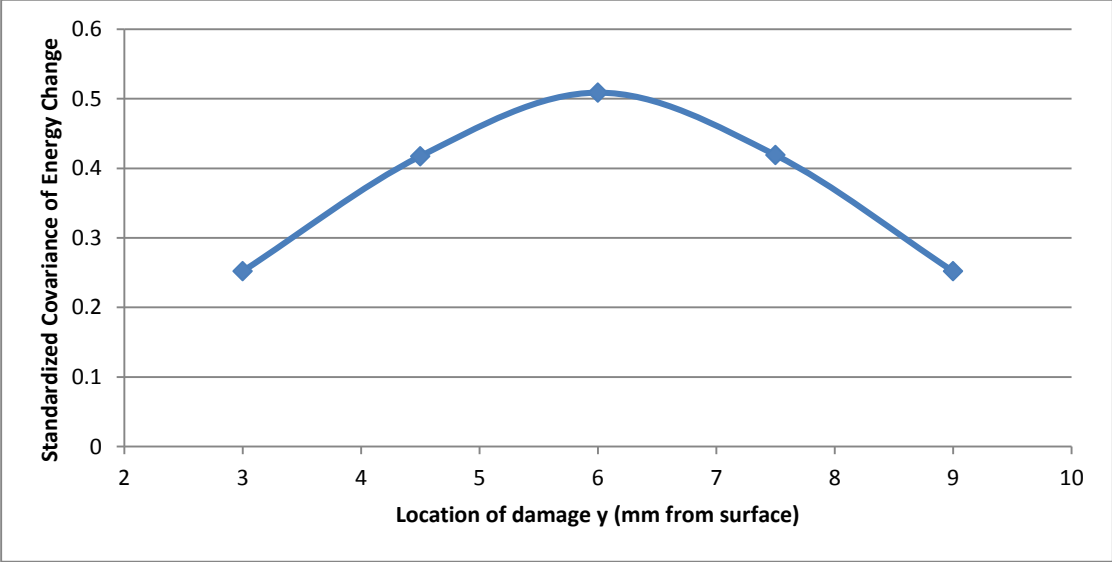


Figure 49. Covariance of energy change at section 1 with varying damage depth

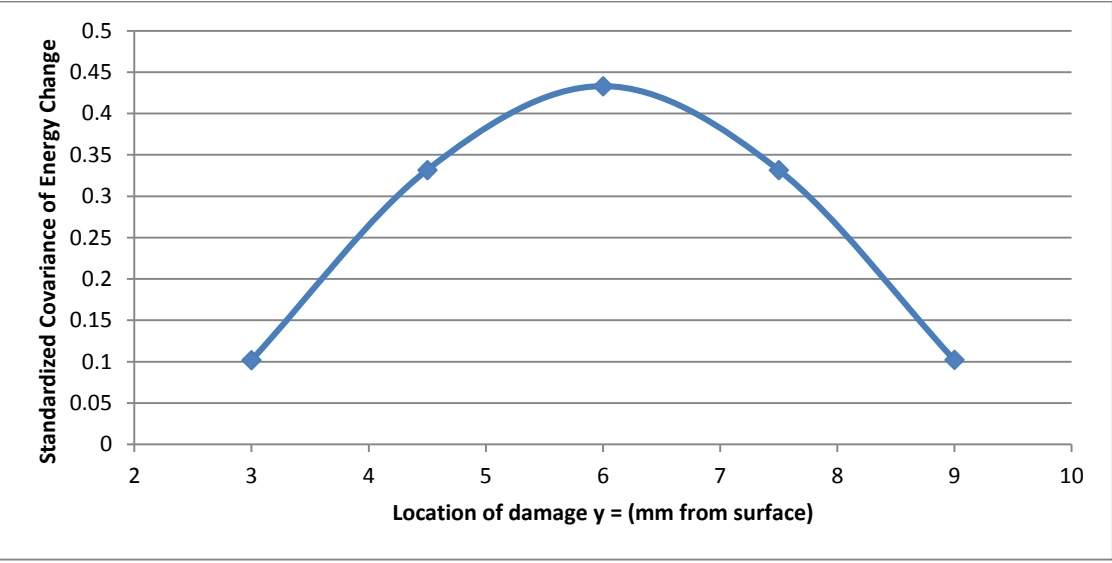
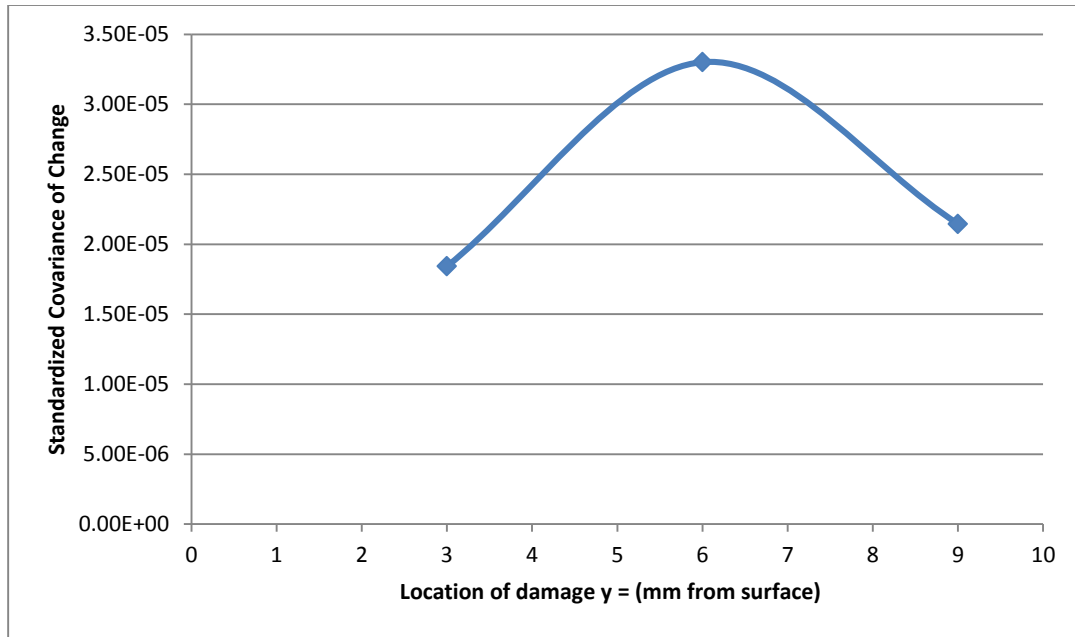
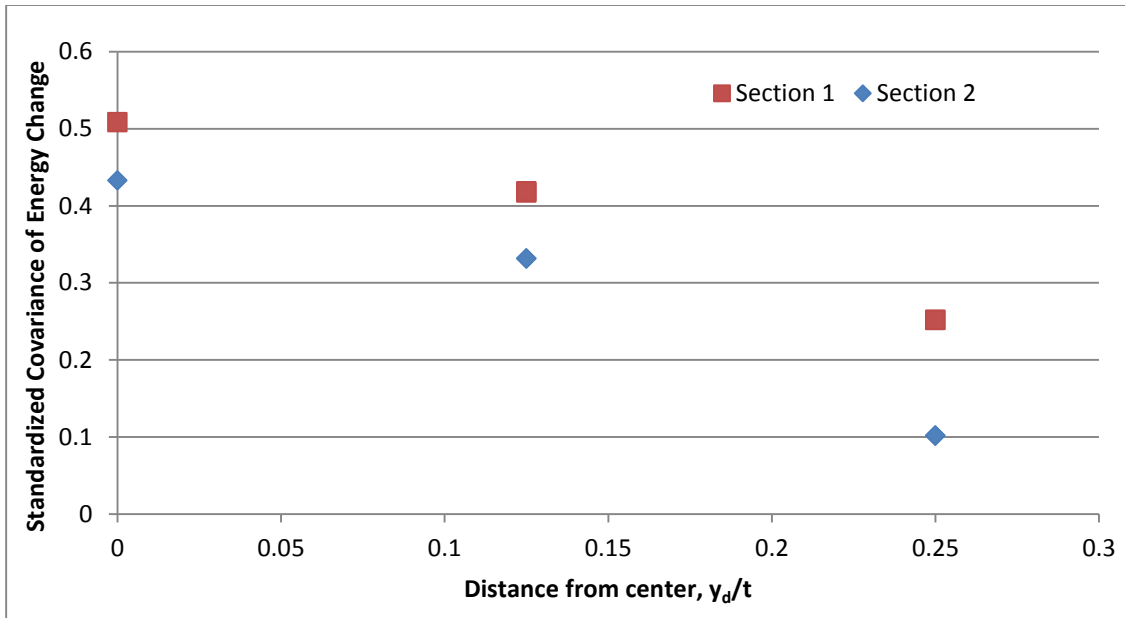


Figure 50. Covariance of energy change at section 2 with varying damage depth



*Figure 51. Covariance of energy change for full section with varying damage depth*

The figures above show a higher change of covariance of energy with damage near the center of the beam. This too can be explained by the amount of material confining the damage. When the damage is near the center, the material contains the vibration and reduces the energy of the wave passing through. Since the behavior is symmetric as expected, a standardized relation between distance from the center ( $y_d$ ), thickness ( $t$ ) and covariance of energy change can be developed.



*Figure 52. Covariance of energy change vs distance of damage from center*

### 3.3.8. Full section convergence study

Results above for the “full section” were found using a window size of 0.0017 s. Since the time window was based on an approximate wave speed, a convergence study was done to ensure the entirety of the third wave path was incorporated.

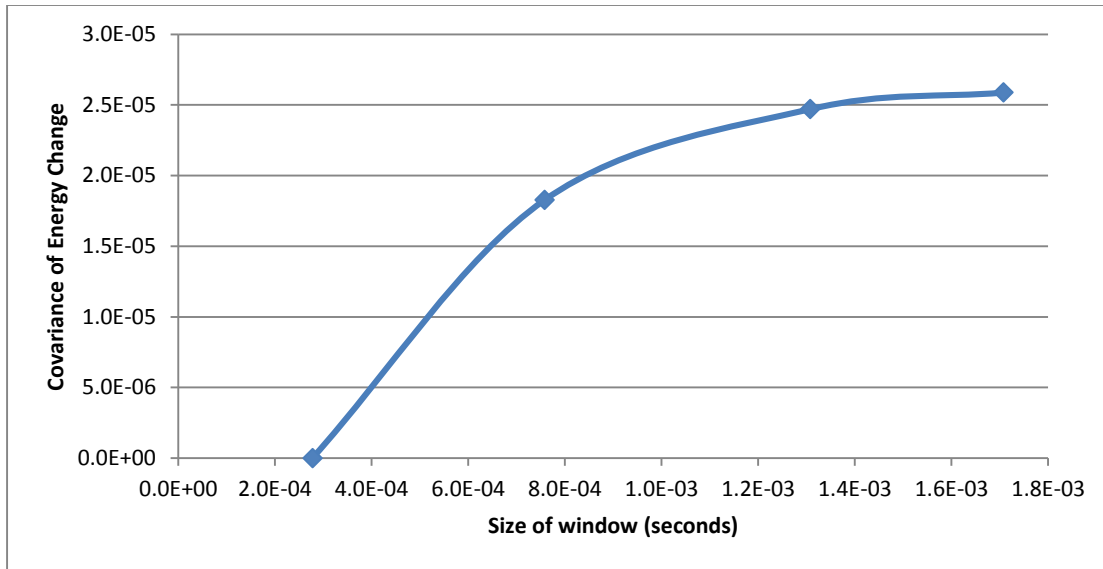


*Figure 53. Convergence study of covariance of energy change of damaged beam based on window size*

The convergence study shows that the window selected was of appropriate size.

### 3.3.9. Multiple delamination detection

To explore the possibility of locating multiple sources of delamination, a beam with two areas of delamination was modeled. The damages were 60 mm by 0.25 mm and placed at  $X = 600$  and  $X = 800$ . Figure 54 shows the wave response of this beam compared with the undamaged beam as well as a damaged beam with a singular delamination.

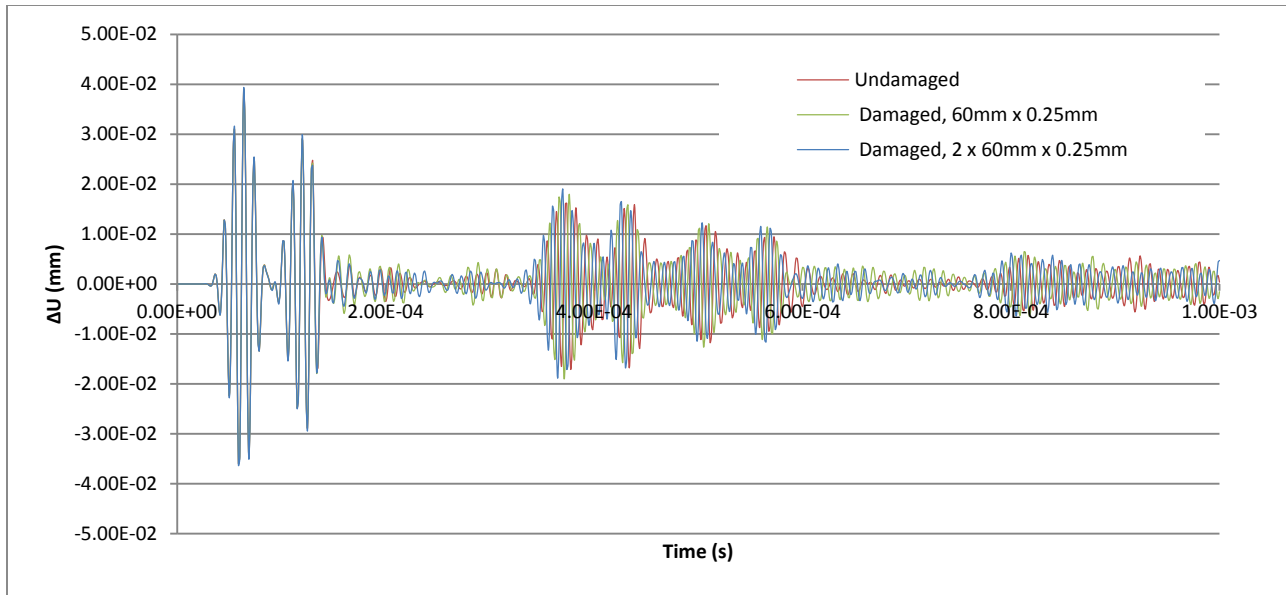


*Figure 54. Wave response comparison for a beam with multiple damages*

The differences in wave response is again difficult to interpret. The wave response in the boxed area shows differences in all three beams, which can be assumed to be caused by the delamination areas. Further study may be done for cases of multiple delamination damages in order to more clearly identify the effects from such damage.

### **3.4. Summary**

In this chapter a method for modeling and assessing composite beams with delamination damage was developed. Previous works had cited the small change in Lamb wave response due to delamination as a prohibitive factor in accurately analyzing such damage. Through the use of FFT as a data reduction method, these small changes were able to be more easily analyzed. Using FFT analysis and covariance of the located signals, an index was developed for relating the damage size with the covariance of energy change.

# **CHAPTER 4. EXPERIMENTAL DETECTION OF DELAMINATION IN LAMINATED COMPOSITE BEAMS THROUGH COVARIANCE OF ENERGY CHANGE OF ULTRASONIC WAVES**

## **4.1. Introduction**

In order to show the methods developed in this thesis are applicable, testing of the method on real samples is necessary. This chapter will manufacture the carbon fiber experimental specimen, perform experimental testing of carbon fiber reinforced polymer beams, and verify the modeling techniques discussed in Chapter 3. Through the innovative data reduction methods suggested in Chapter 3, it was proven that a correlation exists between delamination sizes and wave responses.

## **4.2. Beam manufacturing**

The beams used for the wave propagation experiments were manufactured in the mechanical engineering labs here at NDSU, allowing for easy control over the delamination size and location. The beams are composed of 8 layers of a unidirectional, 6k carbon fiber and Araldite LY 8604 resin. The composites were arranged with a  $[0/90/\pm 45]_s$  layup. A total of 10 beams were produced, with varying delamination depths and sizes. These two parameters were chosen as the variables because they showed the strongest correlation to the covariance of energy change in the modeling portion. The geometry of all beams was held constant for comparison and are shown below.

Table 7. Beam geometry

$L$	1200 mm
$w$	25 mm
$t$	3.4 mm

Where  $L$  = length,  $w$  = width and  $t$  = thickness. Table 11 shows the beams and their respective delamination sizes, depths and locations.

Table 8. Beam specifications

	Delamination Location (mm from left end)	Delamination Size (mm)	Delamination Depth (mm from surface)*
Beam 1	500 - 520	20	0.425
Beam 2	500 - 520	20	0.425
Beam 3	500 - 520	20	0.425
Beam 4	500 - 560	60	0.85
Beam 5	500 - 560	60	0.85
Beam 6	500 - 560	60	0.85
Beam 7	500 - 600	100	1.275
Beam 8	500 - 600	100	1.275
Beam 9	500 - 600	100	1.275
Beam 10	Undamaged	N/A	N/A

\*Depth based on assumption of equal layer thicknesses

In the interest of time and cost, beam properties were taken from a similar composite and then verified using a tensile strength test for comparison. The calculated properties were taken

from a common carbon fiber composite, with the thickness and layout of the beam used in our experiments. The beam used for approximation had the properties shown in Table 12.

Table 9. Beam properties

$L$	1200 mm	$G_{xy}$	22,640 MPa
$t$	3.4 mm	$G_{xz}$	5,833 MPa
$w$	Unit width	$G_{yz}$	5,833 MPa
$E_x$	58,190 MPa	$\nu_{xy}$	0.289
$E_y$	58,190 MPa	$\nu_{xz}$	0.289
$E_z$	6,000 MPa	$\nu_{yz}$	0.500
$\rho$	1.56 g/cm <sup>3</sup>		

Where  $L$  = beam length,  $t$  = beam thickness  $w$  = beam width,  $E$  = modulus of elasticity,  $\rho$  = material density,  $G$  = shear modulus, and  $\nu$  = Poisson’s ratio. Samples were then tested in order to verify the properties calculated.



Figure 55. Tensile test of the composite beam



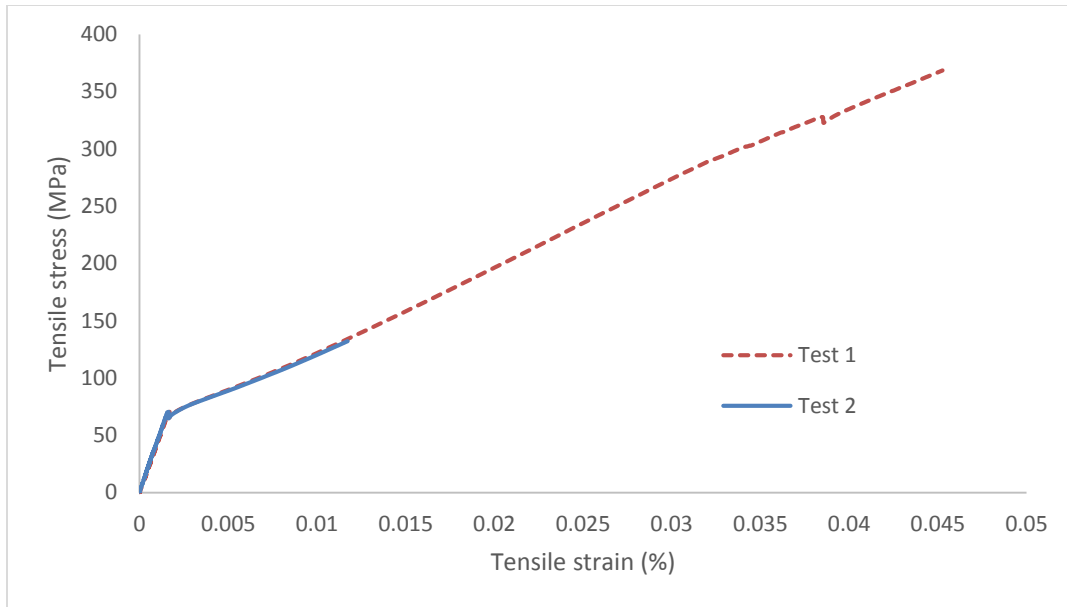


*Figure 56. Tensile test results*

From this test, the longitudinal modulus of elasticity was determined to be roughly 45,000 MPa. While this value is close, there is some disparity which can be accounted for by the cross sectional area of the specimen. The value of 45,000 MPa is calculated under the assumption of constant thickness for the entire width. Figure 57 shows this is not the case.

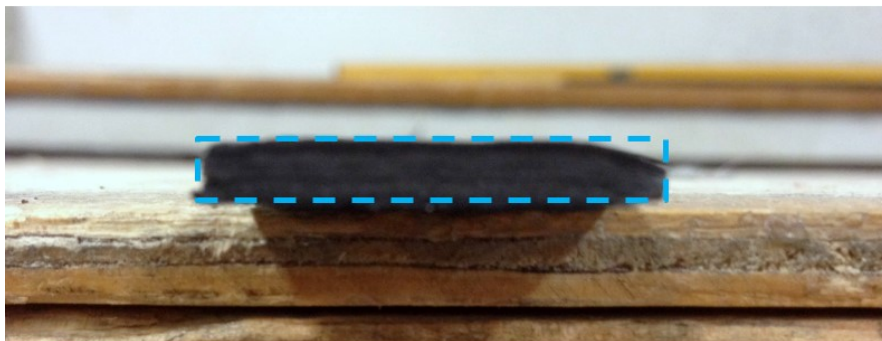


*Figure 57. Cross section of composite beam*

The modulus of elasticity can then be converted to a more accurate value using the proportion of actual cross sectional area to constant thickness cross sectional area. On average

the actual cross sectional area was found to be  $78 \text{ mm}^2$  compared to the constant thickness cross sectional area of  $85 \text{ mm}^2$ . This gives a ratio of 0.92. Applying this ratio to the modulus of elasticity, which is inversely proportional to the cross sectional area, an adjusted modulus of  $48,913 \text{ MPa}$  is found. This is relatively close to the calculated value of  $58,190 \text{ MPa}$ , proving the approximate properties used for modeling to be acceptable.

#### 4.2.1. Creating delamination damage in the beams

Delamination damage was made during the manufacturing process through the use of a very thin Teflon sheet. The sheet was placed at the desired location between the appropriate layers during the layup process. After curing the sheet was removed, creating a void in the beam which simulates normal delamination damage. This damage can still be difficult to detect with the naked eye as shown in Figure 58.

Size range of delamination was chosen to closely mimic the beams analyzed during the modeling performed in Chapter 3. The depth of the delamination was controlled by introducing delamination between differing layers. For example, delamination introduced between the exterior most layers has a depth of  $0.425 \text{ mm}$ , assuming all layers are of equal thickness.



Figure 58. Close up of a damaged (a) and an undamaged (b) beam

### 4.3. Experimental delamination detection in composite beams

#### 4.3.1. Set up

An experiment is set up with locations of actuators and sensors following the configuration in Fig. 78.

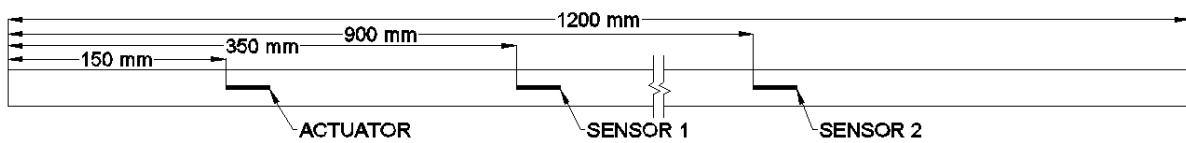


Figure 59. Layout of experimental beams

**i) Boundary Conditions**

The boundary conditions for the experiments were taken as free-free. These were simulated using low-resistance elastic bands. The beams were hung from the bands, allowing displacement in both the vertical and horizontal axes.

**ii) Actuator and Sensors**

The actuator and sensors used in the experiments were small PZTs which could be used to both send and receive a signal. Voltage is supplied to the actuator, causing it to deform and transfer the desired wave to the beam. PZTs acting as sensors undergo deformation from the wave and send the corresponding voltage to a recording device. The PZTs were bonded to the composite beams at the 150 mm, 350 mm and 900 mm locations. The first acted as the actuator, while the remaining two were used as sensors to capture the Lamb waves.



*Figure 60. Bonded PZT – top view*



*Figure 61. Bonded PZT – side view*

The actuator was then connected to an output device, the Agilent 33220A Waveform Generator. An oscilloscope, the Tektronix TDS 2012B, was used for data collection.



*Figure 62. Agilent 33220A waveform generator*



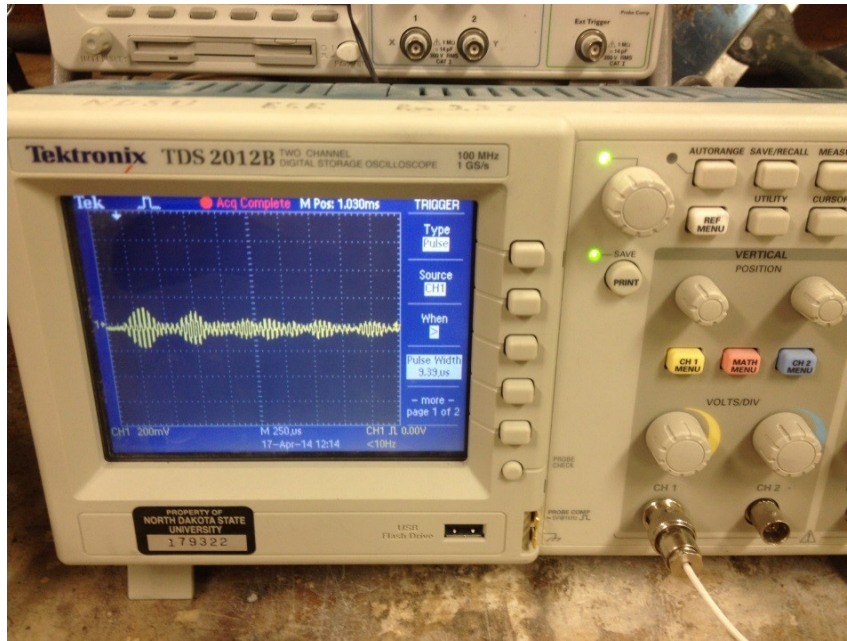


*Figure 63. Tektronix TDS 2012B oscilloscope*

The PZTs were connected to the devices by soldering wires to the designated areas, which in turn were connected to the oscilloscope and waveform generator via coaxial cables. To enhance the output signal, a 10X amplifier was connected between the sensor and the oscilloscope.

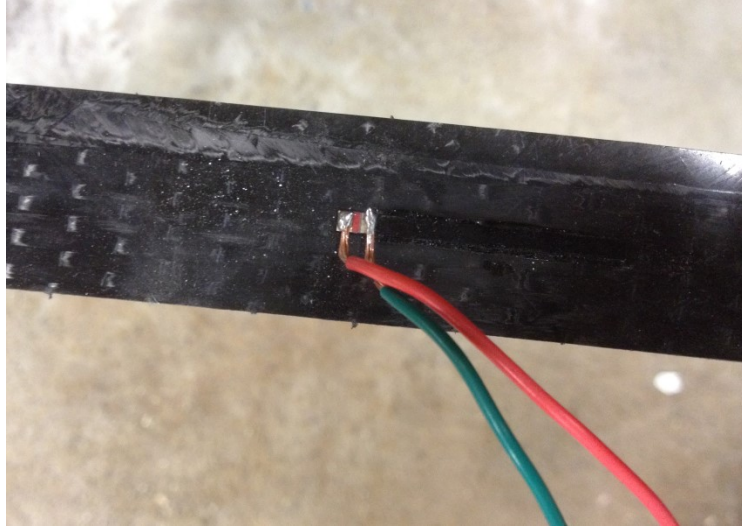


*Figure 64. Wire connection to bonded PZT*

### **iii) Loading**

The input wave used for the experiments was a five count Hanning window burst, as consistent with the previous discussion in this thesis. To determine the frequency to be used, a frequency sweep was performed with the waveform generator. The frequency that proved to optimize the sensor output was found to be 5 kHz. A maximum of 10 volts peak to peak was used for the amplitude.

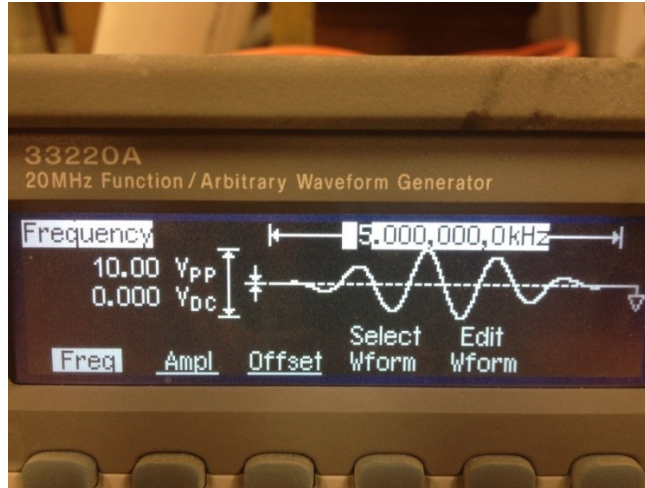


Figure 65. Output wave

#### 4.3.2. Data collection and reduction

For all ten beams the time domain graphs were obtained at both sensor locations. Similar to the comparisons of the time domain graphs from the modeling in Chapter 3, it was difficult to determine which waves were affected or produced by the delamination damage.

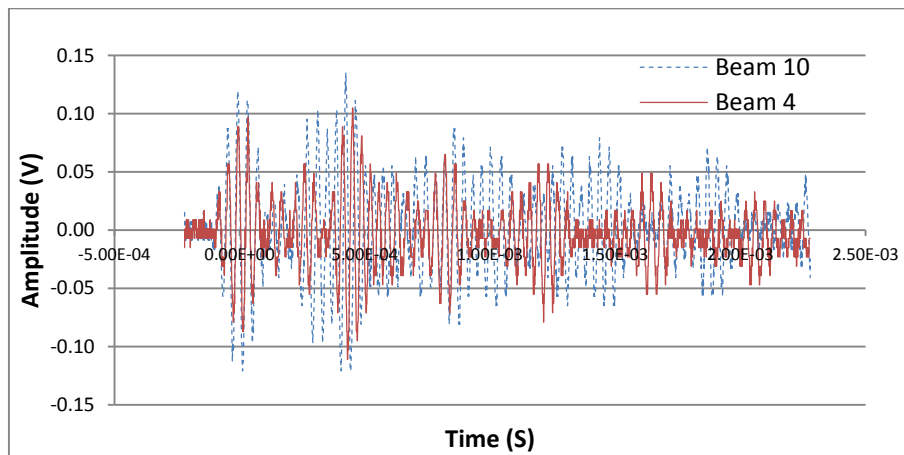


Figure 66. Time domain comparison of wave responses in beams 4 and 10, sensor 1

As shown in the figure above, the initial wave captured by the sensor is very similar. After this, however, the two graphs diverge. Interpreting the changes would prove to be quite



difficult. This is where the data reduction method introduced in Chapter 3 becomes helpful. Implementing the data reduction by the FFT method discussed in Chapter 3, the covariance of energy change is used as a method to analyze the damage.

Wave packages to be studied were selected in the same manner as those in Chapter 3. For Sensor 1, analysis was done on two sections that appear to have major differences in the time domain graph, as well as the “full section” based on time of flight. Details can be found in Section 3.3.5. For Sensor 2, only the full section analysis was performed. A convergence study of the full section time window is included for each sensor at the end of the results.

#### **4.4. Results**

Results were compiled for each beam and section in the same manner as Chapter 3. The covariance of energy change was found and compared for each variable.

##### **4.4.1. Varying delamination size**

###### **i) Sensor 1 Section 1**

Results were separated into graphs of the same delamination depth with varying delamination sizes.

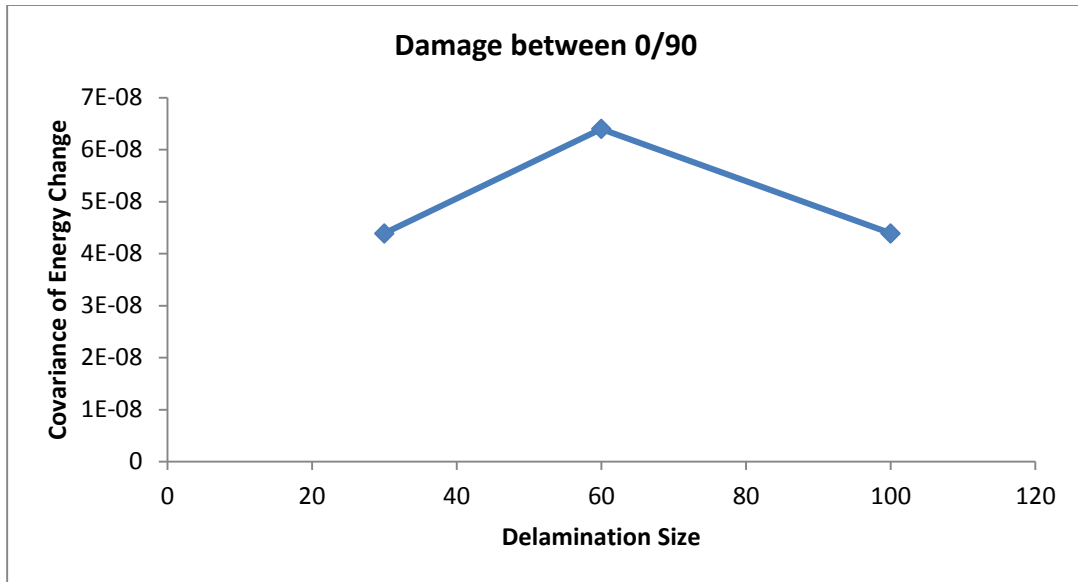


Figure 67. Covariance of energy change at sensor 1, section 1, between 0/90

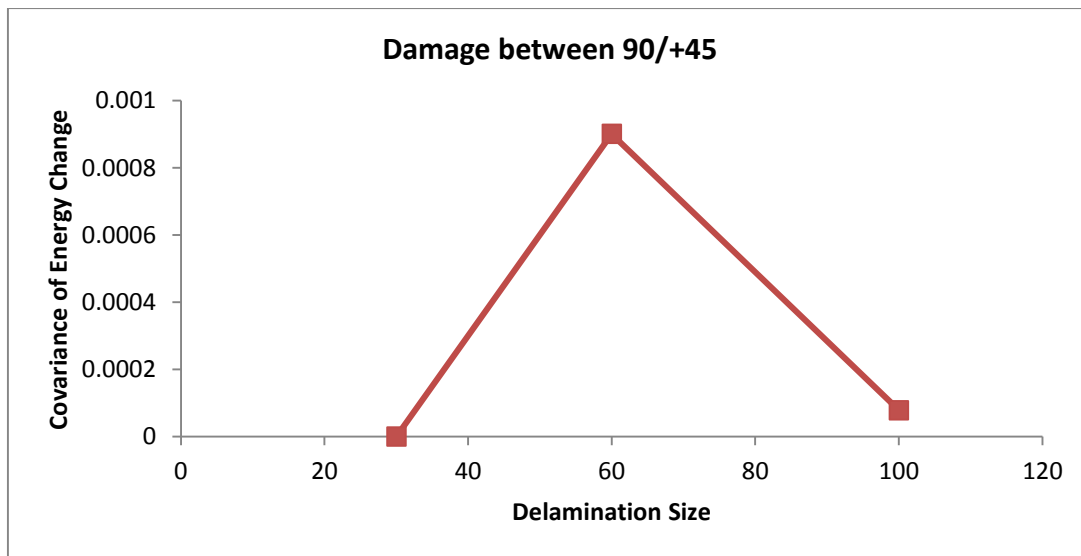


Figure 68. Covariance of energy change at sensor 1, section 1, between 90/+45

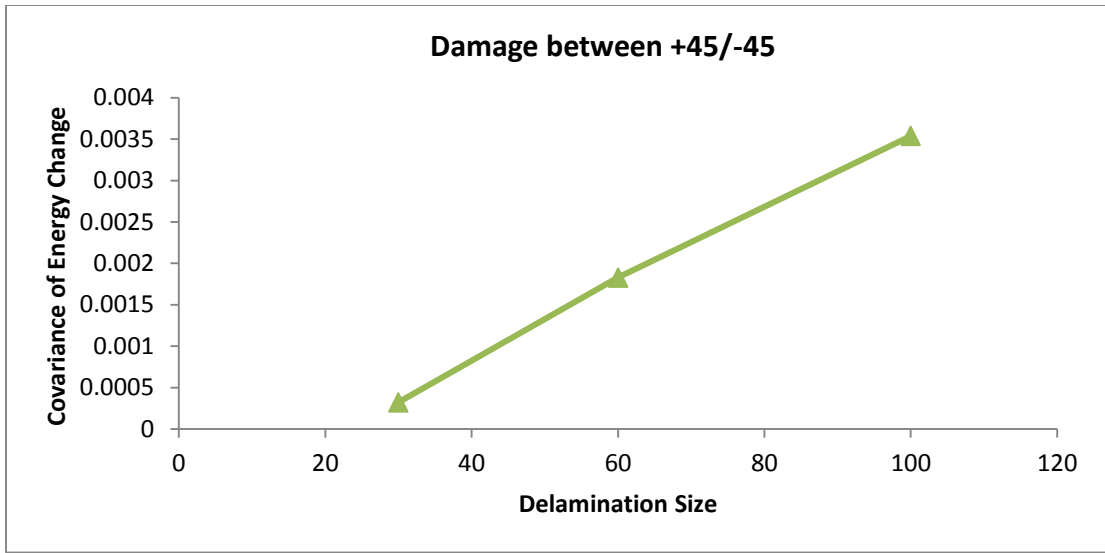


Figure 69. Covariance of energy change at sensor 1, section 1, between +45/-45

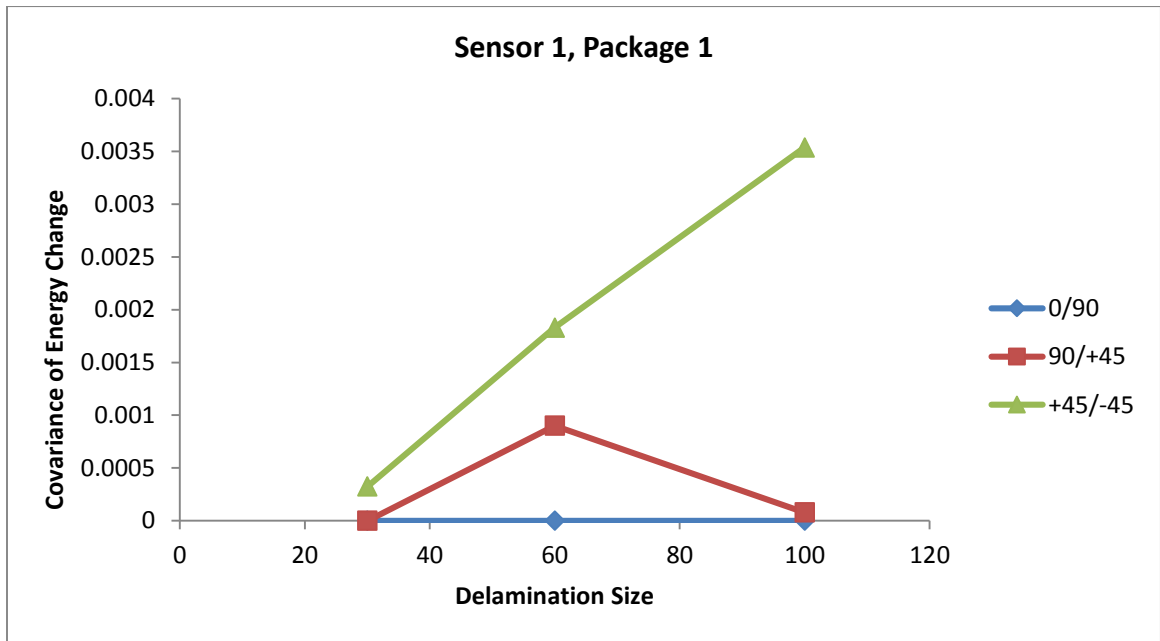


Figure 70. Covariance of energy change at sensor 1, comparison

ii) **Sensor 1 Section 2**

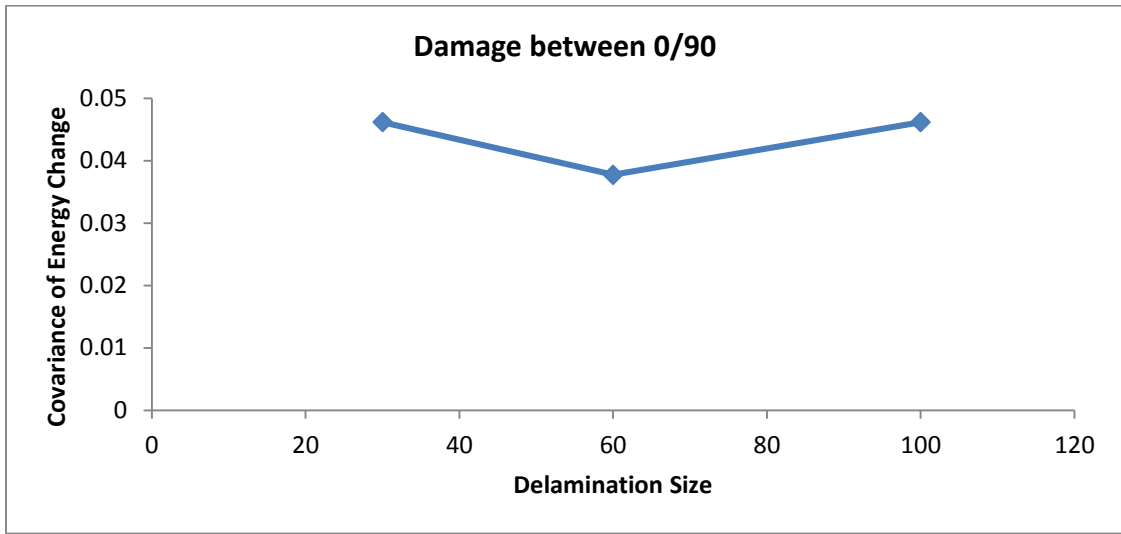


Figure 71. Covariance of energy change at sensor 1, section 2, between 0/90

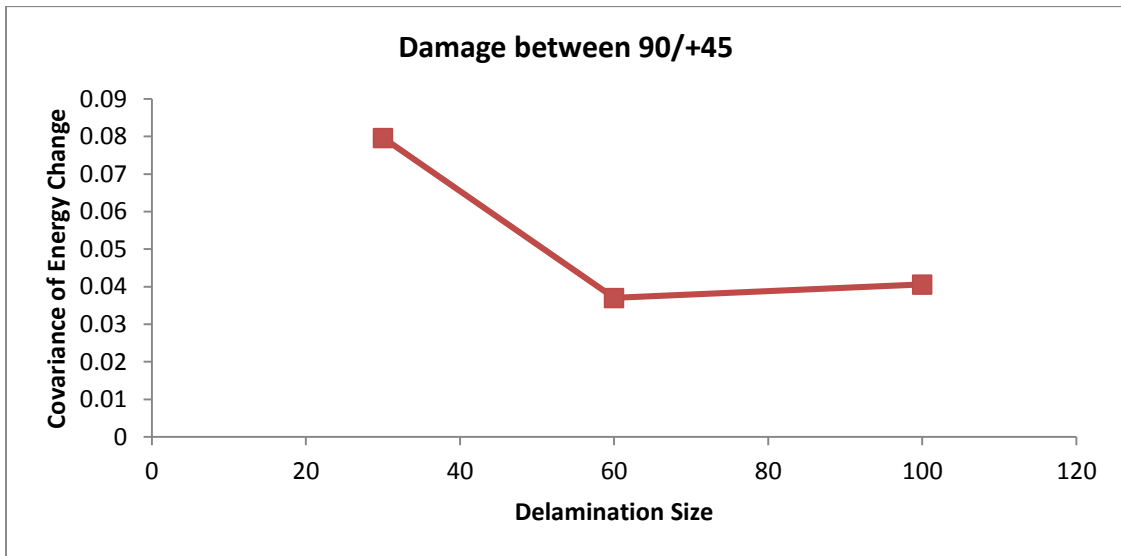


Figure 72. Covariance of energy change at sensor 1, section 2, between 90/+45

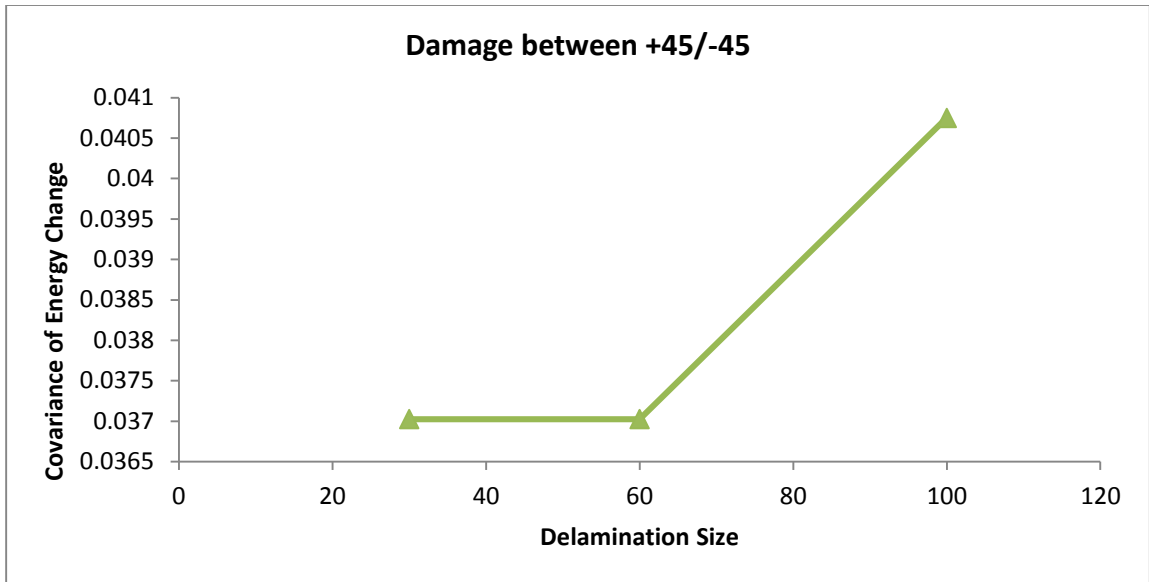


Figure 73. Covariance of energy change at sensor 1, section 2, between +45/-45

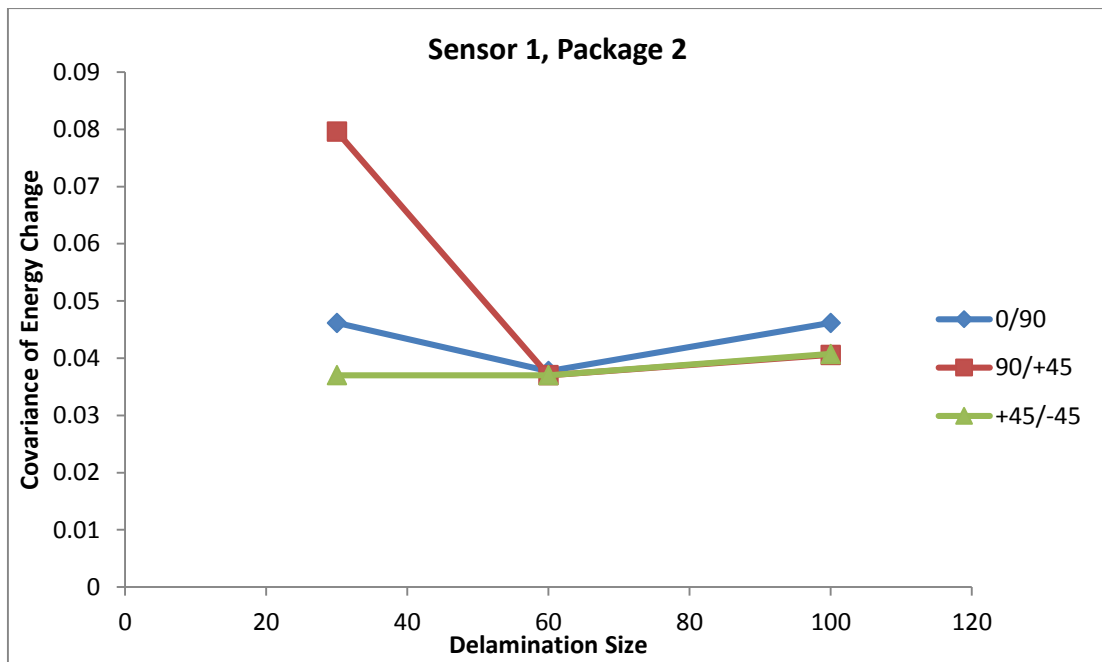


Figure 74. Covariance of energy change at sensor 1, section 2, comparison

iii) **Sensor 1 Full Section**

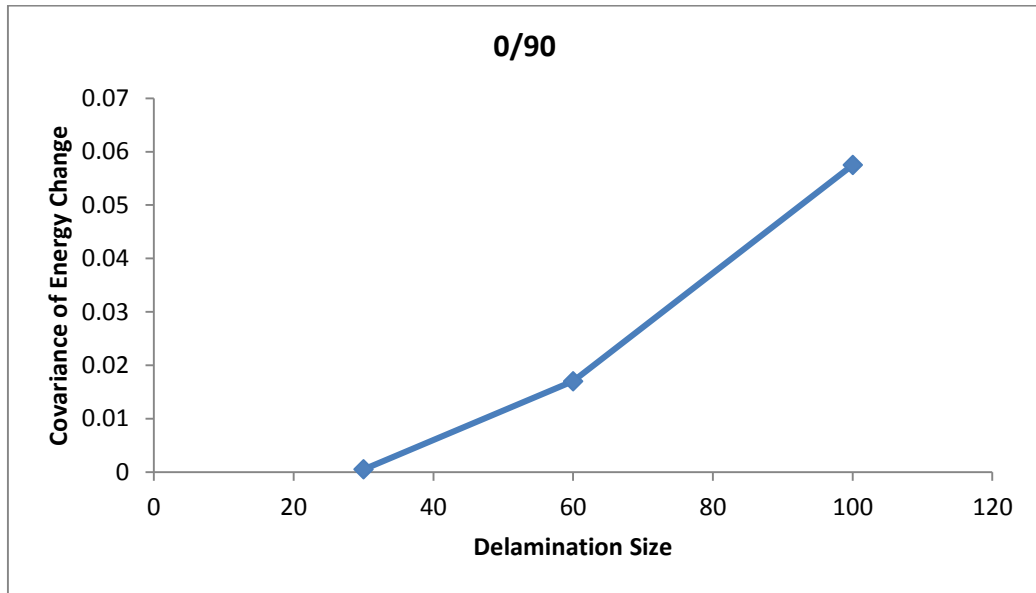


Figure 75. Covariance of energy change at sensor 1, full section, between 0/90

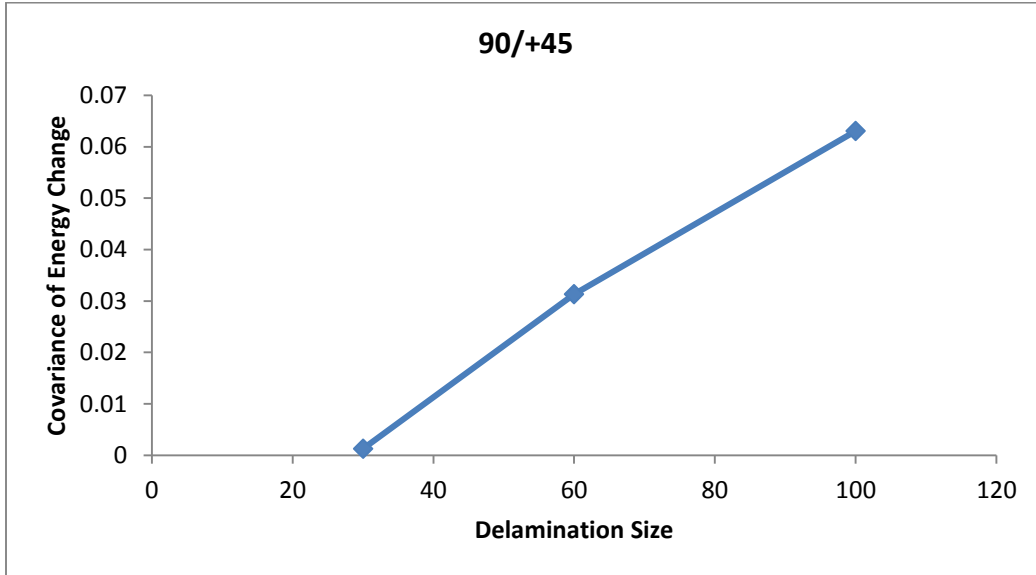


Figure 76. Covariance of energy change at sensor 1, full section, between 90/+45

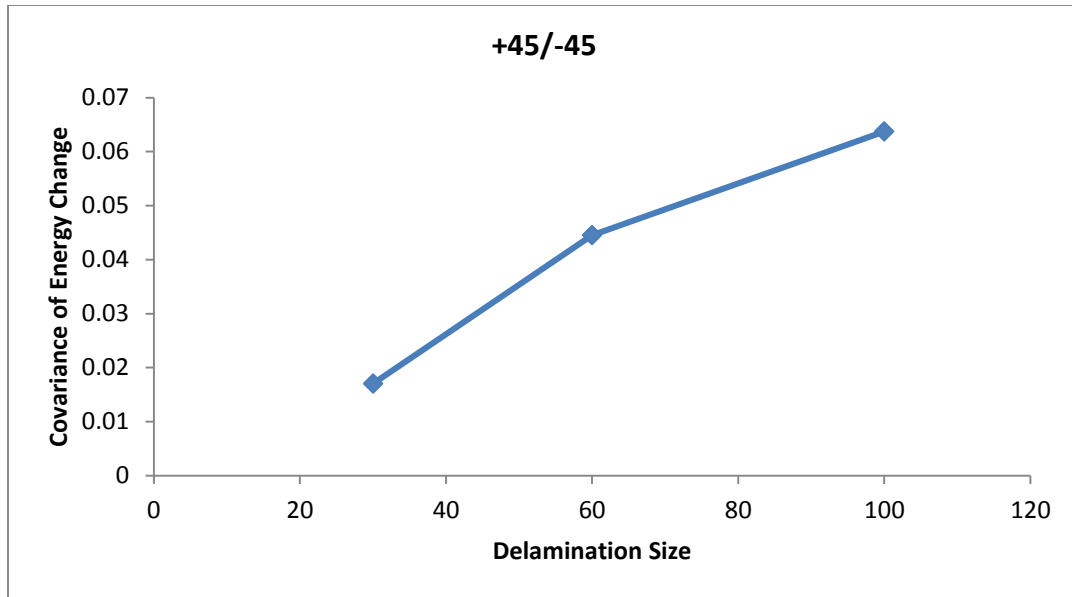


Figure 77. Covariance of energy change at sensor 1, full section, between +45/-45

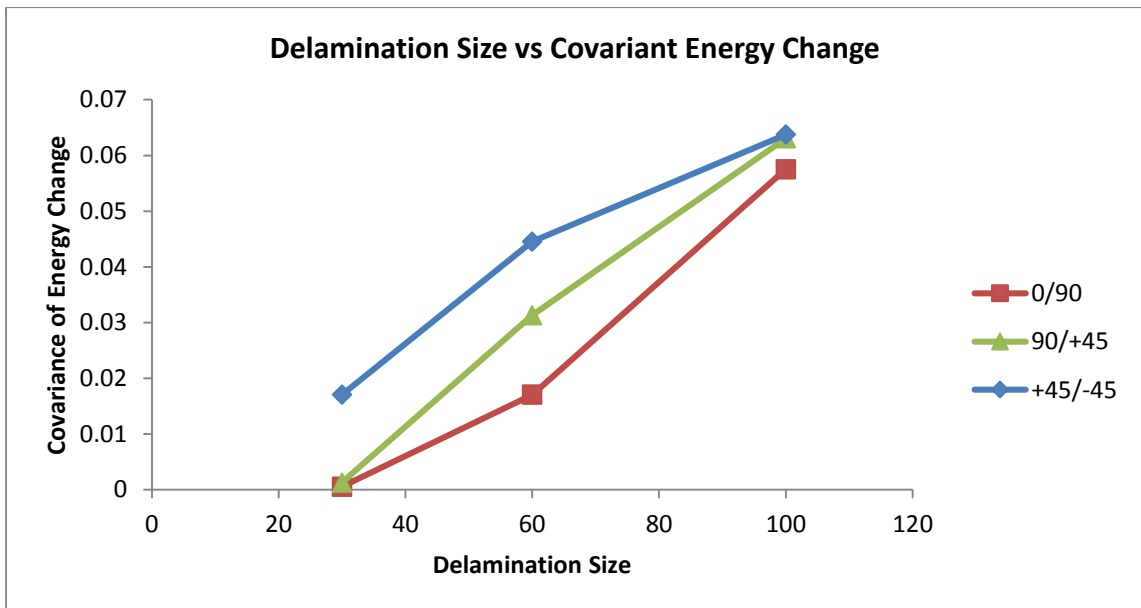


Figure 78. Covariance of energy change at sensor 1, full section, comparison

iv) **Sensor 2 Full Package**

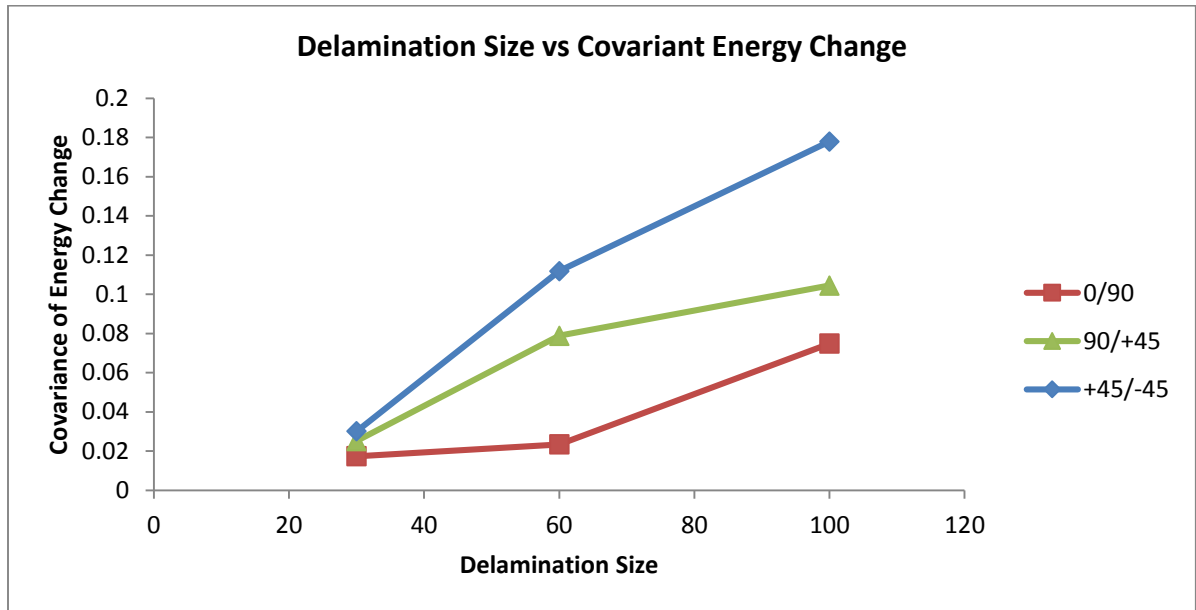


Figure 79. Covariance of energy change at sensor 2, full section, comparison

v) **Summary**

As shown in the results above, the two individual wave packages did not show a definite correlation between delamination size and covariance of energy change. However, when looking at the full section results, it can be seen that with increasing delamination size the covariance of energy change increases. The correlation is consistent to what was found in the modeling. This strengthens the case for using the full section method rather than arbitrarily choosing wave sections that appear different in the time domain. By including the entire section, the chance of missing a wave that has transformed or generated by the damage is much less likely.



#### 4.4.2. Varying delamination depth

This section shows the results of the experimental testing with variable delamination depth.

##### i) Sensor 1 Full Package

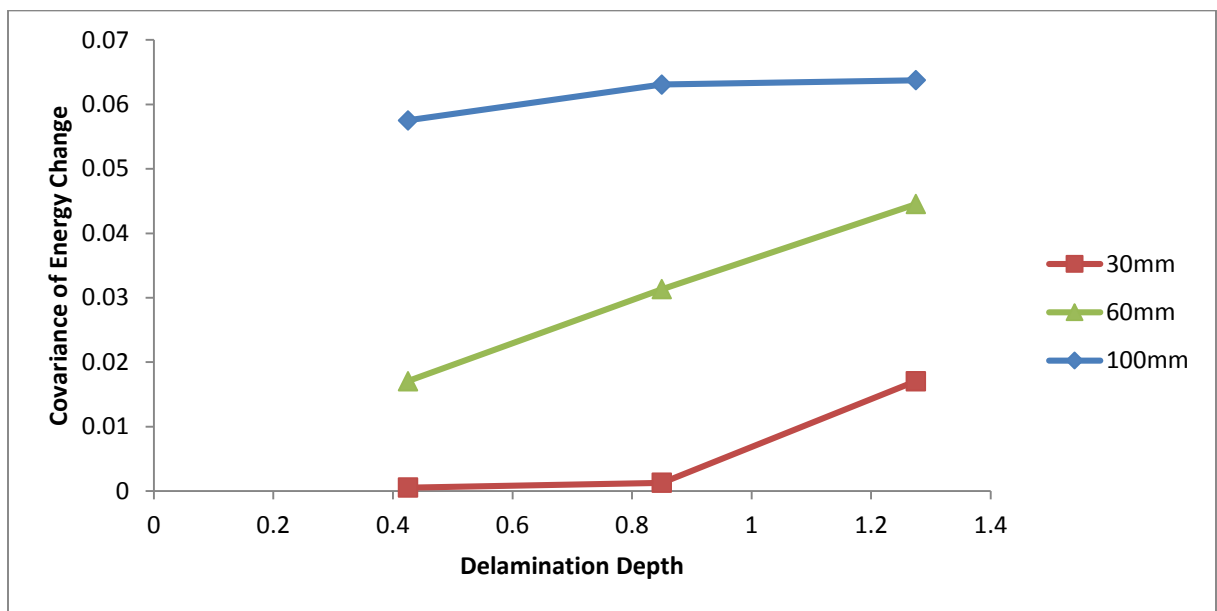
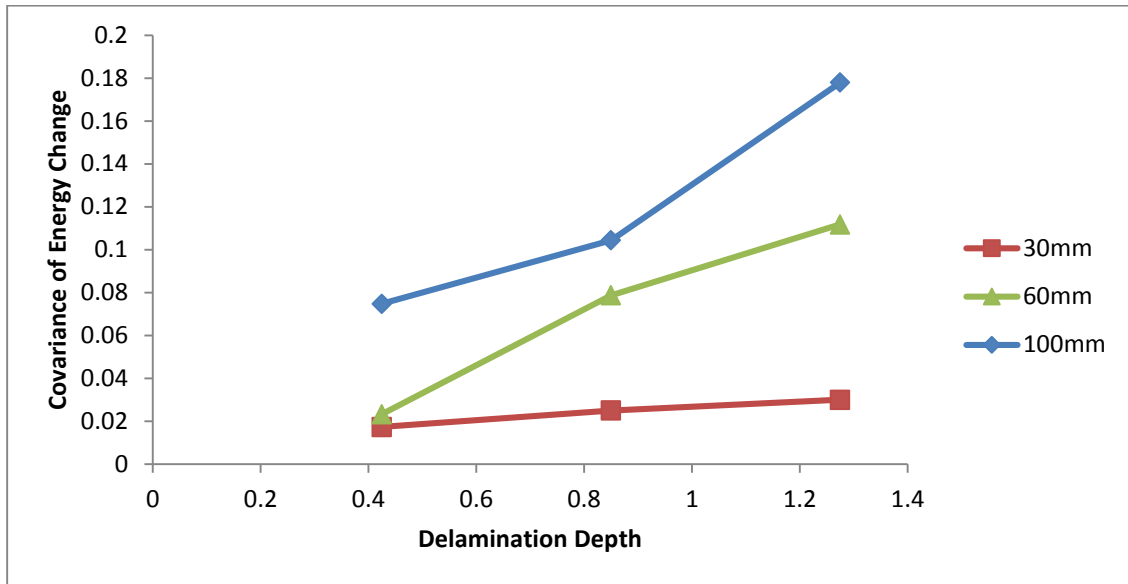


Figure 80. Covariance of energy change at sensor 1, full section, comparison

**ii) Sensor 2 Full Package**



*Figure 81. Covariance of energy change at sensor 2, full section, comparison*

**iii) Summary**

The graphs show a correlation between depth of delamination and covariance of energy change for both Sensor 1 and 2. This correlation of increased change as the delamination approaches the center of the composite is consistent with the results found in Chapter 3 modeling. Again this helps prove the case for using the full section analysis method.

**4.4.3. Convergence study of time window**

To validate the size of window used for the full section analysis, convergence studies were performed for both sensors. A range of near 2.00E-3 seconds was set using the previously described technique involving time of flight. This length of wave package is assumed to capture the most important propagation paths based on the time of flight.

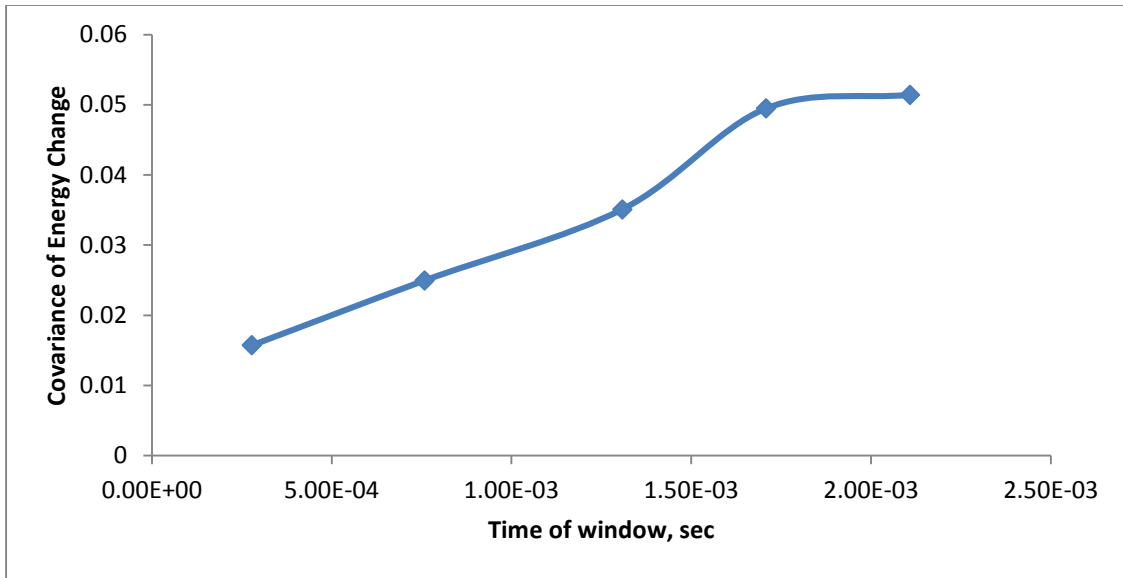


Figure 82. Convergence of time window size for sensor 1

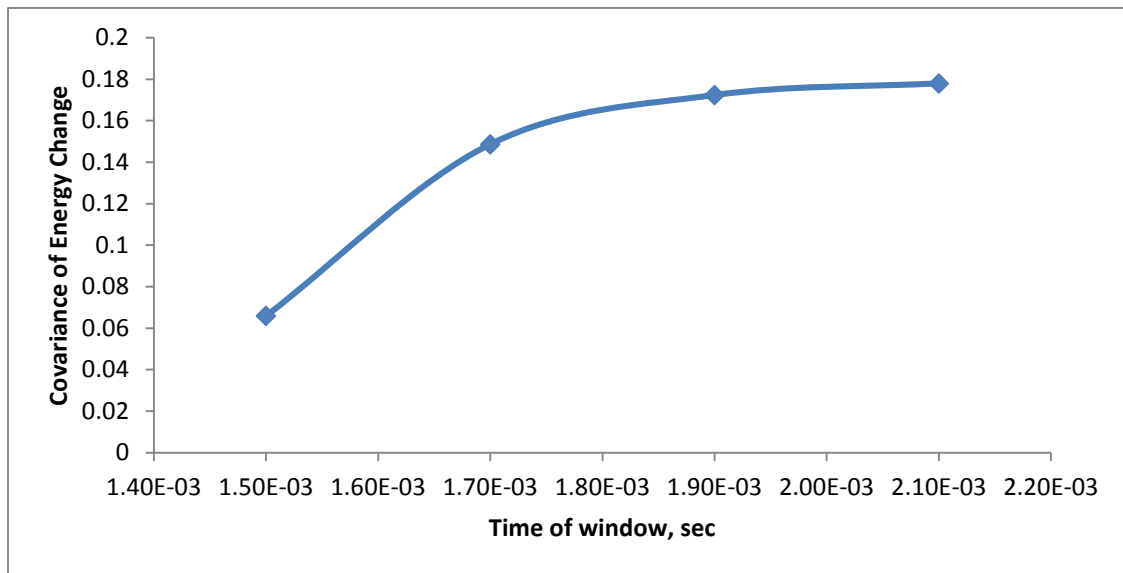


Figure 83. Convergence of time window size for sensor 2

For both sensors, a wave package window of  $2.10 \times 10^{-3}$  s was used. Figures 82 and 83 show that this captured the majority of the covariance of energy change within this range.

#### **4.5. Modeling validation**

As a means of validating both the results found from the experimentation and the modeling portion of this thesis, data from the experiment and a model to replicate the experiment were compared. By using the same methods outlined in Chapter 3 for modeling delamination damage, correlation can be found between experimental and modeling results.

Using the properties calculated for the experimental beam, a model was created using the ANSYS software. The model was subjected to loading very similar to the load used for experimentation. The frequency and length of the loading remained constant. Due to differences of input method, the amplitude varied slightly between model and experiment. This change does not affect the wave response in any vital facet, such as wave speed or wave type. Rather, the amplitude of the responses will differ in a manner proportional to the input.

In the model, a delamination thickness of 0.05 mm was used. This value was chosen from the thickness of the sheet used to simulate delamination damage during production. As discussed in Chapter 3, contact elements were used at the faces of delamination to simulate contact due to vibration. The signal responses from a damaged and an undamaged beam were compared.

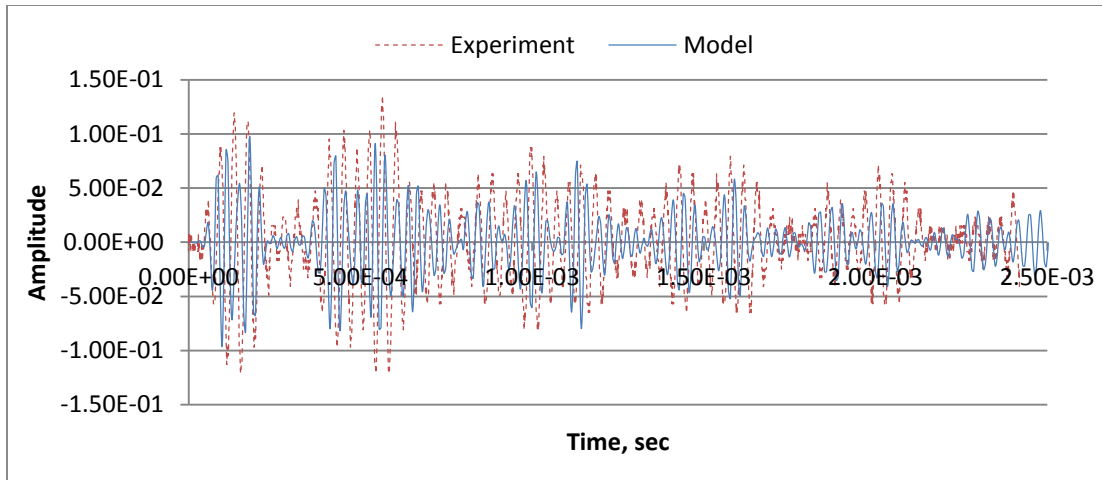


*Figure 84. Comparison of model vs experiment wave responses, undamaged beam*

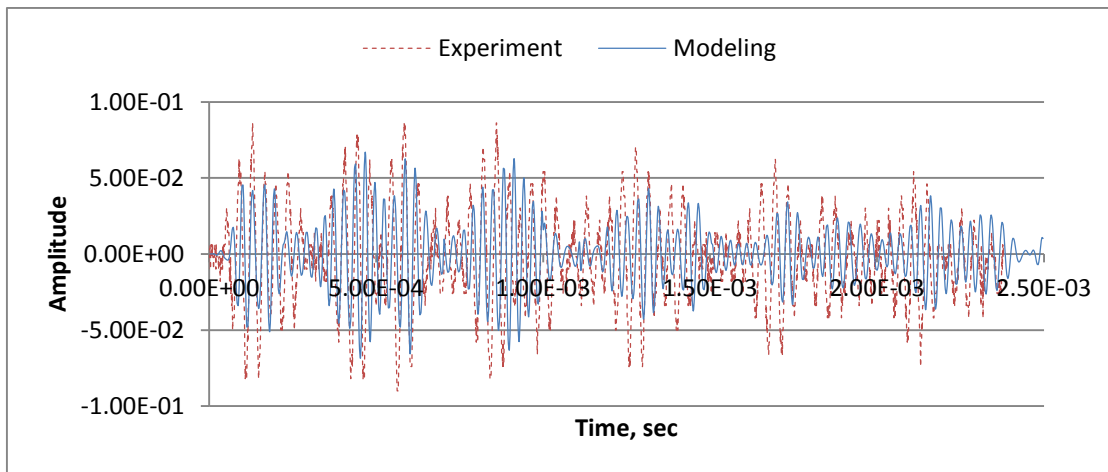


*Figure 85. Comparison of model vs experiment, damaged beam*

It can be shown that while there are some minor differences in the graphs, the response is very well mimicked by the model. Amplitude is different in both graphs, however it is a consistent difference which shows similar dissipation. The accurate response of both the undamaged and damaged models validates the modeling techniques used.

#### **4.6. Summary**

In this chapter delamination damage in composite beams was detected and analyzed through laboratory experiments. Composite beams were manufactured through collaboration with the mechanical engineering department, which also aided in the finding of the beam properties. The purpose of this chapter was to validate the data reduction methods introduced in Chapter 3. By producing similar results in real applications, the concepts of data reduction by FFT were validated. Data analysis was performed on small sections as well as a more complete wave package, similar to Chapter 3. The full wave package method proved to be the more reliable method, showing a correlation with covariance of energy change in both damage size and depth. The correlations closely mirrored those found in the modeling, further strengthening the validity of our innovative data reduction method.

## CHAPTER 5. CONCLUSIONS AND RECOMMENDATIONS

### 5.1. Conclusions

This thesis introduced an innovative data reduction method for easier detection of delamination damage in composite laminates. Using the existing technique of introducing Lamb waves as a means of structural health monitoring, data was collected and interpreted by means of data reduction through FFT. By applying FFT to response waves, the key frequencies and corresponding amplitudes were able to be identified. This led to the concept of covariance of energy, which was used to quantify the change of response to Lamb waves due to delamination damage.

In the modeling portion of the thesis, Chapter 3, different aspects of damage were tested in long, thin carbon fiber composite beams. These included delamination length, thickness, depth and location. It was proven that correlations between covariance of energy change and delamination length, thickness and depth exist. The method was tested both over small wave packages and a full wave package. As both delamination length and thickness increased, it was seen that so did covariance of energy change. Regarding the depth of the damage, results showed that as the damage approached mid-thickness, the covariance of energy change increased. These results were consistent through both small packages analyzed as well as the full package.

Chapter 4 included the experimental testing of carbon fiber laminate beams. The beams were manufactured on site, with simulated delamination damage introduced. Although we were unable to vary the thickness of delamination, the length, location and depth of the damage was controlled. With these beams, testing was performed to closely follow the conditions used in

Chapter 3. Two small wave packages and one full wave package were analyzed using the new data reduction technique. Results showed that the full wave package produced the same correlations found in Chapter 3. As length of the delamination increased, the covariance of energy change did too. Similarly, as damage approached mid-thickness of the beam the covariance of energy change increases. The same trends were not found using the smaller wave packages. This suggests it is better to use the larger wave package, which was defined in size by the relation of specimen length and wave speed. In some cases the smaller package may show the same trends, but due to the somewhat arbitrary selection of the window size it may not be indicative of the true conditions.

## **5.2. Recommendations and future work**

The principles developed in this thesis will be helpful in furthering the field of structural health monitoring. One area for future work related to this research includes further investigation of multiple delamination detection. In real application, delamination is not likely to be contained to a single region. In order to be effective, one must be able to find multiple sources of delamination and their severity.

Another area for future work would be the application to complex structures. In order to monitor structures such as aircraft bodies, the detection method must be able to travel in multiple directions. From the groundwork provided in this thesis, progress can continue toward using the methods introduced to real world applications.



## REFERENCES

- [1] Kessler, S.S., Spearing, S.M., Soutis, C. "Damage detection in composite materials using Lamb wave methods". *Smart Mater Struct* 2002, 11:269–78.
- [2] Hall, S. R. "The total data integrity initiative—structural health monitoring, the next generation". *Proc. USAF ASIP Conf.* 2nd edition. Savannah, GA, 1999.
- [3] Bhat, N. *Delamination Growth in Graphite/Epoxy Composite Laminates under Tensile Load.* Cambridge, MA: Massachusetts Institute of Technology, 1993.
- [4] Wang, S. S. "Delamination crack growth in unidirectional fiber-reinforced laminates under static and cyclic loading." *Composite Material*, 1979.
- [5] Sun, G., Zhou, Z., Chen, X. and Wang, J. "Ultrasonic characterization of delamination in aeronautical composites using noncontact laser generation and detection". *Appl. Opt.*, 2013, 52: 6481-6486.
- [6] Sabin, G. E. *Delamination in Composite Materials as Observed Using an Optical Fiber Strain Gage.* Annapolis, MD: Naval Academy, 1993.
- [7] Yu, L., Giurgiutiu, V. "In situ 2-D piezoelectric wafer active sensors arrays for guided wave damage detection." *Ultrasonics*, 2008, 48:117-134.
- [8] Viktorov, I. A. *Rayleigh and Lamb waves: physical theory and applications.* New York: Plenum Press, 1967.
- [9] Wilson, A.B., Coppens, O.B. *Elements of sound transmission in beams.* Final Report. Monterey, CA: Naval Postgraduate School, 1978.
- [10] Worlton, D.C. "Experimental confirmation of Lamb waves at megacycle frequencies." *Journal of Applied Physics*, 1961, 32:967–971.

- [11] Lin, X., Yuan, F.G. "Diagnostic Lamb waves in an integrated piezoelectric sensor/actuator plate: analytical and experimental studies". *Smart Materials and Structures*, 2001, 10: 907–913.
- [12] Ihn, J.B., Change, F.K. "Built-in diagnostics for monitoring crack growth in aircraft structures." *Proceedings of the SPIE 9th International Symposium on Smart Structures and Materials*, San Diego, CA, 2002, 4702-04.
- [13] Raghavan, A., Cesnik, C.E.S. "Finite-dimensional piezoelectric transducer modeling for guided wave based structural health monitoring." *Journal of Smart Materials and Structures*, 2005, 14:1448–1461.
- [14] Nieuwenhuis, J.H., Neumann, J.J., Greve, D.W., Oppenheim, I.J. "Generation and detection of guided waves using PZT wafer transducers". *IEEE Transactions on Ultrasonics*, 2005, 2103–2111.
- [15] Han, J., Kim, C.G., Kim, J.Y. "The propagation of Lamb waves in a laminated composite plate with a variable stepped thickness". *Journal of Composite Structures*, 2006, 76:388–396.
- [16] Meyer, PA., Rose, J.L., and Barshinger, J., "Ultrasonic Guided Wave Inspection of a 747 Tear Strap Structure", ASNT's 1997 Fall Conference and Quality Testing Show, Pittsburgh, PA, 1997.
- [17] Cawley, P., and Alleyne, D. "The use of Lamb waves for the long range inspection of large structures". *Ultrasonics*, 1996, 34: 287-290.
- [18] Worden, K., Manson, G., Allman, D. "Experimental validation of a structural health monitoring methodology: Part I. Novelty detection on a laboratory structure." *Journal of Sound and Vibration*, 2003, 259(2): 323–343.

- [19] Rose, J.L. "A vision of ultrasonic guided wave inspection potential." Proceedings of the Seventh ASME NDE Topical Conference, San Antonio, TX, NDE-Vol.20: 1-5, 2001.
- [20] Wait, J. R., Park, G., and Charles, R. F. "Integrated Structural Health Assessment Using Piezoelectric Active Sensors". Shock and Vibration, 2005, 12: 389-405.
- [21] Se, Z.Q., Ye, L., Lu, Y. "Guided Lamb waves for identification of damage in composite structures: A review." Journal of Sound and Vibration, 2006, 753-780.
- [22] Yang M, Qiao P. "Modeling and experimental detection of damage in various materials using the pulse-echo method and piezoelectric sensors/actuators." Smart Materials and Structures, 2005, 14:1083–1100.
- [23] Raghavan, A., Cesnik, C.E.S. "Review of guided-wave structural health monitoring." Shock Vib Dig, 2007, 39: 91–114.
- [24] Cooley, J. W. and Tukey, J. W. "An algorithm for the machine calculation of complex Fourier series". Math. Comput. 1965, 19: 297–301.
- [25] Giurgiutiu, V., Cuc, A. "Embedded non-destructive evaluation for structural health monitoring, damage detection, and failure prediction." Shock Vib Dig, 2005, 37: 83–105.
- [26] Tsai, S. W. Composite Materials: Testing and Design Fifth Conference. Baltimore, MD: American Society for Testing and Materials, 1979.
- [27] Frieden, J., Cugnoni, J., Botsis, J., Gmür, T. "Low energy impact damage monitoring of composites using dynamic strain signals from FBG sensors – Part I: Impact detection and localization." Compos Struct , 2012, 438–45.
- [28] Kirkby E., de Oliver, R., Michaud, V., Månson, J.A. "Impact localisation with FBG for a self-healing carbon fibre composite structure". Compos Struct, 2011, 8–14.

- [29] Takeda, S., Aoki, Y., Nagao Y. "Damage monitoring of CFRP stiffened panels under compressive load using FBG sensors". *Compos Struct*, 2012, 813–9.
- [30] Scalea, F.L., Salamone, S. "Temperature effects in ultrasonic Lamb wave structural health monitoring systems". *J Acoust Soc Am*, 2008, 161–74.
- [31] Lu, Y., Michaels, J.E. "A methodology for structural health monitoring with diffuse ultrasonic waves in the presence of temperature variations". *Ultrasonics*, 2005, 717–31.
- [32] Palmos, E. Modeling of Lamb waves and application to crack identification. Master's Thesis. Monterey, CA: Naval Postgraduate School, 2009.
- [33] Han, S.J. Finite element analysis of lamb waves acting within a thin aluminum plate. Master's thesis. Dayton, OH: Air force Institute of Technology, 2007.
- [34] Olson, S.E., Derriso, M.M., DeSimio, M.P. "Analytical modeling of lamb waves for structural health monitoring". *Third European Workshop on Structural Health Monitoring*. Granada, Spain, 2006.
- [35] Min Y., Hoon S., Jeong B.I., Hyung J.L. "Instantaneous delamination detection in a composite plate using a dual piezoelectric transducer network." *Composite Structures*, 2012, 94(12): 3490-3499.
- [36] Giurgiutiu, V. "Tuned Lamb wave excitation and detection with piezoelectric wafer sensors for structural health monitoring". *Journal of Intelligent Material Systems and Structures*, 2005, 291–305.
- [37] Giurgiutiu, V. *Structural Health Monitoring with Piezoelectric Wafer Active Sensors*. Academic Press, 2008.

- [38] Chang, F.-K. "Built-In Damage Diagnostics for Composite Structures". Proceedings of the 10th International Conference on Composite Structures (ICCM-10). Whistler, B.C., Canada, 1995, 283–289.
- [39] Marckerle, J. "Finite-element modeling of non-destructive material evaluation, an addendum: A bibliography (1997–2003)". Modeling and Simulation in Material Science and Engineering, 2004, 799–834.
- [40] Moulin, E., Assaad, J., Delebarre, C., Kaczmarek, H. and Balageas, D. "Piezoelectric transducer embedded in composite plate: application to Lamb wave generation." Journal of Applied Physics, 1997, 2049–2055.
- [41] Soutis, C., Valdez, S.H.D. "Structural integrity monitoring of CFRP laminates using piezoelectric devices." Proc. Eur. Conf. on Composite Materials, Venice, Italy, 2000.
- [42] Soutis, C., Valdez, S.H.D. "Health monitoring of composites using Lamb waves generated by piezoelectric devices last. Rubber Compos". Plast. Rubber Compos, 2000, 475–81.
- [43] Soutis, C., Valdez, S.H.D. "A structural health monitoring system for laminated composites." Proc. 18th Biennial Conf. on Mechanical Vibration and Noise, , 2001.
- [44] Barbero, E.J. Finite Element Analysis of Composite Materials Using ANSYS. Taylor & Francis Group, LLC, 2013.

## **APPENDIX. COMPOSITE MODELING**

The appendix includes examples to show that composite materials are able to be modeled correctly using the ANSYS software. There are several methods for modeling composites in this software. A complete overview of the modeling methods and appropriate element types can be found in Barbero's 2013 book devoted solely to this topic [44]. Composites can be modeled using either shell or solid elements. This section includes examples using both methods.

In addition to verifying the ability to model composites correctly, it is important to show damage can be simulated in the materials. Since the focus of this research deals with delamination detection, an example showing how to model delamination is necessary.

### **A.1. Loading responses of undamaged composite**

A simple example from Barbero's book will be followed to demonstrate one method of modeling a composite laminate material. The example can be found on pages 82-83 [44]. Modeling will be recreated and the results will be verified to confirm correctness of the model.

#### ***i) Problem Statement***

A simply supported square composite plate is subjected to a tensile loading. Find the maximum deflection at the edge of the plate. Properties are given in Appendix Table 1.

Table A1. Plate properties

Layup	[0/90/±45] <sub>s</sub>	Loading	100 N/mm
$a_x$	1000 mm	$G_{xy}$	4.306 GPa
$a_y$	1000 mm	$G_{xz}$	4.306 GPa
$t$	10mm	$G_{yz}$	2.76GPa
$E_x$	133.86 GPa	$\nu_{xy}$	0.301
$E_y$	7.706 GPa	$\nu_{xz}$	0.301
$E_z$	7.706 GPa	$\nu_{yz}$	0.396

Where  $a_x$  = length in x direction,  $a_y$  = length in y direction ,  $t$  = thickness,  $E$  = modulus of elasticity,  $G$  = shear modulus and  $\nu$  = Poisson's ratio.

**ii) Element Type**

The element to be used for this model is the four node SHELL 181 element. Six degrees of freedom are added to the model: UX, UY, UZ, ROTX, ROTY, ROTZ. The options to use full integration (K3) and to store data for all layers (K8) are chosen.

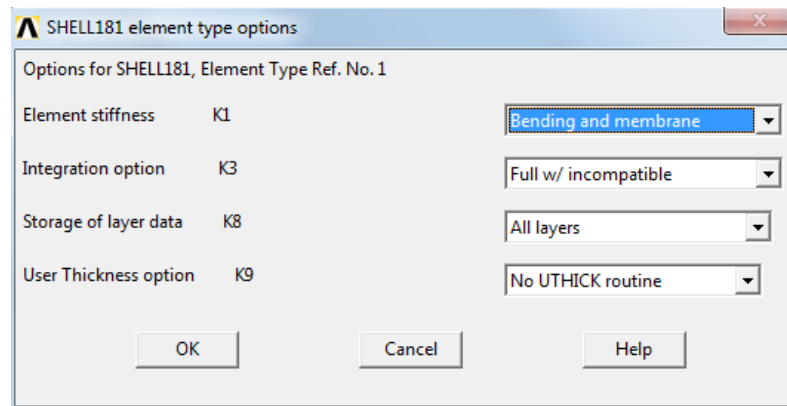


Figure A1. Element type

### iii) Defining a Material

A material is defined with the properties given in the problem statement.

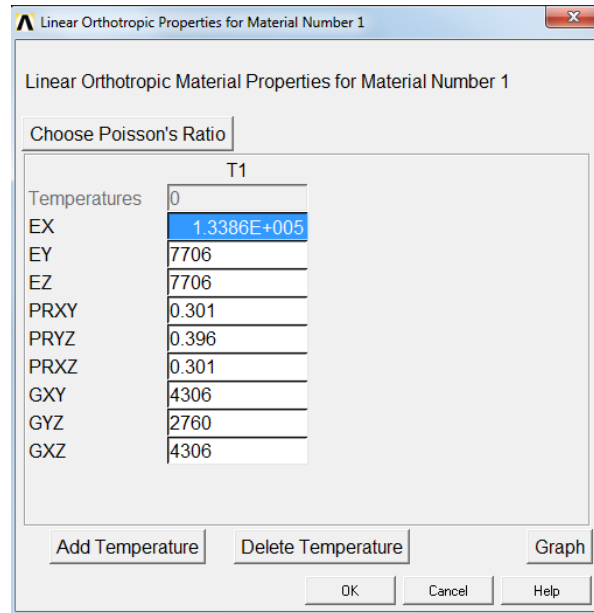


Figure A2. Material properties

### iv) Creating a Section

Using the material just created, the appropriate layup of the composite laminate can now be constructed. The section can be defined under Shell → Lay-up. Since there are 8 layers with a total thickness of 10 mm, each layer will be 1.25 mm thick. The number of integration points is chosen as 3 for each layer; top surface, bottom surface, and mid-plane.



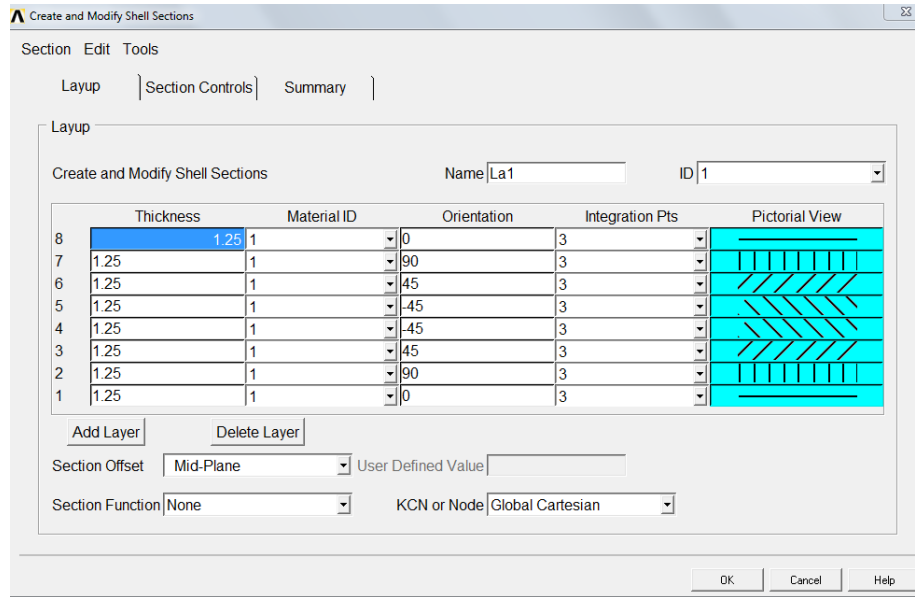


Figure A3. Composite layer arrangement

Once the section is defined, a preview of the entire section can be viewed to confirm the correct layups.

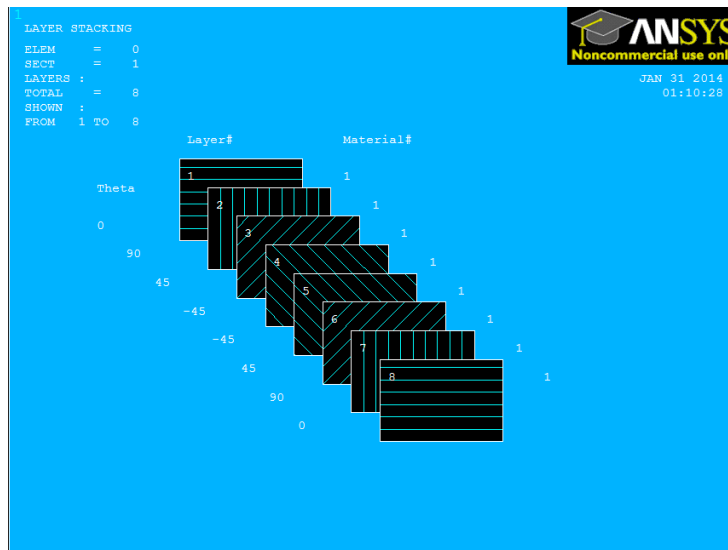
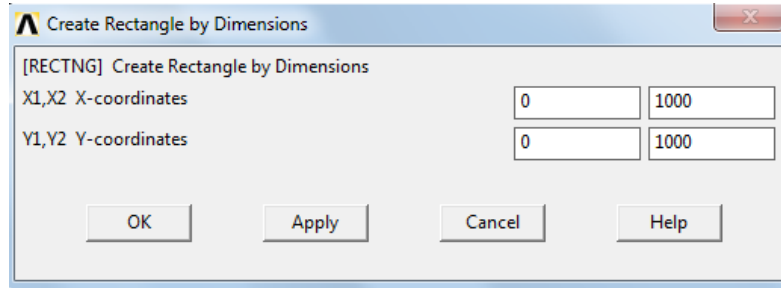


Figure A4. Composite lay-up

**v) Creating the Plate**

The plate is simply created as a rectangle using the Geometry tool.



*Figure A5. Composite plate geometry*

**vi) Meshing**

In order to stay consistent with the reference problem, an element of size of 250 mm is used. However, when creating a model of this type one may want to perform a convergence study to ensure accurate results are found with varying the meshes.

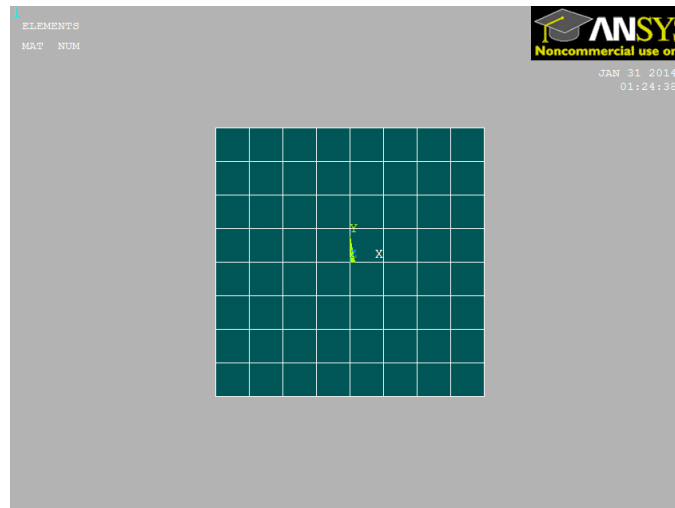


*Figure A6. Composite plate meshing*

### **vii) Applying the Load**

The load is applied as a pressure to two opposite edges of the composite. The input for pressure has input units of (N/mm) when using the MPa unit convention. Sign convention for the pressure input is: compression (+), tension (-).

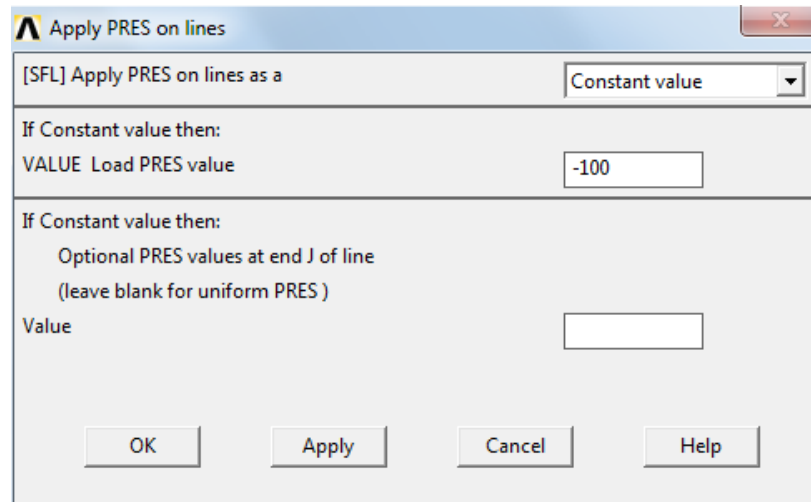


*Figure A7. Pressure application*

### **viii) Analysis/Results**

A static analysis is used, since the only load is a static load. After solving the model, a variety of post-processing options are available to review the results. The problem called for the maximum deflection. From the model, maximum displacement is given as 0.206 mm. This matches the answer given in [44].

### **ix) Comments**

By recreating the model and producing identical results, the use of ANSYS to model orthotropic composite materials is validated.

## A.2. Loading responses of damaged composite

It is important to verify delamination damage can be represented accurately using the ANSYS software. This section provides an example that will confirm modeling of delamination damage in composite is possible. The example was taken from the ANSYS Verification Models (VM) provided in the software. VM248 shows the modeling process for delamination of a 2-D double cantilever beam. The principles from this model will later be applied in Chapter 3 when modeling full composite laminates with delamination damage.

### i) *Problem Statement*

A double cantilever beam is subjected to delamination damage at its free end. Show the behavior of the beam as the delaminated sections undergo displacement in opposing directions.

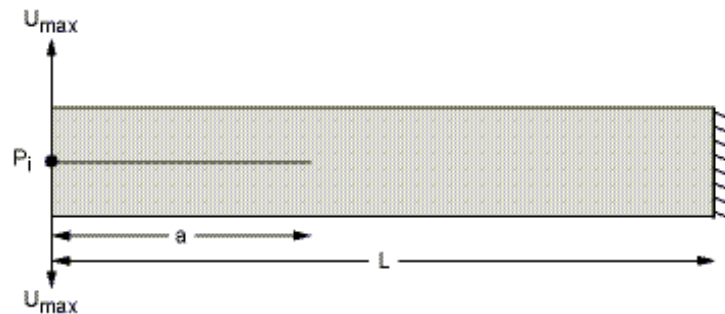


*Figure A8. Double cantilever beam*

Table A2. Double cantilever beam properties

$L$	100 mm	$U_{max}$	10 mm
$a$	30 mm	$G_{xy}$	5.2 GPa
$w$	20 mm	$G_{xz}$	5.2 GPa
$h$	3 mm	$G_{yz}$	3.08 GPa
$E_x$	135.3 GPa	$\nu_{xy}$	0.24
$E_y$	9.0 GPa	$\nu_{xz}$	0.24
$E_z$	9.0 GPa	$\nu_{yz}$	0.46

Where  $L$  = beam length,  $a$  = delamination length,  $w$  = beam width,  $h$  = beam thickness,  $E$  = modulus of elasticity,  $U_{max}$  = maximum deflection,  $G$  = shear modulus, and  $\nu$  = Poisson's ratio.

## ii) Element Types

Three element types are defined. Type 1 and 2 are 4-node SOLID 182 with the options for enhanced strain and plane strain selected. Two identical element types are defined so the beam may be effectively split along the delamination. Type 3 is a Cohesive Zone Element 202. This element type is used when defining contact surface behavior between the 2D quadrilateral elements.

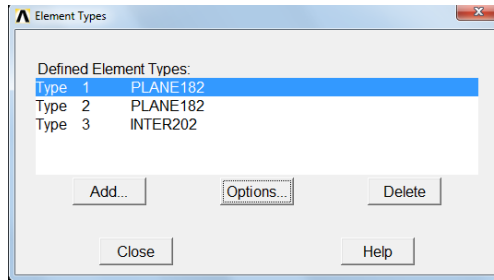


Figure A9. Element selection

### iii) Defining Materials

Two materials are defined for this example. The first is the composite material, which is defined as a linear orthotropic material with the properties shown in Figure 95.

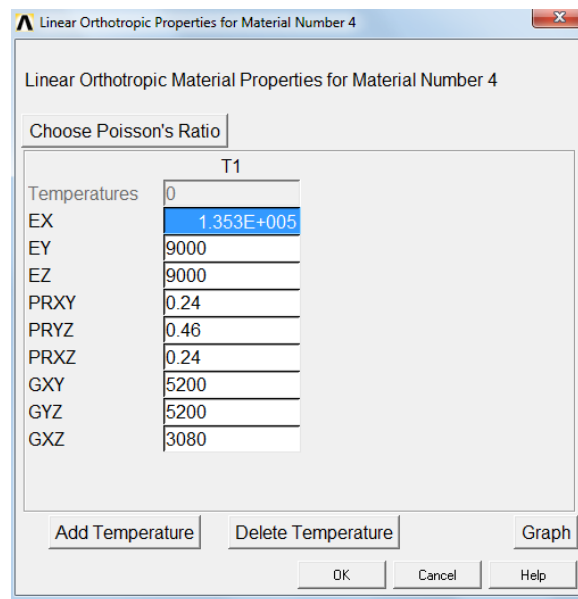


Figure A10. Composite properties

The second material is a cohesive zone material (CZM). This will be used to connect the two layers of composite in areas where delamination has occurred. The input parameters for this material are: C1, maximum stress ( $\sigma_{max}$ ); C2, normal separation ( $\delta_n$ ); and C3, shear separation ( $\delta_t$ ). The reference provides these values as 25 GPa, 0.004 mm, and 1000 mm respectively.

#### **iv) Meshing**

The beam is split into two layers, top and bottom. Element size throughout the beam is taken as 0.75 mm x 50 mm. The top layer is defined as element type 1, while the bottom is element type 2. Next comes the interface meshing. The elements joining the two layers, which are not in the delamination zone, are meshed using the CZMESH command. This applies the CZM previously defined to the contact areas.

#### **v) Boundary Conditions/Loading**

The right end of the beam is fixed, creating the cantilever action. Displacements are applied to the top most and bottom most nodes on the free end.

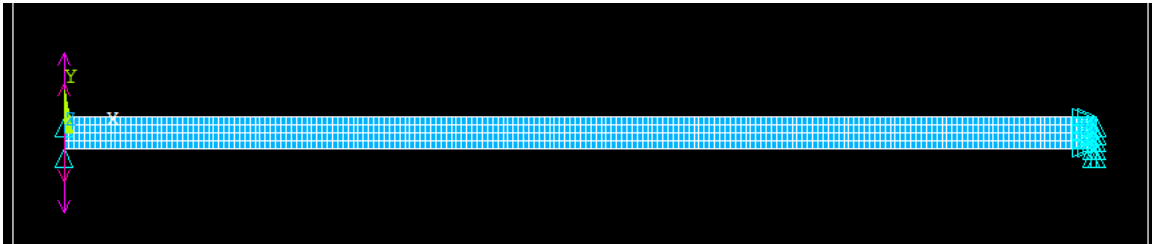


*Figure A11. Meshed composite beam*

#### **vi) Analysis**

Static analysis is performed for this model. Since the loading involved sizable deformation, the option for “Large Displacement” is used. The solution is divided into 40 subsets so a relationship between force and increasing deflection may be obtained.

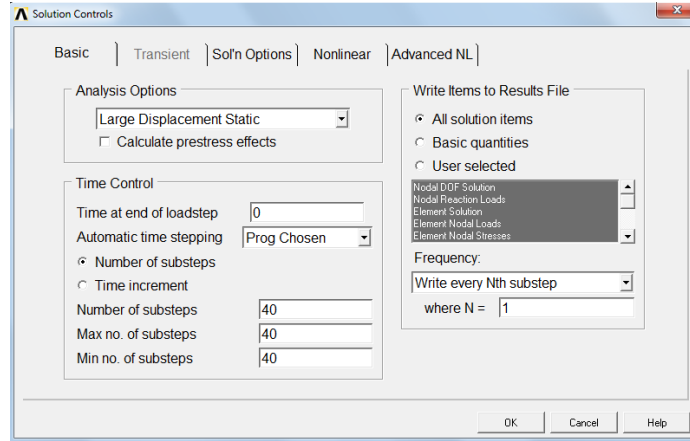


Figure A12. Solution options

**vii) Results/Comparison**

From the post-processor there are many ways to observe and present the solution data. To validate the modeling process, VM248 provides several values to compare. Shown below are the target values for the example and the corresponding values found from the model.

Table A3. Comparison of results

		Target	Model
Max value	$F_y$ (N)	60.0	60.1
	$U_y$ (mm)	1.0	1.0
At free end	$F_y$ (N)	24.0	24.3
	$U_y$ (mm)	10.0	10.0

Where  $F_y$  = reaction force in the y-direction and  $U_y$  = displacement in the y-direction.